

# Atmospheric Circulation of Exoplanets

**Adam P. Showman**

University of Arizona

**James Y-K. Cho**

Queen Mary, University of London

**Kristen Menou**

Columbia University

We survey the basic principles of atmospheric dynamics relevant to explaining existing and future observations of exoplanets, both gas giant and terrestrial. Given the paucity of data on exoplanet atmospheres, our approach is to emphasize fundamental principles and insights gained from Solar-System studies that are likely to be generalizable to exoplanets. We begin by presenting the hierarchy of basic equations used in atmospheric dynamics, including the Navier-Stokes, primitive, shallow-water, and two-dimensional nondivergent models. We then survey key concepts in atmospheric dynamics, including the importance of planetary rotation, the concept of balance, and simple scaling arguments to show how turbulent interactions generally produce large-scale east-west banding on rotating planets. We next turn to issues specific to giant planets, including their expected interior and atmospheric thermal structures, the implications for their wind patterns, and mechanisms to pump their east-west jets. Hot Jupiter atmospheric dynamics are given particular attention, as these close-in planets have been the subject of most of the concrete developments in the study of exoplanetary atmospheres. We then turn to the basic elements of circulation on terrestrial planets as inferred from Solar-System studies, including Hadley cells, jet streams, processes that govern the large-scale horizontal temperature contrasts, and climate, and we discuss how these insights may apply to terrestrial exoplanets. Although exoplanets surely possess a greater diversity of circulation regimes than seen on the planets in our Solar System, our guiding philosophy is that the multi-decade study of Solar-System planets reviewed here provides a foundation upon which our understanding of more exotic exoplanetary meteorology must build.

## 1. INTRODUCTION

The study of atmospheric circulation and climate began hundreds of years ago with attempts to understand the processes that determine the distribution of surface winds on the Earth (e.g., Hadley 1735). As theories of Earth's general circulation became more sophisticated (e.g., Lorenz 1967), the characterization of Mars, Venus, Jupiter, and other Solar-System planets by spacecraft starting in the 1960s demonstrated that the climate and circulation of other atmospheres differ, sometimes radically, from that of Earth. Exoplanets, occupying a far greater range of physical and orbital characteristics than planets in our Solar System, likewise plausibly span an even greater diversity of circulation and climate regimes. This diversity provides a motivation for extending the theory of atmospheric circulation beyond our terrestrial experience. Despite continuing questions, our understanding of the circulation of the modern Earth atmosphere is now well developed (see, e.g., Held 2000; Schneider 2006; Vallis 2006), but attempts to unravel the atmospheric dynamics of Venus, Jupiter, and other Solar-System planets remain ongoing, and the study of atmo-

spheric circulation of exoplanets is in its infancy.

For exoplanets, driving questions fall into several overlapping categories. First, we wish to understand and explain new observations constraining atmospheric structure, such as light curves, photometry, and spectra obtained with the *Spitzer*, *Hubble*, or *James Webb Space Telescopes (JWST)*, thus helping to characterize specific exoplanets as remote worlds. Second, we wish to extend the theory of atmospheric circulation to the wide range of planetary parameters encompassed by exoplanets. Existing theory was primarily developed for conditions relevant to Earth, and our understanding of how atmospheric circulation depends on atmospheric mass, composition, stellar flux, planetary rotation rate, orbital eccentricity, and other parameters remains rudimentary. Significant progress is possible with theoretical, numerical, and laboratory investigations that span a wider range of planetary parameters. Third, we wish to understand the conditions under which planets are habitable, and answering this question requires addressing the intertwined issues of atmospheric circulation and climate.

What drives atmospheric circulation? Horizontal temperature contrasts imply the existence of horizontal pres-

## What drives the atmospheric circulation?

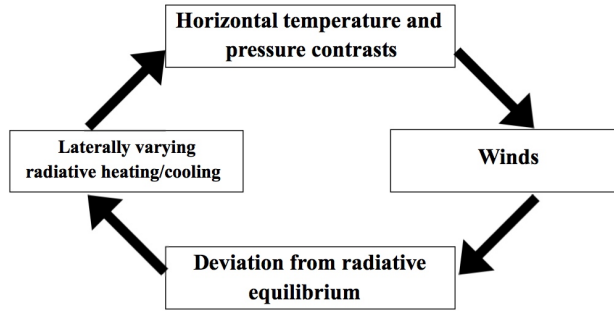


Fig. 1.— Atmospheric circulation results from a coupled interaction between radiation and hydrodynamics: horizontal temperature and pressure contrasts generate winds, which drive the atmosphere away from local radiative equilibrium. This in turn allows the spatially variable thermodynamic (radiative) heating and cooling that maintains the horizontal temperature and pressure contrasts.

sure contrasts, which drive winds. The winds in turn push the atmosphere away from radiative equilibrium by transporting heat from hot regions to cold regions (e.g., from the equator to the poles on Earth). This deviation from radiative equilibrium allows net radiative heating and cooling to occur, thus helping to maintain the horizontal temperature and pressure contrasts that drive the winds (see Fig. 1). Spatial contrasts in thermodynamic heating/cooling thus fundamentally drive the circulation, yet it is the existence of the circulation that allows these heating/cooling patterns to exist. (In the absence of a circulation, the atmosphere would relax into a radiative-equilibrium state with a net heating rate of zero.) The atmospheric circulation is thus a coupled radiation-hydrodynamics problem. On the Earth, for example (see Fig. 2), the equator and poles are not in radiative equilibrium. The equator is subject to net heating, the poles to net cooling, and it is the mean latitudinal heat transport that is both responsible for and driven by these net imbalances.

The mean climate (e.g., the global-mean surface temperature of a planet) depends foremost on the absorbed stellar flux and the atmosphere's need to reradiate that energy to space. Yet even the global-mean climate is strongly affected by the atmospheric mass, composition, and circulation. On a terrestrial planet, for example, the circulation helps to control the distribution of clouds and surface ice, which in turn determine the planetary albedo and the mean surface temperature. In some cases, a planetary climate can have multiple equilibria (e.g., a warm, ice-free state or a cold, ice-covered “snowball Earth” state), and in such cases the circulation plays an important role in determining the relative stability of these equilibria.

Understanding the atmosphere/climate system is challenging because of its nonlinearity, which involves multiple positive and negative feedbacks between radiation, clouds, dynamics, surface processes, planetary interior, and life (if any). The inherent nonlinearity of fluid motion further implies that even atmospheric-circulation models neglecting the radiative, cloud, and surface/interior components can

exhibit a large variety of behaviors.

From the perspective of studying the atmospheric circulation, transiting exoplanets are particularly intriguing because they allow constraints on key planetary attributes that are a prerequisite to characterizing an atmosphere's circulation regime. When combined with Doppler velocity data, transit observations permit a direct measurement of the exoplanet's radius, mass and thus surface gravity<sup>1</sup>. With the additional expectation that close-in exoplanets are tidally locked if on a circular orbit, or pseudo-synchronized<sup>2</sup> if on an eccentric orbit, the planetary rotation rate is thus indirectly known as well. Knowledge of the radius, surface gravity, rotation rate and external irradiation conditions for several exoplanets, together with the availability of direct observational constraints on their emission, absorption and reflection properties, opens the way for the development of comparative atmospheric science beyond the reach of our own Solar System.

The need to interpret these astronomical data reliably, by accounting for the effects of atmospheric circulation and understanding its consequences for the resulting planetary emission, absorption and reflection properties, is the central theme of this chapter. Tidally locked close-in exoplanets, for example, are subject to an unusual situation of permanent day/night radiative forcing, which does not exist in our Solar System<sup>3</sup>. To address the new regimes of forcings and responses of these exoplanetary atmospheres, a discussion of fundamental principles of atmospheric fluid dynamics and how they are implemented in multi-dimensional, coupled radiation-hydrodynamics numerical models of the GCM (General Circulation Model) type is required.

Contemplating the wide diversity of exoplanets raises

<sup>1</sup>Combining Doppler velocity and transit measurements lifts the mass-inclination degeneracy.

<sup>2</sup>Pseudo-synchronization refers to a state of tidal synchronization achieved only at periastron passage (=closest approach), as expected from the strong dependence of tides with orbital separation.

<sup>3</sup>Venus may provide a partial analogy, which has not been fully exploited yet.

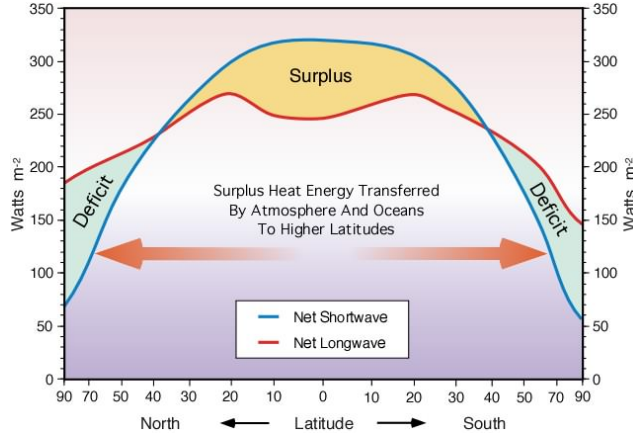


Fig. 2.—Earth’s energy balance. The Earth absorbs more sunlight at the equator than the poles (blue curve, denoted “shortwave”). The Earth also radiates more infrared energy to space at the equator than the poles (red curve, denoted “longwave”). However, because the atmospheric/oceanic circulation act to mute the latitudinal temperature contrasts (relative to radiative equilibrium), the longwave radiation exhibits less latitudinal variation than the shortwave absorption. Thus, the circulation leads to net heating at the equator and net cooling at the poles, which in turn drives the circulation. Data are an annual-average for 1987 obtained from the NASA Earth Radiation Budget Experiment (ERBE) project. Copyright M. Pidwirny, [www.physicalgeography.net](http://www.physicalgeography.net), used with permission.

a number of fundamental questions. What determines the mean wind speeds, direction, and 3D flow geometry in atmospheres? What controls the equator-to-pole and day-night temperature differences? What controls the frequencies and spatial scales of temporal variability? What role does the circulation play in controlling the mean climate (e.g., global-mean surface temperature, composition) of an atmosphere? How do these answers depend on parameters such as the planetary rotation rate, gravity, atmospheric mass and composition, and stellar flux? And, finally, what are the implications for observations and habitability of exoplanets?

At present, only partial answers to these questions exist (see reviews by Showman et al. 2008b; Cho 2008). With upcoming observations of exoplanets, constraints from Solar-System atmospheres, and careful theoretical work, significant progress is possible over the next decade. While a rich variety of atmospheric flow behaviors is realized in the Solar System alone—and an even wider diversity is possible on exoplanets—the fundamental physical principles obeyed by all planetary atmospheres are nonetheless universal. With this unifying notion in mind, this chapter provides a basic description of atmospheric circulation principles developed on the basis of extensive Solar-System studies and discusses the prospects for using these principles to better understand physical conditions in the atmospheres of remote worlds.

The plan of this chapter is as follows. In Section 2, we introduce several of the equation sets that are used to investigate atmospheric circulation at varying levels of complexity. This is followed (Section 3) by a tutorial on basic ideas in atmospheric dynamics, including atmospheric energetics, timescale arguments, force balances relevant to the large-scale circulation, the important role of rotation in generating east-west banding, and the role of waves and

eddies in shaping the circulation. In Section 4, we survey the atmospheric dynamics of giant planets, beginning with generic arguments to constrain the thermal and dynamical structure and proceeding to specific models for understanding the circulation of our “local” giant planets (Jupiter, Saturn, Uranus, Neptune) as well as hot Jupiters and hot Neptunes.<sup>4</sup> In Section 5, we turn to the climate and circulation of terrestrial exoplanets. Observational constraints in this area do not yet exist, and so our goal is simply to summarize basic concepts that we expect to become relevant as this field expands over the next decade. This includes a description of climate feedbacks (Section 5.1), global circulation regimes (Section 5.2), Hadley-cell dynamics (Section 5.3), the dynamics of the so-called midlatitude “baroclinic” zones where baroclinic instabilities dominate (Section 5.4), the slowly rotating regime relevant to Venus and Titan (Section 5.5), and finally a survey of how the circulation responds to the unusual forcing associated with synchronous rotation, extreme obliquities, or extreme orbital eccentricities (Section 5.6). The latter topics, while perhaps the most relevant, are the least understood theoretically. In Section 6 we summarize recent highlights, both observational and theoretical, and in Section 7 we finish with a survey of future prospects.

## 2. EQUATIONS GOVERNING ATMOSPHERIC CIRCULATION

A wide range of dynamical models has been developed to explore atmospheric circulation and climate. Such mod-

<sup>4</sup>The terms hot Jupiter and hot Neptune refer to giant exoplanets with masses comparable to those of Jupiter and Neptune, respectively, with orbital semi-major axes less than  $\sim 0.1$  AU, leading to high temperatures.

els are used to explain observations, understand mechanisms that govern the circulation/climate system, determine the sensitivity of a planet's circulation/climate to changes in parameters, test hypotheses about how the system works, and make predictions.

Developing a good understanding of atmospheric circulation requires the use of a hierarchy of atmospheric fluid dynamics models. Complex models that properly represent the full range of physical processes may be required for detailed predictions or comparisons with observations, but their very complexity can obscure the specific physical mechanisms causing a given phenomenon. In contrast, simpler models contain less physics, but they are easier to diagnose and can often lead to a better understanding of cause-and-effect in an idealized setting. Whether a given model contains sufficient physics to explain a given phenomenon is a question that can only be answered by exploring a hierarchy of models with a range of complexity. Exploring a hierarchy of models is therefore invaluable because it allows one to determine the minimal set of physical ingredients that are needed to generate a specific atmospheric behavior—insight that typically cannot be obtained from one type of model alone.

The equations governing atmospheric behavior derive from conservation of momentum, mass, and energy for a fluid, which we here assume to be an electrically neutral continuum. For three-dimensional models, where momentum is a three-dimensional vector, this implies five governing equations, which are generally represented as five coupled partial differential equations for the three-dimensional velocity, density, and internal energy per mass (with other thermodynamic state variables determined from density and internal energy by the equation of state). The *Navier-Stokes equations*, described in § 2.1, constitute the canonical example and provide a complete representation of a continuum, electrically neutral, viscous fluid in three dimensions.

So-called *reduced* models simplify the dynamics in one or more ways, for example by reducing specified equations to their leading-order balances. For example, because most atmospheres have large aspect ratios (with characteristic horizontal length scales for the global circulation typically 10–100 times the characteristic vertical scales), the vertical momentum balance is typically close to a local hydrostatic balance, with the local weight of fluid parcels balancing the local vertical pressure gradient [see, e.g., Holton (2004, pp. 41–42) or Vallis (2006, pp. 80–84) for a derivation]. The *primitive equations*, described in § 2.2, formalize this fact by replacing the full vertical momentum equation with local vertical hydrostatic balance. Although the system is still governed by five equations, this alteration simplifies the dynamics by removing vertically propagating sound waves, which are unimportant for most meteorological phenomena. It also leads to mathematical simplification, making it easier to obtain analytic and numerical solutions. This is the equation set that forms the basis for most cutting-edge global-scale climate models used for studying atmospheres of Solar-System planets, although some global-scale high-

resolution models now include non-hydrostatic effects.

A further common reduction is to simplify the dynamics to a one-layer model representing (for example) the vertically averaged flow. The most important example is the *shallow-water model*, described in § 2.3, which govern the behavior of a thin layer of constant-density fluid of variable thickness. This implies three coupled equations for horizontal momentum and mass conservation (governing the evolution of the two horizontal velocity components and the layer thickness) as a function of longitude, latitude, and time. Although highly idealized, the shallow-water model has proven surprisingly successful at capturing a wide range of atmospheric phenomena and has become a time-honored process model in atmospheric dynamics (see, for example, Pedlosky 1987, Chapter 3).

A further reduction results from assuming the fluid-layer thickness is constant in the shallow-water model. Given that density is also constant, the mass conservation equation then becomes a statement that horizontal convergence/divergence is zero. This constraint, which has the effect of removing gravity (buoyancy) waves from the system, allows the horizontal velocity components to be represented using a streamfunction, leading finally to a single governing partial differential equation for the streamfunction as a function of longitude, latitude, and time. § 2.4 describes this *two-dimensional, non-divergent model*. The impressive reduction from five coupled equations in five dependent variables (as for the Navier-Stokes or primitive equations) to one equation in one variable leads to great mathematical simplification, enabling analytic solutions in cases when they are otherwise difficult to obtain. Moreover, the exclusion of buoyancy effects, gravity waves, and vertical structure leads to a conceptual simplification, allowing the exploration of (for example) vortex and jet formation in the most idealized possible setting.

A comparison of results from the full range of models described here provides a path toward identifying the relative roles of acoustic waves, vertical structure, buoyancy effects, and gravity waves in affecting any given meteorological phenomenon of interest. We now present the equations associated with each of these models.

## 2.1. Navier-Stokes Equations

Let  $\mathbf{u} = \mathbf{u}(\mathbf{x}, t)$  be velocity at position  $\mathbf{x}$  and time  $t$ , where  $\mathbf{x}, \mathbf{u} \in \mathbb{R}^3$ . If the frictional force per unit area of the fluid is linearly proportional to shear in the fluid, then it is a Newtonian fluid (e.g., Batchelor 1967). Such fluids are described by the Navier-Stokes equations:

$$\frac{D\mathbf{u}}{Dt} = -\frac{1}{\rho}\nabla p + \mathbf{f}_b + \frac{1}{\rho}\nabla \cdot \left\{ 2\mu \left[ \mathbf{e} - \frac{1}{3}(\nabla \cdot \mathbf{u})\mathbb{I} \right] \right\}, \quad (1a)$$

where

$$\frac{D}{Dt} = \frac{\partial}{\partial t} + \mathbf{u} \cdot \nabla \quad (1b)$$

is the material derivative (i.e., the derivative following the motion of a fluid element). Here,  $\rho$  is density,  $p$  is pres-

sure,  $\mathbf{f}_b$  represents various body forces per mass (e.g., gravity and Coriolis),  $\mu$  is molecular dynamic viscosity, and  $\mathbf{e} = \frac{1}{2}[(\nabla \mathbf{u}) + (\nabla \mathbf{u})^\top]$  and  $\mathbb{I}$  are the strain-rate and unit tensors, respectively. In Eq. (1a) the quantity inside the braces is the viscous stress tensor. Here, as in Eq. (3) below, the average normal viscous stress (bulk viscosity) has been assumed to be zero.

Eq. (1a) is closed with the following equations for mass (per unit volume), internal energy (per unit mass), and state:

$$\frac{D\rho}{Dt} = -\rho \nabla \cdot \mathbf{u}, \quad (2)$$

$$\begin{aligned} \frac{D\epsilon}{Dt} = & -\frac{p}{\rho} (\nabla \cdot \mathbf{u}) + \frac{2\mu}{\rho} \left[ \mathbf{e} : (\nabla \mathbf{u})^\top - \frac{1}{3} (\nabla \cdot \mathbf{u})^2 \right] \\ & + \frac{1}{\rho} \nabla \cdot (K_T \nabla T) + \mathcal{Q}, \end{aligned} \quad (3)$$

$$p = p(\rho, T), \quad (4)$$

where  $\epsilon = \epsilon(T, s)$  is specific internal energy,  $s$  is specific entropy,  $K_T$  is heat conduction coefficient,  $T$  is temperature, and  $\mathcal{Q}$  is thermodynamic heating rate per mass. In Eq. (3) “:” is scalar-product (i.e., component-wise multiplication) operator for two tensors. Eqs. (1–4) constitute 6 equations for 6 independent unknowns,  $\{\mathbf{u}, p, \rho, T\}$ . Note that for a homogeneous thermodynamic system, which involves a single phase, only two state variables can vary independently; hence, there are only two thermodynamic degrees of freedom for such a system.

The neutral atmosphere is well described by Eqs. (1–4) when the characteristic length scale  $L$  is much larger than the mean free path of the constituents that make up the atmosphere. Hence, the equations are valid up to heights where ionization is not significant and the continuum hypothesis does not break down. Under normal conditions, the atmosphere behaves like an ideal gas. The parameters  $\mu$ ,  $K_T$ , and other physical properties of the fluid depend on  $T$ , as well as  $\rho$ . When appreciable temperature differences exists in the flow field, these properties must be regarded as a function of position. For large-scale atmosphere applications, however, the terms involving  $\mu$  in Eqs. (1a) and (3) are small and can be neglected in most cases. The typical boundary conditions are  $\mathbf{u} \cdot \mathbf{n} = 0$  at the lower boundary, where  $\mathbf{n}$  is the normal to the boundary, and  $\rho, p \rightarrow 0$  as  $z \rightarrow \infty$ . For local, limited area models, periodic boundary conditions are often used.

## 2.2. The Primitive Equations

On the large scale (to be more precisely quantified below), the motion of an atmosphere is governed by the primitive equations. They read (e.g., Salby 1996):

$$\frac{D\mathbf{v}}{Dt} = -\nabla_p \Phi - f \mathbf{k} \times \mathbf{v} + \mathcal{F} - \mathcal{D} \quad (5a)$$

$$\frac{\partial \Phi}{\partial p} = -\frac{1}{\rho} \quad (5b)$$

$$\frac{\partial \varpi}{\partial p} = -\nabla_p \cdot \mathbf{v} \quad (5c)$$

$$\frac{D\theta}{Dt} = \frac{\theta}{c_p T} \dot{q}_{\text{net}}, \quad (5d)$$

where

$$\frac{D}{Dt} = \frac{\partial}{\partial t} + \mathbf{v} \cdot \nabla_p + \varpi \frac{\partial}{\partial p}. \quad (5e)$$

Note here that  $p$ , rather than the geometric height  $z$ , is used as the vertical coordinate. This coordinate, which simplifies the gradient term in Eq. (5a), is common in atmospheric studies; it renders  $z = z(\mathbf{x}, p, t)$  a dependent variable, where now  $\mathbf{x} \in \mathbb{R}^2$ . In Eq. (5)  $\mathbf{v}(\mathbf{x}, t) = (u, v)$  is the (eastward<sup>5</sup>, northward) velocity in a frame rotating with  $\Omega$ , where  $\Omega$  is the planetary rotation vector as represented in inertial space;  $\Phi = gz$  is the geopotential, where  $g$  is the gravitational acceleration (assumed to be constant and to include the centrifugal acceleration contribution; see Holton 2004, pp. 13–14) and  $z$  is the height above a fiducial geopotential surface;  $\mathbf{k}$  is the local upward unit vector;  $f = 2\Omega \sin \phi$  is the Coriolis parameter, the locally vertical component of the planetary vorticity vector  $2\Omega$ ;  $\nabla_p$  is the horizontal gradient on a  $p$ -surface;  $\varpi = Dp/Dt$  is the vertical velocity;  $\mathcal{F}$  and  $\mathcal{D}$  represent the momentum sources and sinks, respectively;  $\theta = T(p_{\text{ref}}/p)^\kappa$  is the potential temperature<sup>6</sup>, where  $p_{\text{ref}}$  is a reference pressure and  $\kappa = R/c_p$  with  $R$  the specific gas constant and  $c_p$  the specific heat at constant pressure; and  $\dot{q}_{\text{net}}$  is the net diabatic heating rate (heating minus cooling). Note that  $\dot{q}_{\text{net}}$  can include not only radiative heating/cooling but latent heating and, at low pressures where the thermal conductivity becomes large, conductive heating. The Newtonian cooling scheme, which relaxes temperature toward a prescribed radiative-equilibrium temperature over a specified radiative time constant, is one simple parameterization of  $\dot{q}_{\text{net}}$ .

The fundamental presumption in the use of Eqs. (5) is that small scale processes are parameterizable within the framework of large-scale dynamics. Here by “large” scales, it is meant typically  $L \gtrsim a/10$ , where  $a$  is the planetary radius. By “small” scales, it is meant those scales that are not resolvable numerically by global models—typically  $\lesssim a/10$ . Regions of the atmosphere where small scale processes are important are often highly concentrated (e.g., fronts and convective updrafts). Their characteristic scales are  $\ll a/10$ . Therefore, it is possible that the Eq. (5) set—as with all the other equation sets discussed in this chapter—leaves out some processes important for large-scale dynamics.

To arrive at Eq. (5), one begins with Eqs. (1–4) in spherical geometry (e.g., Batchelor 1967). Two approximations are then made. These are the “shallow atmosphere” and

<sup>5</sup>Cardinal directions are defined here consistent with everyday usage; east is defined to be the prograde direction, that is, the direction in which the planet rotates. North is the direction along which  $\Omega \cdot \mathbf{k}$  becomes more positive.

<sup>6</sup>The potential temperature  $\theta$  is related to the entropy  $s$  by  $ds = c_p d \ln \theta$ . When  $c_p$  is constant, this yields  $\theta = T(p_{\text{ref}}/p)^\kappa$ .

the “traditional” approximations (e.g., Salby (1996)). The first assumes  $z/a \ll 1$ . The second is formally valid in the limit of strong stratification, when the Prandtl ratio ( $N^2/\Omega^2 \gg 1$ ). Here,  $N = N(\mathbf{x}, z, t)$  is the Brunt–Väisälä (buoyancy) frequency, the oscillation frequency for an air parcel that is displaced vertically under adiabatic conditions:

$$N = \left[ g \frac{\partial(\ln \theta)}{\partial z} \right]^{1/2}. \quad (6)$$

These approximations allow the Coriolis terms involving vertical velocity to be dropped from Eq. (1a) and vertical accelerations to be assumed small. The latter is explicitly embodied in Eq. (5b), the hydrostatic balance, which we discuss further below.

Hydrostatic balance renders the primitive equations valid only when  $N^2/\omega^2 \gg 1$ , where  $2\pi/\omega$  is the timescale of the motion under consideration. This condition, which is distinct from the Prandtl ratio condition, restricts the vertical length scale of motions to be small compared to the horizontal length scale. Therefore, the hydrostatic balance approximation breaks down in weakly stratified regions (here we refer to the dynamically evolving hydrostatic balance associated with circulation-induced perturbations in pressure and density; the mean background density and pressure—i.e., those that would exist in absence of dynamics—will remain hydrostatically balanced even when the circulation-induced perturbations are not). The hydrostatic assumption filters vertically propagating sound waves from the equations.

According to Eq. (5d), when  $\dot{q}_{\text{net}} = 0$ , individual values of  $\theta$  are retained by fluid elements as they move with the flow. In this case, Eq. (5) also admit a dynamically important conserved quantity, the potential vorticity:

$$q_{\text{PE}} = \left[ \frac{(\zeta + f) \mathbf{k}}{\rho} \right] \cdot \nabla \theta, \quad (7a)$$

where  $\zeta = \mathbf{k} \cdot \nabla \times \mathbf{v}$  is the relative vorticity. This quantity provides the crucial connection between the primitive equations and the physically simpler models that follow. For example, undulations of potential vorticity are often a direct manifestation of Rossby waves, which are represented in all the models presented in this section. The conservation of the potential vorticity  $q_{\text{PE}}$  following the flow,

$$\frac{D q_{\text{PE}}}{Dt} = 0, \quad (7b)$$

and the redistribution of  $q_{\text{PE}}$  implied by it, is one of the most important properties in atmospheric dynamics.

### 2.3. Shallow-Water Model

For many applications, Eq. (5) is too complex and broad in scope. In the absence of observational information to properly constrain the model parameters, reduction of the equations is beneficial. A commonly used approach is to collapse the 3D primitive equations to a two-dimensional

(2D), one-layer model. Such reduction allows investigation of horizontal vortex and jet interactions in an idealized setting.

Among the most widely used one-layer models is the shallow-water model. Consider a thin layer of homogeneous (i.e., constant-density) fluid, bounded above by a free surface and below by an impermeable boundary, so that its thickness is  $h(\mathbf{x}, t)$ . The dynamics of such a layer is governed by the following equations (e.g., Pedlosky 1987, chapter 3):

$$\frac{D \mathbf{v}}{Dt} = -g \nabla h - f \mathbf{k} \times \mathbf{v} \quad (8a)$$

$$\frac{Dh}{Dt} = -h \nabla \cdot \mathbf{v}, \quad (8b)$$

where

$$\frac{D}{Dt} = \frac{\partial}{\partial t} + \mathbf{v} \cdot \nabla. \quad (8c)$$

Forcing and dissipation are not included in Eq. (8), but they can be added in the usual way. In the absence of forcing and dissipation, the equations preserve the potential vorticity,

$$q_{\text{sw}} = \frac{\zeta + f}{h}, \quad (9)$$

following the flow.

If Eq. (8) is derived as the vertical mean of the flow of an isentropic atmosphere with a free upper boundary,  $h$  must be replaced by  $h^\kappa$  in the geopotential gradient term. If they are derived as a vertical mean of the flow of an isentropic atmosphere between rigid upper and lower boundaries,  $h$  must be replaced by  $h^{\kappa/(1-\kappa)}$  in the geopotential gradient term. Note that while  $\nabla \cdot \mathbf{v} \neq 0$  in Eq. (8b),  $\nabla \cdot \mathbf{u} = 0$ , since the layer is homogeneous (i.e., density is constant). Hence, the sound speed  $c_s \rightarrow \infty$ , and the sound waves are filtered out from the system. However, the system does retain gravity waves, which propagate at speed  $c_g = \sqrt{gh}$ .

The shallow-water equations are widely used as a process model in geophysical fluid dynamics. They are much simpler than the primitive equations, yet they still describe a wealth of phenomena—including vortices, jet streams, Rossby waves, gravity waves, and the interactions between them. Excluded are any processes that depend on the details of the vertical structure—including vertically propagating waves, baroclinic instabilities (see §3.7), and depth-dependent flow. However, because both rotational and buoyancy processes are included (the latter via the variable layer thickness), the shallow-water model—as well as all the models discussed so far—includes a fundamental length scale called the *Rossby radius of deformation* (often simply called the deformation radius), which is a natural length scale for a variety of phenomena that depend on both rotation and stratification. In the shallow-water system, this length scale is

$$L_D = \frac{\sqrt{gh}}{f}. \quad (10)$$

## 2.4. Two-Dimensional, Nondivergent Model

This is the simplest useful one-layer model for large-scale dynamics. For large-scale weather systems characterized by  $U/c_g \ll 1$ , we can apply a rigid upper boundary to the shallow-water model, since  $c_g$  represents external gravity wave speed in the model. Then,  $H$  is large and Eq. (8b) implies  $\nabla \cdot \mathbf{v} \ll 1$ . Taking  $\nabla \cdot \mathbf{v} = 0$  then gives the 2D nondivergent equation:

$$\frac{D\mathbf{v}}{Dt} = -g\nabla h - f\mathbf{k} \times \mathbf{v}, \quad (11)$$

where  $D/Dt$  is same as in (8c). The  $\nabla \cdot \mathbf{v} = 0$  restriction on the velocity implies that we can define a streamfunction,  $\psi(\mathbf{x}, t)$ , such that

$$\mathbf{v} = \left( -\frac{\partial\psi}{\partial y}, \frac{\partial\psi}{\partial x} \right). \quad (12)$$

Using this definition, Eq. (11) can finally be written as a single governing equation for the evolution of the streamfunction:

$$\frac{D}{Dt}(\nabla^2\psi + f) = 0. \quad (13)$$

From Eq. (13), we see that  $q_{2D} = \nabla^2\psi + f$  is the materially conserved potential vorticity for the 2D nondivergent model. This also results simply by letting  $h \rightarrow \text{constant}$  in Eq. (9).

In addition to the nonlinear vorticity advection, this equation—along with all the other equation sets described in this section—represents the dynamical effects of latitudinally varying Coriolis parameter. This is the so-called “beta effect,” where  $\beta \equiv df/dy$  is the northward gradient of the Coriolis parameter.

Eq. (13) describes Rossby waves, non-linear advection, and phenomena—such as the formation of zonal jet streams—that require the interaction of all these aspects (see §3.6). However, it lacks a finite deformation radius ( $L_D \rightarrow \infty$ ) and does not possess gravity wave solutions. Therefore, any phenomena that depend on finite deformation radius, gravity waves, or buoyancy cannot be captured. (These assumptions render the equation valid only for  $U/c_g \ll 1$  and  $L/L_D \ll 1$ .) As a result, the 2D nondivergent model cannot serve as an accurate predictive tool for most applications; however, its very simplicity renders it a valuable process model for investigating jet formation in the simplest possible setting. For a review of examples, see for example Vasavada and Showman (2005) or Vallis (2006).

## 2.5. Conserved Quantities

Potential vorticity conservation has been emphasized throughout because of its central importance in atmospheric dynamics. There are other useful conserved quantities. For example, the full Navier-Stokes equation gives

$$\frac{D}{Dt}(\mathbf{r} \times \mathbf{u}) = \mathbf{r} \times \left( -\frac{1}{\rho} \nabla p - 2\boldsymbol{\Omega} \times \mathbf{u} - \nabla \Phi^* + \mathbf{F} \right), \quad (14)$$

where  $\Phi^*$  is effective geopotential and  $\mathbf{F}$  represents any additional forces on the fluid. From this, we obtain the conservation law for specific, axial angular momentum  $\mathcal{M}$ :

$$\frac{D\mathcal{M}}{Dt} = -\frac{1}{\rho} \frac{\partial p}{\partial \lambda} + \mathcal{F}_\lambda \cos \phi, \quad (15a)$$

where

$$\mathcal{M} = (\Omega r \cos \phi + u) r \cos \phi. \quad (15b)$$

Eq. (15) relates the material change of  $\mathcal{M}$  to the axial components of torques present. For a thin atmosphere,  $r$  can be replaced with  $a$ .

Eq. (1) also gives the material conservation law for the specific total energy  $E$ :

$$\frac{DE}{Dt} = -\frac{1}{\rho} \nabla \cdot (\rho \mathbf{u}) + (\dot{Q}_{\text{net}} + \mathbf{u} \cdot \mathbf{F}), \quad (16)$$

where  $E$  is the total energy including kinetic, potential, and internal contributions:  $E = \frac{1}{2}\mathbf{u}^2 + \Phi + c_v T$  with  $c_v$  the specific heat at constant volume and  $T$  the temperature. In flux form, the conservation law is:

$$\frac{\partial}{\partial t}(\rho E) + \nabla \cdot [(\rho E + p)\mathbf{u}] = \rho(\dot{Q}_{\text{net}} + \mathbf{u} \cdot \mathbf{F}). \quad (17)$$

As already noted for  $\mathcal{M}$ , the total energy reduces in the appropriate way for the various simpler physical situations discussed in previous subsections. For example,  $\Phi$  and  $c_v T$  terms do not exist for the 2D nondivergent case. An important issue in the study of atmospheric energetics is the extent to which  $\Phi$  and  $c_v T$  are available to be converted to  $\frac{1}{2}\mathbf{u}^2$ .

## 3. BASIC CONCEPTS

The equation sets summarized in §2 describe nonlinear, potentially turbulent flows with many degrees of freedom. Unfortunately, due to the nonlinearity and complexity, analytic solutions rarely exist, and one must resort to solving the equations numerically on a computer. To represent the atmospheric circulation of a particular planet, the chosen equation set is solved numerically with a specified spatial resolution and timestep, subject to appropriate parameter values (e.g., composition, gravity, planetary rotation rate), boundary conditions, and forcing/damping (e.g., prescriptions for heating/cooling and friction).

Such models vary greatly in complexity and numerical method. General Circulation Models (GCMs) in the Solar-System studies literature, for example, typically solve the 3D primitive equations with sophisticated representations of radiative transfer, cloud formation, surface/atmosphere interactions, surface ice formation, and (if relevant) oceanic processes. These models are useful for exploring the interaction of dynamics with surface processes, radiation, and climate and are needed for quantitative comparisons with observational records.

However, because of their complexity, numerical simulations with full GCMs are computationally expensive, limiting such simulations to only moderate spatial resolution and making it difficult to broadly survey the relevant parameter space. Even more problematic, because of the inherent complexity of nonlinear fluid dynamics and its possible interactions with radiation and surface processes, it is rarely obvious *why* a given GCM simulation produces the output it does. By itself, the output of a sophisticated 3D model often provides little more fundamental understanding than the observations of the actual atmosphere themselves. To understand how a given atmospheric circulation would vary under different planetary parameters, for example, an understanding of the *mechanisms* shaping the circulation is required. Although careful diagnostics of GCM results can provide important insights into the mechanisms that are at play, a deep mechanistic understanding does not always flow naturally from such simulations.

Rather, obtaining a robust understanding requires a diversity of model types, ranging from simple to complex, in which various processes are turned on and off and the results carefully diagnosed. This is called a modeling hierarchy and its use forms the backbone of forward progress in the field of atmospheric dynamics of Earth and other Solar-System planets (see, e.g., Held 2005). For example, despite the existence of numerous full GCMs for modern Earth climate, significant advances in our understanding of the *mechanisms* shaping the atmospheric circulation rely heavily on the usage of linear models, simplified one-layer non-linear models (such as the 2D non-divergent or shallow-water models), and 3D models that do not include the sophisticated treatments of radiation and sub-grid scale convective processes included in full GCMs.<sup>7</sup> Even more fundamentally, obtaining understanding requires the development of basic theory that can (at least qualitatively) explain the results of these various models as well as observations of actual atmospheres. One of the major goals in performing simplified models is to aid in the construction of such a theory (see, e.g., Schneider 2006).

Exoplanet GCMs will surely be useful in the coming years. But, as with Solar-System planets, we expect that a fundamental understanding will require use of a modeling hierarchy as well as basic theory. In this section we survey key concepts in atmospheric dynamics that provide insight into the expected atmospheric circulation regimes. Emphasis is placed on presenting a conceptual understanding and as such we describe not only GCM results but basic theory and the results of highly simplified models as well. Here we focus on basic aspects relevant to both gaseous and terrestrial planets. Detailed presentations of issues specific to giant and terrestrial exoplanets are deferred to §4 and §5.

---

<sup>7</sup>To illustrate, a summary of the results of such a hierarchy for understanding Jupiter's jet streams can be found in Vasavada and Showman (2005).

### 3.1. Energetics of atmospheric circulation

Atmospheric circulations involve an energy cycle. Absorption of starlight and emission of infrared energy to space creates potential energy, which is converted to kinetic energy and then lost via friction. Each step in the process involves nonlinearities, and generally the atmosphere self-adjusts so that, in a time mean sense, the conversion rates balance.

What matters for driving the circulation is not the *total* potential energy but rather the *fraction* of the potential energy that can be extracted by adiabatic atmospheric motions. For example, a stably stratified, horizontally uniform atmosphere can contain vast potential energy, but none can be extracted—any adiabatic motions can only *increase* the potential energy of such a state. Uniformly heating the top layers of such an atmosphere would further increase its potential energy but would still preclude an atmospheric circulation.

For convecting atmospheres, creating extractable potential energy requires heating the fluid at lower altitudes than it is cooled. This creates buoyant air parcels (positively buoyant at the bottom, negatively buoyant at the top); vertical motion of these buoyant parcels releases potential energy and drives convection.<sup>8</sup> But, most atmospheres are stably stratified, and in this case extractable energy—called *available potential energy*—only exists when density varies horizontally on isobars (Peixoto and Oort 1992, chapter 14). In this case, the denser regions can slide laterally and downward underneath the less-dense regions, decreasing the potential energy and creating kinetic energy (winds). Continual generation of available potential energy (required to balance its continual conversion to kinetic energy and loss via friction) requires heating the regions of the atmosphere that are already hot (e.g., the tropics on Earth) and cooling the regions that are already cold (e.g., the poles). For Earth, available potential energy is generated at a global-mean rate of  $\sim 2 \text{ W m}^{-2}$ , which is  $\sim 1\%$  of the global-mean absorbed and radiated flux of  $240 \text{ W m}^{-2}$  (Peixoto and Oort 1992, pp. 382–385).

The rate of frictional dissipation can affect the mean state, but rigorously representing such friction in models is difficult. For Solar-System planets, kinetic-energy loss occurs via turbulence, waves, and friction against the surface (if any). Ohmic dissipation may be important in the deep interiors of gas giants (Kirk and Stevenson 1987; Liu et al. 2008), as well as in the upper atmosphere where ionization becomes important. These processes sometimes have length scales much smaller (by up to several orders of magnitude) than can easily be resolved in global, 3D numerical models. In Earth GCMs, such frictional dissipation mechanisms are therefore often *parameterized* by adding to

---

<sup>8</sup>To emphasize the importance of the distinction, consider a hot, isolated giant planet. The cooling caused by its radiation to space *decreases* its *total* potential energy, yet (because the cooling occurs near the top) this *increases* the fraction of the remaining potential energy that can be extracted by motions. This is what can allow convection to occur on such objects.

the equations quasi-empirical damping terms (e.g., a vertical diffusion to represent turbulent kinetic-energy losses by small-scale shear instabilities and breaking waves). A difficulty is that such prescriptions, while physically motivated, are often non-rigorous and the extent to which they can be extrapolated to other planetary environments is unclear. Perhaps for this reason, models of hot Jupiters published to date do not include such parameterizations of frictional processes (although they all include small-scale viscosity for numerical reasons).<sup>9</sup> Nevertheless, Goodman (2009) has highlighted the possible importance that such processes could play in the hot-Jupiter context, and future models of hot Jupiters will surely explore the possible effect that friction may have on the mean states.

Solar-System planets offer interesting lessons on the role of friction. Despite absorbing a greater solar flux than any other thick atmosphere in our Solar System, Earth's winds are relatively slow, with a mean wind speed of  $\sim 20 \text{ m sec}^{-1}$ . In contrast, Neptune absorbs a solar flux only 0.1% as large, but has wind speeds reaching  $400 \text{ m sec}^{-1}$ . Presumably, Neptune can achieve such fast winds despite its weak radiative forcing because its frictional damping is extremely weak. Qualitatively, this makes sense because Neptune lacks a surface, which is a primary source of frictional drag on Earth. More puzzling is the fact that Neptune has significantly stronger winds than Jupiter (Table 1) despite absorbing only 4% the solar flux absorbed by Jupiter. Possible explanations are that Jupiter experiences greater frictional damping than Neptune or that it has equilibrated to a state that has relatively slow wind speeds despite weak damping. This is not well understood and argues for humility in efforts to model the circulations of exoplanets.

### 3.2. Timescale arguments for the coupled radiation-dynamics problem

The atmospheric circulation represents a coupled radiation-hydrodynamics problem. The circulation advects the temperature field and thereby influences the radiation field; in turn, the radiation field (along with atmospheric opacities and surface conditions) determines the atmospheric heating and cooling rates that drive the circulation. Rigorously attacking this problem requires coupled treatment of both radiation and dynamics. However, crude insight into the thermal response of an atmosphere can be obtained with simple timescale arguments. Suppose  $\tau_{\text{advect}}$  is an advection time (e.g., the characteristic time for air to advect across a hemisphere) and  $\tau_{\text{rad}}$  is the radiative time (i.e., the characteristic time for radiation to induce large fractional entropy changes). When  $\tau_{\text{rad}} \ll \tau_{\text{advect}}$ , we expect temperature to deviate only slightly from the (spatially varying) radiative equilibrium temperature structure. Because the radiative

equilibrium temperature typically varies greatly from day-side to night-side (or from equator to pole), this implies that such a planet would exhibit large fractional temperature contrasts. On the other hand, when  $\tau_{\text{rad}} \gg \tau_{\text{advect}}$ , dynamical transport dominates and air will tend to homogenize its entropy, implying that lateral temperature contrasts should be modest.

In estimating the advection time, one must distinguish north-south from east-west advection; east-west advection (relative to the pattern of stellar insolation) will often be dominated by the planetary rotation. For synchronously rotating planets, a characteristic horizontal advection time is

$$\tau_{\text{advect}} \sim \frac{a}{U}, \quad (18)$$

where  $U$  is a characteristic horizontal wind speed. A similarly crude estimate of the radiative time can be obtained by considering a layer of pressure thickness  $\Delta p$  that is slightly out of radiative equilibrium and radiates to space as a blackbody. If the radiative equilibrium temperature is  $T_{\text{rad}}$  and the actual temperature is  $T_{\text{rad}} + \Delta T$ , with  $\Delta T \ll T_{\text{rad}}$ , then the net flux radiated to space is  $4\sigma T_{\text{rad}}^3 \Delta T$  and the radiative timescale is (Showman and Guillot 2002; James 1994, pp. 65-66)

$$\tau_{\text{rad}} \sim \frac{\Delta p}{g} \frac{c_p}{4\sigma T^3}. \quad (19)$$

In deep, optically thick atmospheres where the radiative transport is diffusive, a more appropriate estimate might be a diffusion time, crudely given by  $\tau_{\text{rad}} \sim H^2/D$ , where  $H$  is the vertical height of a thermal perturbation and  $D$  is the radiative diffusivity.

Showman et al. (2008b) estimated advective and radiative time constants for Solar-System planets and found that, as expected, planets with  $\tau_{\text{rad}} \gg \tau_{\text{advect}}$  generally have small horizontal temperature contrasts and vice versa.

For hot Jupiters, most models suggest peak wind speeds of  $\sim 1\text{--}3 \text{ km sec}^{-1}$  (§4.3), implying advection times of  $\sim 10^5 \text{ sec}$  based on the peak speed. Eq. (19) would then suggest that  $\tau_{\text{rad}} \ll \tau_{\text{advect}}$  at  $p \ll 1 \text{ bar}$  whereas  $\tau_{\text{rad}} \gg \tau_{\text{advect}}$  at  $p \gg 1 \text{ bar}$ . Thus, one might crudely expect large day-night temperature differences at low pressure and small day-night temperature difference at high pressure, with the transition occurring at  $\sim 0.1\text{--}1 \text{ bar}$ . These estimates are generally consistent with the observational inference of Barman (2008) and 3D numerical simulations (e.g., Showman et al. 2009; Dobbs-Dixon and Lin 2008) of hot Jupiters—though some uncertainties still exist with modeling and interpretation.

For synchronously rotating terrestrial planets in the habitable zones of M dwarfs, a mean wind speed of  $20 \text{ m sec}^{-1}$  (typical for terrestrial planets in our Solar System; see Table 1) would imply an advection time of  $\sim 3 \text{ Earth days}$ . For a temperature of  $300 \text{ K}$ , Eq. (19) would then imply that  $\tau_{\text{rad}}$  is much smaller (greater) than  $\tau_{\text{advect}}$  when the surface pressure is much less (greater) than  $\sim 0.2 \text{ bars}$ . This argument suggests that synchronously rotating terrestrial

<sup>9</sup>Note that a statistically steady (or quasi-steady) state can still occur in such a case; this requires the atmosphere to self-adjust so that the rates of generation of available potential energy and its conversion to kinetic energy become small.

exoplanets with a surface pressure much less than  $\sim 0.2$  bars should develop large day-night temperature differences, whereas if the surface pressure greatly exceeds  $\sim 0.2$  bars, day-night temperature differences would be modest. As with hot Jupiters, these estimates are consistent with 3D GCM simulations (Joshi et al. 1997), which suggest that this transition should occur at  $\sim 0.1$  bars. These estimates may have relevance for whether CO<sub>2</sub> atmospheres would collapse due to nightside condensation and hence whether such planets are habitable.

### 3.3. Basic force balances: importance of rotation

Planets rotate, and this typically constitutes a dominant factor in shaping the circulation. The importance of rotation can be estimated by performing a *scale analysis* on the equation of motion. Suppose the circulation has a mean speed  $U$  and that we are interested in flows with characteristic length scale  $L$  (this might approach a planetary radius for global-scale flows). To order-of-magnitude, the strength of the acceleration term is  $U^2/L$  (namely,  $U$  divided by a time  $L/U$  to advect fluid across a distance  $L$ ), while the magnitude of the Coriolis term is  $fU$ . The ratio of the acceleration term to the Coriolis term can therefore be represented by the *Rossby number*,

$$Ro \equiv \frac{U}{fL}. \quad (20)$$

Whenever  $Ro \ll 1$ , the acceleration terms  $D\mathbf{v}/Dt$  are weak compared to the Coriolis force per unit mass in the horizontal momentum equation. Because friction is generally weak, the only other term that can balance the horizontal Coriolis force is the pressure-gradient force, which is just  $-\nabla_p\Phi$  in pressure coordinates. The resulting balance, called *geostrophic balance*, is given by

$$fu = -\left(\frac{\partial\Phi}{\partial y}\right)_p \quad fv = \left(\frac{\partial\Phi}{\partial x}\right)_p \quad (21)$$

where  $x$  and  $y$  are eastward and northward distance, respectively and the derivatives are evaluated at constant pressure. In our Solar System, geostrophic balance holds at large scales in the mid- and high-latitude atmospheres of Earth, Mars, Jupiter, Saturn, Uranus, and Neptune. Rossby numbers range from 0.01–0.1 for these rapidly rotating planets, but exceed unity in the stratosphere of Titan<sup>10</sup> and reach  $\sim 10$  for Venus, implying in the latter case that the Coriolis force plays a less important role in the force balance (Table 1). Note that, even on rapidly rotating planets, horizontal geostrophy breaks down at the equator, where the horizontal Coriolis forces go to zero.

Determining Rossby numbers for exoplanets requires estimates of wind speeds, which are unknown. Some models of hot Jupiter atmospheres have generally suggested peak winds of several km sec<sup>-1</sup> near the photosphere,<sup>11</sup> with

mean values perhaps a factor of several smaller. To illustrate the possibilities, Table 1 presents  $Ro$  values for several hot Jupiters assuming a range of wind speeds of 100–4000 m sec<sup>-1</sup>. Generally, if mean wind speeds are fast (several km sec<sup>-1</sup>), Rossby numbers approach or exceed unity. If mean wind speeds are hundreds of m sec<sup>-1</sup> or less, Rossby numbers should be much less than one, implying that geostrophy approximately holds. One might thus plausibly expect a situation where the Coriolis force plays an important but not overwhelming role (i.e.  $Ro \sim 1$ ) near photosphere levels, with the flow transitioning to geostrophy in the interior if winds are weaker there.

Geostrophy implies that, rather than flowing from pressure highs to lows as often occurs in a non-rotating fluid, the primary horizontal wind flows *perpendicular* to the horizontal pressure gradient. Thus, the primary flow does not erase the horizontal pressure contrasts; rather, the Coriolis forces associated with that flow actually help preserve large-scale pressure gradients in a rotating atmosphere. Geostrophy explains why the isobar contours included in most mid-latitude weather maps (say of the U.S. or Europe) are so useful: the isobars describe not only the pressure field but the large-scale wind field, which flows along the isobar contours.

In many cases, rotation inhibits the ability of the circulation to equalize horizontal temperature differences. On rapidly rotating planets like the Earth, which is heated by sunlight primarily at low latitudes, the mean horizontal temperature gradients in the troposphere<sup>12</sup> generally point from the poles toward the equator. Integration of the hydrostatic equation (Eq. 5b) implies that the mean pressure gradients also point north-south. Thus, on a rapidly rotating planet where geostrophy holds and the primary temperature contrast is between equator and pole, the mean midlatitude winds will be *east-west* rather than *north-south*—thus limiting the ability of the circulation to homogenize its temperature differences in the north-south direction. We might thus expect that, everything else being equal, a more rapidly rotating planet will harbor a greater equator-to-pole temperature difference.

In rapidly rotating atmospheres, a tight link exists between horizontal temperature contrasts and the vertical gradients of the horizontal wind. This can be shown by taking the derivative with pressure of Eq. (21) and invoking the hydrostatic balance equation (5b) and the ideal-gas law. We obtain the *thermal-wind equation* for a shallow atmosphere (Holton 2004, pp. 70–75):

$$f \frac{\partial u}{\partial \ln p} = \frac{\partial(RT)}{\partial y} \quad f \frac{\partial v}{\partial \ln p} = -\frac{\partial(RT)}{\partial x} \quad (22)$$

<sup>10</sup>The troposphere is the bottommost, optically thick layer of an atmosphere, where temperature decreases with altitude and convection may play an important role; the tropopause defines the top of the troposphere, and the stratosphere refers to the stably stratified, optically thin region overlying the troposphere. In some cases, a stratosphere's temperature may increase with altitude due to absorption of sunlight by gases or aerosols; in other cases, however, the stratosphere's temperature can be nearly constant with altitude.

<sup>11</sup>Titan's Rossby number is smaller near the surface, where winds are weak.

<sup>12</sup>Defined here as the approximate pressure at which infrared photons can escape directly to space.

TABLE 1  
PLANETARY PARAMETERS

Planet	$a^*$ ( $10^3$ km)	Rotation period $^\sharp$ (Earth days)	$\Omega$ (rad sec $^{-1}$ )	gravity $^\aleph$ (m sec $^{-2}$ )	$F_*^\square$ (W m $^{-2}$ )	$T_e^\spadesuit$ (K)	$H_p^\dagger$ (km)	$U^\ddagger$ (m sec $^{-1}$ )	$Ro^\P$	$L_D/a^\clubsuit$	$L_\beta/a^\diamondsuit$
Venus	6.05	243	$3 \times 10^{-7}$	8.9	2610	232	5	$\sim 20$	10	70	7
Earth	6.37	1	$7.27 \times 10^{-5}$	9.82	1370	255	7	$\sim 20$	0.1	0.3	0.5
Mars	3.396	1.025	$7.1 \times 10^{-5}$	3.7	590	210	11	$\sim 20$	0.1	0.6	0.6
Titan	2.575	16	$4.5 \times 10^{-6}$	1.4	15	85	18	$\sim 20$	2	10	3
Jupiter	71.4	0.4	$1.7 \times 10^{-4}$	23.1	50	124	20	$\sim 40$	0.02	0.03	0.1
Saturn	60.27	0.44	$1.65 \times 10^{-4}$	8.96	15	95	39	$\sim 150$	0.06	0.03	0.3
Uranus	25.56	0.72	$9.7 \times 10^{-5}$	8.7	3.7	59	25	$\sim 100$	0.1	0.1	0.4
Neptune	24.76	0.67	$1.09 \times 10^{-4}$	11.1	1.5	59	20	$\sim 200$	0.1	0.1	0.6
WASP-12b	128	1.09	$6.7 \times 10^{-5}$	11.5	$8.8 \times 10^6$	2500	800	-	0.01–0.3	0.1	0.2–1.5
HD 189733b	81	2.2	$3.3 \times 10^{-5}$	22.7	$4.7 \times 10^5$	1200	200	-	0.03–1	0.3	0.4–3
HD 149026b	47	2.9	$2.5 \times 10^{-5}$	21.9	$1.8 \times 10^6$	1680	280	-	0.06–2	0.8	0.6–4
HD 209458b	94	3.5	$2.1 \times 10^{-5}$	10.2	$1.0 \times 10^6$	1450	520	-	0.04–1	0.4	0.5–3
TrES-2	87	2.4	$2.9 \times 10^{-5}$	21	$1.1 \times 10^6$	1475	260	-	0.03–1	0.3	0.4–3
TrES-4	120	3.5	$2.0 \times 10^{-5}$	7.8	$2.5 \times 10^6$	1825	870	-	0.03–1	0.4	0.4–3
HAT-P-7b	97	2.2	$3.3 \times 10^{-5}$	25	$4.7 \times 10^6$	2130	320	-	0.02–1	0.3	0.4–3
GJ 436b	31	2.6	$2.8 \times 10^{-5}$	9.8	$4.3 \times 10^4$	660	250	-	0.1–3	0.7	0.8–5
HAT-P-2b	68	5.6	$1.3 \times 10^{-5}$	248	$9.5 \times 10^5$	1400	21	-	0.1–3	1	0.8–5
Corot-Exo-4b	85	9.2	$7.9 \times 10^{-6}$	13.2	$3.0 \times 10^5$	1080	300	-	0.1–4	1	0.9–5

NOTE.—\*Equatorial planetary radius.  $^\sharp$  Assumes synchronous rotation for exoplanets.  $^\aleph$  Equatorial gravity at the surface.  $^\square$  Mean incident stellar flux.  $^\spadesuit$  Global-average blackbody emission temperature, which for exoplanets is calculated from Eq. (51) assuming zero albedo.  $^\dagger$  Pressure scale height, evaluated at temperature  $T_e$ .  $^\ddagger$  Rough estimates of characteristic horizontal wind speed. Estimates for Venus and Titan are in the high-altitude superrotating jet; both planets have weaker winds (few m sec $^{-1}$ ) in the bottom scale height. In all cases, peak winds exceed the listed values by factors of two or more.  $^\P$  Rossby number, evaluated in mid-latitudes using wind values listed in Table and  $L \sim 2000$  km for Earth, Mars, and Titan, 6000 km for Venus, and  $10^4$  km for Jupiter, Saturn, Uranus, and Neptune. For exoplanets, we present a range of possible values evaluated with  $L = a$  and winds from 100 to 4000 m sec $^{-1}$ .  $^\clubsuit$  Ratio of Rossby deformation radius to planetary radius, evaluated in mid-latitudes with  $H$  equal to the pressure scale height and  $N$  appropriate for a vertically isothermal temperature profile.  $^\diamondsuit$  Ratio of Rhines length (Eq. 35) to planetary radius, calculated using the equatorial value of  $\beta$  and the wind speeds listed in the Table.

where  $R$  is the specific gas constant (i.e., the universal gas constant divided by the molar mass). The equation states that, in a geostrophically balanced atmosphere, north-south temperature gradients must be associated with a vertical gradient in the zonal (east-west) wind, whereas east-west temperature gradients must be associated with a vertical gradient in the meridional (north-south) wind. Given the primarily equatorward pointing midlatitude horizontal temperature gradient in the tropospheres of Earth and Mars, for example, and given the weak winds at the surface of a terrestrial planet (a result of surface friction), this equation correctly demonstrates that the mean mid-latitude winds in the upper troposphere must flow to the east—as observed for the mid-latitude tropospheric jet streams on Earth and Mars.

Geostrophy relates the 3D structure of the winds and temperatures at a given time but says nothing about the flow's time evolution. In a rapidly rotating atmosphere, both the temperatures and winds often evolve together, maintaining approximate geostrophic balance as they do so. This time evolution depends on the *ageostrophic* component of the circulation, which tends to be of order  $Ro$  smaller than the geostrophic component. The fact that a time evolving flow maintains approximate geostrophic balance implies that, in a rapidly rotating atmosphere, adjustment mechanisms exist that tend to re-establish geostrophic balance when departures from it occur.

What is the mechanism for establishing and maintaining geostrophy? If a rapidly rotating atmosphere deviates from geostrophic balance, it implies that the horizontal pressure-gradient and Coriolis forces only imperfectly cancel, leaving an unbalanced residual force. This force generates a component of ageostrophic motion between pressure highs and lows. The Coriolis force on this ageostrophic motion, and the alteration of the pressure contrasts caused by the ageostrophic wind, act to re-establish geostrophy.

To give a concrete example, imagine an atmosphere with zero winds and a localized circular region of high surface pressure surrounded on all sides by lower surface pressure. This state has an unbalanced pressure-gradient force, which would induce a horizontal acceleration of fluid radially away from the high-pressure region. The horizontal Coriolis force on this outward motion causes a lateral deflection (to the right in the northern hemisphere and left in the southern hemisphere<sup>13</sup>), leading to a vortex surrounding the high-pressure region. The Coriolis force on this vortical motion points radially toward the high-pressure center, resisting its lateral expansion. This process continues until the inward-pointing Coriolis force balances the outward pressure-gradient force—hence establishing geostrophy and inhibiting further expansion. Although this is an extreme example, radiative heating/cooling, friction, and other forcings gradually push the atmosphere away from

geostrophy, and the process described above re-establishes it.

This process, called *geostrophic adjustment*, tends to occur with a natural length scale comparable to the Rossby radius of deformation, given in a 3D system by

$$L_D = \frac{NH}{f} \quad (23)$$

where  $N$  is Brunt-Väisälä frequency (Eq. 6),  $H$  is the vertical scale of the flow, and  $f$  is the Coriolis parameter. Thus, geostrophic adjustment naturally generates large-scale atmospheric flow structures with horizontal sizes comparable to the deformation radius (see Holton (2004) or Vallis (2006) for a detailed treatment).

Equation (22), as written, applies to atmospheres that are vertically thin compared to their horizontal dimensions (i.e., shallow atmospheres). However, a non-shallow analog of Eq. (22) can be obtained by considering the 3D vorticity equation. In a geostrophically balanced fluid where the friction force is weak, the vorticity balance is given by (see Pedlosky 1987, p. 43)

$$2(\boldsymbol{\Omega} \cdot \nabla)\mathbf{u} - 2\boldsymbol{\Omega}(\nabla \cdot \mathbf{u}) = -\frac{\nabla\rho \times \nabla p}{\rho^2}, \quad (24)$$

where  $\boldsymbol{\Omega}$  is the planetary rotation vector and  $\mathbf{u}$  is the 3D wind velocity. The term on the right, called the baroclinic term, is nonzero when density varies on constant-pressure surfaces. In the interior of a giant planet, however, convection tends to homogenize the entropy, in which case fractional density variations on isobars are extremely small. Such a fluid, where surfaces of constant  $p$  and  $\rho$  align, is called a barotropic fluid. In this case the right side of Eq. (24) can be neglected, leading to the compressible-fluid generalization of the *Taylor-Proudman theorem*:

$$2(\boldsymbol{\Omega} \cdot \nabla)\mathbf{u} - 2\boldsymbol{\Omega}(\nabla \cdot \mathbf{u}) = 0 \quad (25)$$

Consider a Cartesian coordinate system  $(x_*, y_*, z_*)$  with the  $z_*$  axis parallel to  $\boldsymbol{\Omega}$  and the  $x_*$  and  $y_*$  axes lying in the equatorial plane. Eq. (25) can then be expressed in component form as

$$\frac{\partial u_*}{\partial z_*} = \frac{\partial v_*}{\partial z_*} = 0 \quad (26)$$

$$\frac{\partial u_*}{\partial x_*} + \frac{\partial v_*}{\partial y_*} = 0 \quad (27)$$

where  $u_*$  and  $v_*$  are the wind components along the  $x_*$  and  $y_*$  axes, respectively. These equations state that the wind components parallel to the equatorial plane are independent of direction along the axis perpendicular to the equatorial plane, and moreover that the divergence of the winds in the equatorial plane must be zero. The flow thus exhibits a structure with winds constant on columns, called Taylor columns, that are parallel to the rotation axis. In the context of a giant planet, motion of Taylor columns toward or away from the rotation axis is disallowed because the planetary geometry would force the columns to stretch

<sup>13</sup>Northern and southern hemispheres are here defined as those where  $\boldsymbol{\Omega} \cdot \mathbf{k} > 0$  and  $< 0$ , respectively, where  $\boldsymbol{\Omega}$  and  $\mathbf{k}$  are the planetary rotation vector and local vertical (upward) unit vector.

or contract, causing a nonzero divergence in the equatorial plane—violating Eq. (27). Rather, the columns are free to move only along latitude circles. The flow then takes the form of concentric cylinders, centered about the rotation axis, which can move in the east-west direction. This columnar flow provides one model for the structure of the winds in the deep interiors of Jupiter, Saturn, Uranus, Neptune, and giant exoplanets (see §4).

### 3.4. Other force balances: The case of slowly rotating planets

The pressure-gradient force can be balanced by forces other than the Coriolis force. An important example is *cyclostrophic balance*, which is a balance between horizontal centrifugal and pressure-gradient force, expressed in its simplest form as:

$$\frac{u_t^2}{r} = \frac{1}{\rho} \frac{\partial p}{\partial r}, \quad (28)$$

where we are considering circular flow around a central point. Here,  $u_t$  is the tangential speed of the circular flow and  $r$  is the radius of curvature of the flow. The left-hand side of the equation is the centrifugal force per unit mass and the right-hand side is the radial pressure-gradient force per unit mass. Cyclostrophic balance is the force balance that occurs within dust devils and tornadoes, for example.

In the context of a global-scale planetary circulation, if the primary flow is east-west, the centrifugal force manifests as the curvature term  $u^2 \tan \phi / a$ , where  $a$  is planetary radius and  $\phi$  is latitude (see Holton 2004, pp. 31–38 for a discussion of curvature terms). Cyclostrophic balance can then be written

$$\frac{u^2 \tan \phi}{a} = - \left( \frac{\partial \Phi}{\partial y} \right)_p \quad (29)$$

This is the force balance relevant on Venus, for example, where a strong zonal jet with peak speeds reaching  $\sim 100 \text{ m sec}^{-1}$  dominates the stratospheric circulation (Gierasch et al. 1997). Eq. (29) can be differentiated with respect to pressure to yield a cyclostrophic version of the thermal-wind equation:

$$\frac{\partial(u^2)}{\partial \ln p} = - \frac{a}{\tan \phi} \frac{\partial(RT)}{\partial y}, \quad (30)$$

where hydrostatic balance and the ideal-gas law have been invoked.

Thus, on a slowly rotating, cyclostrophically balanced planet like Venus, Eq. (30) would indicate that variation of the zonal winds with height requires latitudinal temperature gradients as occur with geostrophic balance. Note, however, that for zonal winds whose strength increases with height, the latitudinal temperature gradients for cyclostrophic balance point equatorward *regardless* of whether the zonal winds are east or west. This differs from geostrophy, where latitudinal temperature gradients would point equatorward for a zonal wind that becomes more eastward with height but poleward for a zonal wind that becomes more westward with height.

### 3.5. What controls vertical velocities?

In atmospheres, mean vertical velocities associated with the large-scale circulation tend to be much smaller than horizontal velocities. This results from several factors:

*Large aspect ratio:* Atmospheres generally have horizontal dimensions greatly exceeding their vertical dimensions, which leads to a strong geometric constraint on vertical motions. To illustrate, suppose the continuity equation can be approximated in 3D by the incompressibility condition  $\nabla \cdot \mathbf{u} = \partial u / \partial x + \partial v / \partial y + \partial w / \partial z = 0$ . To order of magnitude, the horizontal terms can be approximated as  $U/L$  and the vertical term can be approximated as  $W/H$ , where  $L$  and  $H$  are the horizontal and vertical scales and  $U$  and  $W$  are the characteristic magnitudes of the horizontal and vertical wind. This then suggests a vertical velocity of approximately

$$W \sim \frac{H}{L} U \quad (31)$$

On a typical terrestrial planet,  $U \sim 10 \text{ m sec}^{-1}$ ,  $L \sim 1000 \text{ km}$ , and  $H \sim 10 \text{ km}$ , which would suggest  $W \sim 0.1 \text{ m sec}^{-1}$ , two orders of magnitude smaller than horizontal velocities. However, this estimate of  $W$  is an upper limit, since partial cancellation can occur between  $\partial u / \partial x$  and  $\partial v / \partial y$ , and indeed for most atmospheres Eq. (31) greatly overestimates their mean vertical velocities. On Earth, for example, mean midlatitude vertical velocities on large scales ( $\sim 10^3 \text{ km}$ ) are actually  $\sim 10^{-2} \text{ m sec}^{-1}$  in the troposphere and  $\sim 10^{-3} \text{ m sec}^{-1}$  in the stratosphere, much smaller than suggested by Eq. (31).

*Suppression of vertical motion by rotation:* The geostrophic velocity flows perpendicular to the horizontal pressure gradient, which implies that a large fraction of this flow cannot cause horizontal divergence or convergence (as necessary to allow vertical motions). However, the *ageostrophic* component of the flow, which is  $O(Ro)$  smaller than the geostrophic component, can cause horizontal convergence/divergence. Thus, to order-of-magnitude one might expect  $W \sim Ro U / L$ . Considering the geostrophic flow and taking the curl of Eq. (21), we can show that the horizontal divergence of the horizontal geostrophic wind is

$$\nabla_p \cdot \mathbf{v}_G = \frac{\beta}{f} v = \frac{v}{a \tan \phi} \quad (32)$$

where in the rightmost expression  $\beta/f$  has been evaluated assuming spherical geometry. To order of magnitude,  $v \sim U$ . Eq. (32) then implies that to order-of-magnitude the horizontal flow divergence is not  $U/L$  but rather  $U/a$ . On many planets, the dominant flow structures are smaller than the planetary radius (e.g.,  $L/a \sim 0.1\text{--}0.2$  for Earth, Jupiter, and Saturn). This implies that the horizontal divergence of the geostrophic flow is  $\sim L/a$  smaller than the estimate in Eq. (31). Taken together, these constraints suggest that rapid rotation can suppress vertical velocities by close to an order of magnitude. For Earth parameters, the

estimates imply  $W \sim 0.01 \text{ m sec}^{-1}$ , similar to the mean vertical velocities in Earth's troposphere.

*Suppression of vertical motion by stable stratification:* Most atmospheres are stably stratified, implying that entropy (potential temperature) increases with height. Adiabatic expansion/contraction in ascending (descending) air would cause temperature at a given height to decrease (increase) over time. In the absence of radiation, such steady flow patterns are unsustainable because they induce density variations that resist the motion—ascending air becomes denser and descending air becomes less dense than the surroundings. Thus, in stably stratified atmospheres, the radiative heating/cooling rate exerts major control over the rate of vertical ascent/decent. Steady vertical motion can only occur as fast as radiation can remove the temperature variations caused by the adiabatic ascent/descent (Showman et al. 2008a), when conduction is negligible. The idea can be quantified by rewriting the thermodynamic energy equation (Eq. 5d) in terms of the Brunt-Väisälä frequency:

$$\frac{\partial T}{\partial t} + \mathbf{v} \cdot \nabla_p T - \omega \frac{H_p^2 N^2}{R_p} = \frac{\dot{q}_{\text{net}}}{c_p} \quad (33)$$

where  $H_p$  is the pressure scale height. In situations where the flow is approximately steady and vertical thermal advection is more important than (or comparable to) horizontal thermal advection, an estimate of the magnitude of the vertical velocity in an overturning circulation can be obtained by equating the right side to the last term on the left side. Converting to velocity expressed in height units, we obtain (Showman et al. 2008a; Showman and Guillot 2002)<sup>14</sup>

$$W \sim \frac{\dot{q}_{\text{net}}}{c_p} \frac{R}{H_p N^2}. \quad (34)$$

For Earth's midlatitude troposphere,  $H_p \sim 10 \text{ km}$ ,  $N \sim 0.01 \text{ sec}^{-1}$ , and  $\dot{q}_{\text{net}}/c_p \sim 3 \times 10^{-5} \text{ K sec}^{-1}$ , implying  $W \sim 10^{-2} \text{ m sec}^{-1}$ . In the stratosphere, however, the heating rate is lower, and the stable stratification is greater, leading to values of  $W \sim 10^{-3} \text{ m sec}^{-1}$ .

For a canonical hot Jupiter with a 3-day rotation period, horizontal wind speeds of  $\text{km sec}^{-1}$  imply Rossby numbers of  $\sim 1$ , and for scale heights of  $\sim 300 \text{ km}$  (Table 1) and horizontal length scales of a planetary radius, one thus estimates  $RoUH/L \sim 10 \text{ m sec}^{-1}$ . Likewise, for  $R = 3700 \text{ J kg}^{-1} \text{ K}^{-1}$ ,  $H_p \sim 300 \text{ km}$ ,  $N \approx 0.005 \text{ sec}^{-1}$  (appropriate for an isothermal layer on a hot Jupiter with surface gravity of  $20 \text{ m sec}^{-1}$ ), and  $\dot{q}_{\text{net}}/c_p \sim 10^{-2} \text{ K sec}^{-1}$  (perhaps appropriate for photospheres of a typical hot Jupiter), Eq. (34) suggests mean vertical speeds of  $W \sim 10 \text{ m sec}^{-1}$  (Showman and Guillot 2002; Showman et al. 2008a). Thus, despite the fact that the circulation on hot Jupiters occurs in a radiative zone expected to be stably stratified over most of the planet, vertical overturning can occur near the photosphere over timescales of

$H_p/W \sim 10^5 \text{ sec}$ . Because the interior of a multi-Gyr-old hot Jupiter transports an intrinsic flux of only  $\sim 10-100 \text{ W m}^{-2}$  (as compared with typically  $\sim 10^5 \text{ W m}^{-2}$  in the layer where starlight is absorbed and infrared radiation escapes to space), the net heating  $\dot{q}_{\text{net}}$  should decrease rapidly with depth. The mean vertical velocities should thus plummet with depth, leading to very long overturning times in the bottom part of the radiative zone.

### 3.6. Effect of eddies: jet streams and banding

Although turbulence is a challenging problem, several decades of work in the fields of fluid mechanics and atmosphere/ocean dynamics have led to a basic understanding of turbulent flows and how they interact with planetary rotation. In a 3D turbulent flow, vorticity stretching and straining drives a fluid's kinetic energy to smaller and smaller length scales, where it can finally be removed by viscous dissipation. This process, the so-called *forward* energy cascade, occurs when turbulence has scales smaller than a fraction of a pressure scale height ( $\sim 10 \text{ km}$  for Earth,  $\sim 200 \text{ km}$  for hot Jupiters). On global scales, however, atmospheres are quasi-two-dimensional, with horizontal flow dimensions exceeding vertical flow dimensions by typically factors of  $\sim 100$ . In this quasi-2D regime, vortex stretching is inhibited, and other nonlinear processes, such as vortex merging, assume a more prominent role, forcing energy to undergo an *inverse* cascade from small to large scales (Vallis 2006, pp. 349-361). This process has been well-documented in idealized laboratory and numerical experiments (e.g., Tabeling 2002) and helps explain the emergence of large-scale jets and vortices from small-scale turbulent forcing in planetary atmospheres.

Where the Coriolis parameter  $f$  is approximately constant, this process generally produces turbulence that is horizontally isotropic, that is, turbulence without any preferred directionality (north-south versus east-west). This could explain the existence of some quasi-circular vortices on Jupiter and Saturn, for example; however, it fails to explain the existence of numerous jet streams on Jupiter, Saturn, Uranus, Neptune, and the terrestrial planets. On the other hand, Rhines (1975) realized that the variation of  $f$  with latitude leads to anisotropy, causing elongation of structures in the east-west direction relative to the north-south direction. This anisotropy can cause the energy to reorganize into east-west oriented jet streams with a characteristic latitudinal length scale

$$L_\beta = \pi \left( \frac{U}{\beta} \right)^{1/2} \quad (35)$$

where  $U$  is a characteristic wind speed and  $\beta \equiv df/dy$  is the gradient of the Coriolis parameter with northward distance  $y$ . This length is called the Rhines scale.

Numerous idealized studies of 2D turbulent flow forced by injection of small-scale turbulence have demonstrated jet formation by this mechanism [e.g., Williams (1978), Cho and Polvani (1996a), Cho and Polvani (1996b), Huang

<sup>14</sup>Oscillatory vertical motions associated with (for example) fast waves can occur adiabatically and are not governed by this constraint.

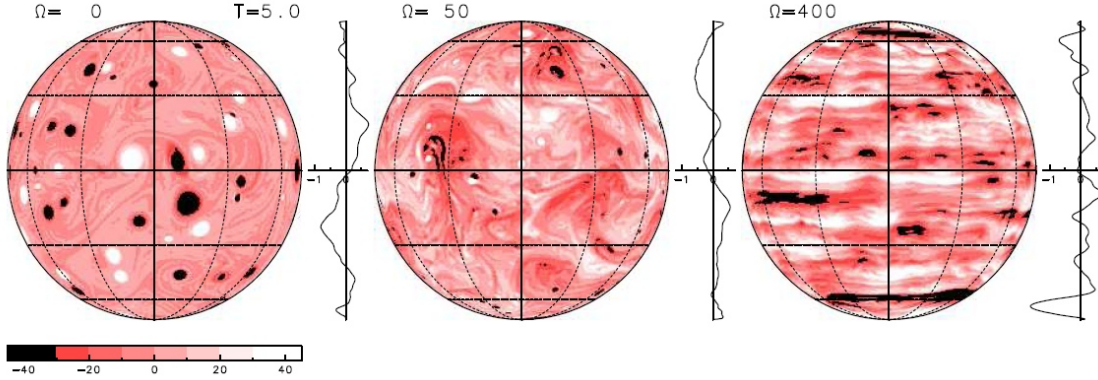


Fig. 3.— Relative vorticity for three 2D non-divergent simulations on a sphere initialized from small-scale isotropic turbulence. The three simulations are identical except for the planetary rotation rate, which is zero on the left, intermediate in the middle, and fast on the right. Forcing and large-scale friction are zero, but the simulations contain a hyperviscosity to maintain numerical stability. The final state consists of isotropic turbulence in the non-rotating case but banded flow in the rotating case, a result of the Rhines effect. The spheres are viewed from the equatorial plane, with the rotation axis oriented upward on the page. After Yoden et al. (1999), Hayashi et al. (2000), Ishioka et al. (1999), and Hayashi et al. (2007).

and Robinson (1998), Marcus et al. (2000); see Vasavada and Showman (2005) for a review]. Figure 3 illustrates an example. In 2D non-divergent numerical simulations of flow energized by small-scale turbulence, the flow remains isotropic at low rotation rates (Fig. 3, left) but develops banded structure at high rotation rates (Fig. 3, right). As shown in Fig. 4, the number of jets in such simulations increases as the wind speed decreases, qualitatively consistent with Eq. (35).

The Rhines scale can be interpreted as a transition scale between the regimes of turbulence and Rossby waves, which are a large-scale wave solution to the dynamical equations in the presence of non-zero  $\beta$ . Considering the simplest possible case of an unforced 2D non-divergent fluid (§2.4), the vorticity equation reads

$$\frac{\partial \zeta}{\partial t} + \mathbf{v} \cdot \nabla \zeta + v\beta = 0, \quad (36)$$

where  $\zeta$  is the relative vorticity,  $\mathbf{v}$  is the horizontal velocity vector, and  $v$  is the northward velocity component. The relative vorticity has characteristic scale  $U/L$ , and so the nonlinear term has characteristic scale  $U^2/L^2$ . The  $\beta$  term has characteristic scale  $\beta U$ . Comparison between these two terms shows that, for length scales smaller than the Rhines scale, the nonlinear term dominates, implying the dominance of nonlinear vorticity advection. For scales exceeding the Rhines scale, the linear  $v\beta$  term dominates over the nonlinear term, and Rossby waves are the primary solutions to the equations.<sup>15</sup>

<sup>15</sup>Adopting a streamfunction  $\psi$  defined by  $u = -\partial\psi/\partial y$  and  $v = \partial\psi/\partial x$ , the 2D non-divergent vorticity equation can be written  $\partial\nabla^2\psi/\partial t + \beta\partial\psi/\partial x = 0$  when the nonlinear term is neglected. In Cartesian geometry with constant  $\beta$ , this equation has wave solutions with a dispersion relationship  $\omega = -\beta k^2/(k^2 + l^2)$  where  $\omega$  is the oscillation frequency and  $k$  and  $l$  are the wavenumbers ( $2\pi$  over the wavelength) in the eastward and northward directions, respectively. These are Rossby waves, which

How does jet formation occur at the Rhines scale? In a 2D fluid where turbulence is injected at small scales<sup>16</sup> an upscale energy cascade occurs, but when the turbulent structures reach sizes comparable to the Rhines scale, the transition from nonlinear to quasi-linear dynamics prevents the turbulence from easily cascading to scales larger than  $L_\beta$ . At the Rhines scale, the characteristic Rossby-wave frequency for a typically oriented Rossby wave,  $-\beta/\kappa$ , roughly matches the turbulent frequency  $U\kappa$ , where  $\kappa$  is the wavenumber magnitude. (The Rossby wave frequency results from the dispersion relation, ignoring the distinction between eastward and northward wavenumbers; the turbulent frequency is one over an advective timescale,  $L/U$ .) At larger length scales (smaller wavenumbers) than the Rhines scale, the Rossby-wave oscillation frequency is faster than the turbulence frequency and so wave/turbulent interactions are inefficient at transporting energy into the Rossby-wave regime. This tends to cause a pile-up of energy at a wavelength  $L_\beta$ . As a result, flow structures with a wavelength of  $L_\beta$  often contain more energy than flow structures at any other wavelength.

But why are these dominant structures generally banded jet streams rather than (say) quasi-circular vortices? The reason relates to the anisotropy of Rossby waves. In a 2D non-divergent fluid, the Rossby-wave dispersion relation can be written

$$\omega = -\frac{\beta k}{k^2 + l^2} = -\frac{\beta \cos \alpha}{\kappa}, \quad (37)$$

where  $k$  and  $l$  are the wavenumbers in the eastward and

have a westward phase speed and a frequency that depends on the wave orientation.

<sup>16</sup>In a 2D model, turbulence behaves in a 2D manner at all scales, but in the atmosphere, flows only tend to behave 2D when the ratio of widths to heights  $\gg 1$  (implying horizontal scales exceeding hundreds of km for Earth).

northward directions,  $\kappa = \sqrt{k^2 + l^2}$  is the total wavenumber magnitude, and  $\alpha$  is the angle between the Rossby-wave propagation direction and east. Equating this frequency to the turbulence frequency  $U\kappa$  leads to an anisotropic Rhines wavenumber

$$k_\beta^2 = \frac{\beta}{U} |\cos \alpha|. \quad (38)$$

When plotted on the  $k$ - $l$  wavenumber plane, this relationship traces out a dumbbell pattern;  $k_\beta$  approaches  $\beta/U$  when  $\alpha \approx 0$  or  $180^\circ$  and approaches zero when  $\alpha \approx \pm 90^\circ$ . The Rhines scale  $L_\beta$  is thus  $\sim \pi(U/\beta)^{1/2}$  for wavevectors with  $\alpha \approx 0$  or  $180^\circ$ , but it tends to infinity for wavevectors with  $\alpha \approx \pm 90^\circ$ . Because of this anisotropic barrier, the inverse cascade can successfully drive energy to smaller wavenumbers (larger length scales) along the  $\alpha = \pm 90^\circ$  axis than along any other direction. Wavevectors with  $\alpha \approx \pm 90^\circ$  correspond to cases with  $k \ll l$ , that is, flow structures whose east-west lengths become unbounded compared to their north-south lengths. The result is usually an east-west banded pattern and jet streams whose latitudinal width is  $\sim \pi(U/\beta)^{1/2}$ . Although these considerations are heuristic, detailed numerical simulations generally confirm that in 2D flows forced by small-scale isotropic turbulence, the turbulence reorganizes to produce jets with widths close to  $L_\beta$  (Fig. 3; for a review see Vasavada and Showman 2005).

In practice, when small-scale forcing is injected into the flow, jet formation does not generally occur as the end product of successive mergers of continually larger and larger vortices but rather by a feedback whereby small eddies interact directly with the large-scale flow and pump up jets (e.g., Nozawa and Yoden 1997; Huang and Robinson 1998). The large-scale background shear associated with jets distorts the eddies, and the interaction pumps momentum up-gradient into the jet cores, helping to maintain the jets against friction or other forces.

The above arguments were derived in the context of a 2D non-divergent model, which is the simplest model where Rossby waves can interact with turbulence to form jets. Such a model lacks gravity waves and has an infinite deformation radius  $L_D$  (Eqs. 10 and 23). It is possible to extend the above ideas to one-layer models exhibiting gravity waves and a finite deformation radius, such as the shallow-water model. Doing so suggests that, as long as  $\beta$  is strong, jets dominate when the deformation radius is large (as in the 2D non-divergent model); however, the flow becomes more isotropic (dominated by vortices rather than jets) when the deformation radius is sufficiently smaller than  $(U/\beta)^{1/2}$  (e.g., Okuno and Masuda 2003; Smith 2004; Showman 2007).

On a spherical planet,  $\beta = 2\Omega a^{-1} \cos \phi$ , which implies that a planet should have a number of jet streams roughly given by

$$N_{\text{jet}} \sim \left( \frac{2\Omega a}{U} \right)^{1/2}. \quad (39)$$

These considerations do a reasonable job of predicting

the latitudinal separations and total number of jets that exist on planets in our Solar System. Given the known wind speeds (Table 1) and values of  $\beta$ , the Rhines scale predicts  $\sim 20$  jet streams on Jupiter/Saturn, 4 jet streams on Uranus and Neptune, and 7 jet streams on Earth. This is similar to the observed numbers ( $\sim 20$  on Jupiter and Saturn, 3 on Uranus and Neptune, and 3 to 7 on Earth depending on how they are defined<sup>17</sup>). Moreover, the scale-dependent anisotropy—with quasi-isotropic turbulence at small scales and banded flow at large scales—is readily apparent on Solar-System planets. Fig. 5 illustrates an example for Saturn: small-scale structures (e.g., the cloud-covered vortices that manifest as small dark spots in the figure) are relatively circular, whereas the large-scale structures are banded.

These considerations yield insight into the degree of banding and size of dominant flow structures to be expected on exoplanets. Equation (39) suggests that the number of bands scales as  $\Omega^{1/2}$ , so rapidly rotating exoplanets will tend to exhibit numerous strongly banded jets, whereas slowly rotating planets will exhibit fewer jets with weaker banding. Moreover, for a given rotation rate, planets with slower winds should exhibit more bands than planets with faster winds. Hot Jupiters are expected to be tidally locked, implying rotation rates of typically a few days. Although wind speeds on hot Jupiters are unknown, various numerical models have obtained (or assumed) speeds of  $\sim 0.5$ – $3$  km sec $^{-1}$  (Showman and Guillot 2002; Cooper and Showman 2005; Langton and Laughlin 2007; Dobbs-Dixon and Lin 2008; Menou and Rauscher 2009; Cho et al. 2003, 2008). Inserting these values into Eq. (39) implies  $N_{\text{jet}} \sim 1$ – $2$ . Consistent with these arguments, simulations of hot-Jupiter atmospheres forced at small scales have obtained typically  $\sim 1$ – $3$  broad jets (Cho et al. 2003, 2008; Langton and Laughlin 2008a).<sup>18</sup> Thus, due to a combination of their slower rotation and presumed faster wind speeds, hot Jupiters should have only a small number of broad jets—unlike Jupiter and Saturn. If the wind speeds are much slower, and/or rotation rates much greater than assumed here, the number of bands would be larger.

### 3.7. Role of eddies in 3D atmospheres

Although atmospheres behave in a quasi-2D manner on large scales due to large horizontal:vertical aspect ratios,

<sup>17</sup>In Earth's troposphere, an instantaneous snapshot typically shows distinct subtropical and high-latitude jets in each hemisphere, with weaker flow between these jets and westward flow at the equator. The jet latitudes exhibit large excursions in longitude and time, however, and when a time- and longitude average is performed, only a single local maximum in eastward flow exists in each hemisphere, with westward flow at the equator.

<sup>18</sup>Published 3D models of hot Jupiters forced by day-night heating contrasts also exhibit only a few broad jets (e.g., Cooper and Showman 2005; Showman et al. 2008a, 2009; Dobbs-Dixon and Lin 2008; Menou and Rauscher 2009) but for a different reason. In this case, the jet width may be controlled by the Rossby deformation radius, which is close to the planetary radius for many hot Jupiters. As a result, the day-night heating contrast injects significant energy into the flow directly at the planetary scale, and the  $\beta$  effect can reorganize this global-scale energy into a banded jet pattern. Because the forcing and jet scales are comparable, such a flow could lack an inverse cascade.

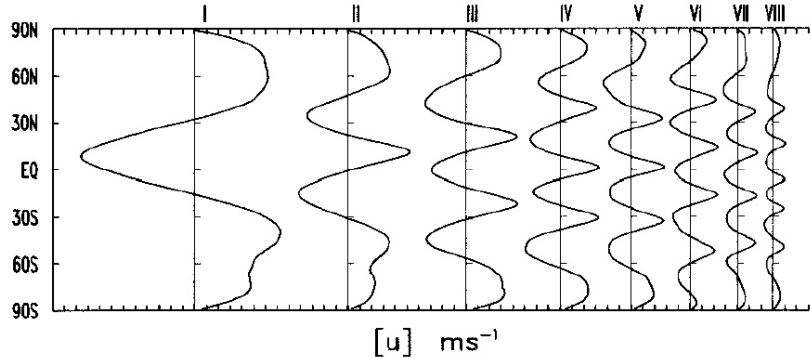


Fig. 4.— Zonal-mean zonal winds versus latitude for a series of global, 2D non-divergent simulations performed on a sphere showing the correlation between jet speed and jet width. The simulations are forced by small-scale turbulence and damped by a linear drag. Each simulation uses different forcing and friction parameters and equilibrates to a different mean wind speed, ranging from fast on the left to slow on the right. Simulations with faster jets have fewer jets and vice versa; the jet widths approximately scale with the Rhines length. From Huang and Robinson (1998).

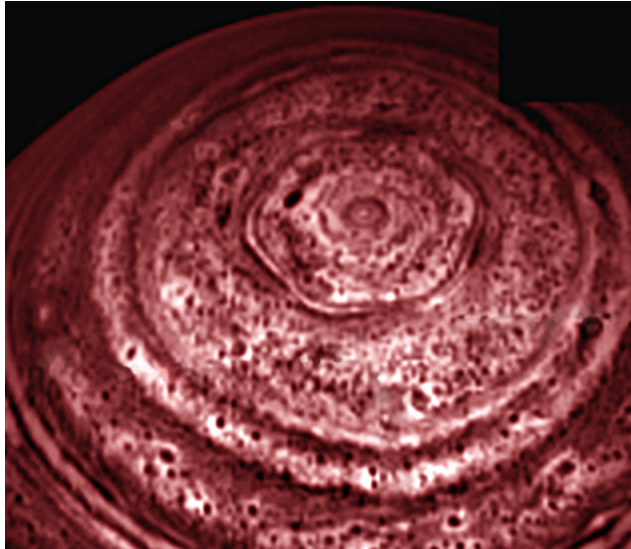


Fig. 5.— Saturn's north polar region as imaged by the Cassini Visible and Infrared Mapping Spectrometer at  $5\mu\text{m}$  wavelengths. At this wavelength, scattered sunlight is negligible; bright regions are cloud-free regions where thermal emission escapes from the deep ( $\sim 3 - 5$  bar) atmosphere, whereas dark regions are covered by thick clouds that block this thermal radiation. Note the scale-dependent anisotropy: small-scale features tend to be circular, whereas the large-scale features are banded. This phenomenon results directly from the Rhines effect (see text). [Photo credit: NASA/VIMS/Bob Brown/Kevin Baines.]

small Rossby numbers, and stable stratification, they are of course three dimensional, and as a result they can experience both upscale and downscale energy cascades depending on the length scales of the turbulence and other factors. Nevertheless, the basic mechanism discussed above for the interaction of turbulence and the  $\beta$  effect still applies and suggests that even 3D atmospheres can generally exhibit a banded structure with a characteristic length scale close to  $L_\beta$ . Consistent with this idea, numerical simulations show that banding can indeed occur in 3D even when  $\beta$  is the only source of horizontal anisotropy (e.g., Sayanagi et al. 2008; Lian and Showman 2009). Nevertheless, on real planets, banding can also result from anisotropic forcing—such as the fact that solar heating is primarily a function of latitude rather than longitude on rapidly rotating planets like Earth and Mars.

A variety of studies show that, in stably stratified, rapidly rotating atmospheres, the characteristic vertical length scale of the flow is approximately  $f/N$  times the characteristic horizontal scale (e.g., Charney 1971; Dritschel et al. 1999; Reinaud et al. 2003; Haynes 2005). For typical horizontal dimensions of large-scale flows, this often implies vertical dimensions of one to several scale heights.

Several processes can generate turbulent eddies that significantly affect the large-scale flow. Convection is particularly important in giant planet interiors and near the surface of terrestrial planets. Shear instabilities can occur when the wind shear is sufficiently large; they transfer energy from the mean flow into turbulence and reduce the shear of the mean flow. A particularly important turbulence-generating process on rapidly rotating planets is *baroclinic instability*, which is a dynamical instability driven by the extraction of potential energy from a latitudinal temperature contrast.<sup>19</sup> On non- (or slowly) rotating planets, the presence of a latitudinal temperature contrast would simply cause a direct Hadley-type overturning circulation, which efficiently mutes the thermal contrasts. However, on a rapidly rotating planet, Hadley circulations cannot penetrate to high latitudes (§5.3), and, in the absence of instabilities and waves, the atmosphere poleward of the Hadley cell would approach a radiative-equilibrium temperature structure, with strong latitudinal temperature gradients and strong zonal winds in thermal-wind balance with the temperature gradients. In 3D, this radiative-equilibrium structure can experience baroclinic instabilities, which develop into three-dimensional eddies that push cold polar air equatorward and down and push warm low-latitude air poleward and up. This process lowers the center of mass of the fluid, thereby converting potential energy into kinetic energy and transporting thermal energy between the equator and poles. The fastest instability growth rates occur at length scales comparable to the Rossby deformation radius (Eq. 23), and the resulting

eddies act as a major driver for the mid-latitude jet streams on Earth, Mars, and perhaps Jupiter, Saturn, Uranus, and Neptune.

A formalism for describing the effect of eddies on the mean flow can be achieved by decomposing the flow into zonal-mean components and deviations from the zonal mean. Here, “eddies” are defined as deviations from the zonal-mean flow and can represent the effects of turbulence, waves, and instabilities. Denoting zonal means with overbars and deviations therefrom with primes, we can write  $u = \bar{u} + u'$ ,  $v = \bar{v} + v'$ ,  $\theta = \bar{\theta} + \theta'$ , and  $\omega = \bar{\omega} + \omega'$ . Substituting these expressions into the 3D primitive equations (Eq. 5) and zonally averaging the resulting equations yields

$$\frac{\partial \bar{\theta}}{\partial t} = \overline{\frac{\partial \theta q}{T c_p}} - \frac{\partial(\bar{\theta} v)}{\partial y} - \frac{\partial(\bar{\theta} \omega)}{\partial p} \quad (40)$$

$$\frac{\partial \bar{u}}{\partial t} = f \bar{v} - \frac{\partial(\bar{u} v)}{\partial y} - \frac{\partial(\bar{u} \omega)}{\partial p} + \bar{\mathcal{F}} - \bar{\mathcal{D}}. \quad (41)$$

It can be shown that

$$\bar{u} \bar{v} = \bar{u} \bar{v} + \overline{u' v'} \quad (42)$$

and similarly for zonal averages of other quadratic terms. Thus, the terms involving derivatives on the right sides of Eqs. (40)–(41) represent the effect of transport by advection of the *mean flow* (e.g.,  $\bar{u} \bar{v}$ ) and the effect of transport by *eddies* (e.g.,  $\overline{u' v'}$ ). For example,  $\overline{u' v'}$  can be thought of as the northward transport of eastward momentum by eddies. If  $\overline{u' v'}$  has the same sign as the background jet shear  $\partial \bar{u} / \partial y$ , then eddies pump momentum up-gradient into the jet cores. If they have opposite signs, the eddies transport momentum down-gradient out of the jet cores. (See Cho 2008, for a brief discussion in the exoplanet context). Molecular diffusion is a down-gradient process, but in many cases eddies can transport momentum up-gradient, strengthening the jets.

To illustrate, consider linear Rossby waves, whose dispersion relation is given by Eq. (37) in the case of a 2D non-divergent flow. For such waves, it can be shown that the product  $\overline{u' v'}$  is opposite in sign to the north-south component of their group velocity (see Vallis 2006, pp. 489–490). Since the group velocity generally points away from the wave source, this implies that Rossby waves cause a flux of eastward momentum *toward* the wave source. The general result is an eastward eddy acceleration at the latitudes of the wave source and a westward eddy acceleration at the latitudes where the waves dissipate or break. This process is a major mechanism by which jet streams can form in planetary atmospheres.

The existence of eddy acceleration and heat transport triggers a mean circulation that has a back-influence on both  $\bar{u}$  and  $\bar{\theta}$ . On a rapidly rotating planet, for example, the eddy accelerations and heat transports tend to push the atmosphere away from geostrophic balance, leading to a mismatch in the mean north-south pressure gradient and Coriolis forces. This unbalanced force drives north-south

<sup>19</sup>When two adjacent, stably stratified air columns have differing temperature profiles, potential energy is released when the colder column slides underneath the hotter column. For this reason, baroclinic instability, which draws on this energy source, is sometimes called “slantwise convection.”

motion, which, through the mass continuity equation, accompanies vertical motions. This circulation induces advection of momentum and entropy, and moreover causes an east-west Coriolis acceleration  $f\bar{v}$ , all of which tend to restore the atmosphere toward geostrophic balance [for descriptions of this, see James (1994, pp. 100-107) or Holton (2004, pp. 313-323)]. Such mean circulations tend to have broad horizontal and vertical extents, providing a mechanism for a localized eddy perturbation to trigger a non-local response.

Clearly, jets on planets do not continually accelerate, so any jet acceleration caused by eddies must (on average) be resisted by other terms in the equation. Near the equator (or on slowly rotating planets where Coriolis forces are small), this jet acceleration is generally balanced by a combination of friction (e.g., as represented by  $\bar{D}$  in Eq. (41)) and large-scale advection. However, in the mid- and high-latitudes of rapidly rotating planets, Coriolis forces are strong, and away from the surface the eddy accelerations are often balanced by the Coriolis force on the mean flow  $f\bar{v}$ .

When averaged vertically, the east-west accelerations due to the Coriolis forces tend to cancel out<sup>20</sup>, and the *vertically integrated* force balance (on a terrestrial planet, for example) is between the vertically integrated eddy accelerations and surface friction (e.g., Peixoto and Oort 1992, Chapter 11). This means that regions without active eddy accelerations must have weak time-averaged surface winds, although the time-averaged winds may still be strong aloft. Conversely, the existence of strong time-averaged winds *at the surface* can only occur at latitudes where eddy accelerations are active. A prime example is the eastward mean surface winds in Earth's mid-latitudes (associated with the jet stream), which are enabled by the eddy accelerations from mid-latitude baroclinic instabilities.

## 4. CIRCULATION REGIMES: GIANT PLANETS

### 4.1. Thermal structure of giant planets: general considerations

Because of the enormous energy released during planetary accretion, the interiors of giant planets are hot, and due to the expected high opacities in their interiors, this energy is thought to be transported through their interiors into their atmospheres primarily by convection rather than radiation (Stevenson 1991; Chabrier and Baraffe 2000; Burrows et al. 2001; Guillot et al. 2004; Guillot 2005; Fortney et al. 2009, this volume). Jupiter, Saturn, and Neptune emit significantly more energy than they absorb from the Sun (by factors of 1.7, 1.8, and 2.6, respectively, implying interior heat fluxes of  $\sim 1-10 \text{ W m}^{-2}$ ) showing that these planets are still cooling off, presumably by convection, even 4.6 Gyr after their formation. Even for giant exoplanets that lie close to their parent stars, the stellar insolation generally

cannot stop the inexorable cooling of the planetary interiors (e.g., Guillot et al. 1996; Saumon et al. 1996; Burrows et al. 2000; Chabrier et al. 2004; Fortney et al. 2007). Thus, we expect that in general the interiors of giant planets will be convective, and hence the interior entropy will be nearly homogenized and the interior temperature and density profiles will lie close to an adiabat.<sup>21</sup>

The interiors will not precisely follow an adiabat because convective heat loss generates descending plumes that are colder than the background fluid. We can estimate the deviation from an adiabat as follows. Solar-System giant planets are rotationally dominated; as a result, convective velocities are expected to scale as (Stevenson 1979; Fernando et al. 1991):

$$w \sim \left( \frac{F\alpha g}{\Omega \rho c_p} \right)^{1/2}, \quad (43)$$

where  $w$  is the characteristic magnitude of the vertical velocity,  $F$  is the heat flux transported by convection, and  $\alpha$  and  $c_p$  are the thermal expansivity and specific heat at constant pressure. To order-of-magnitude, the convected heat flux should be  $F \sim \rho w c_p \delta T$ , where  $\delta T$  is the characteristic magnitude of the temperature difference between a convective plume and the environment. These equations yield

$$\delta T \sim \left( \frac{F\Omega}{\rho c_p \alpha g} \right)^{1/2}. \quad (44)$$

Inserting values for Jupiter's interior ( $F \sim 10 \text{ W m}^{-2}$ ,  $\Omega = 1.74 \times 10^{-4} \text{ sec}^{-1}$ ,  $\rho \sim 1000 \text{ kg m}^{-3}$ ,  $\alpha \sim 10^{-5} \text{ K}^{-1}$ ,  $c_p \approx 1.3 \times 10^4 \text{ J kg}^{-1} \text{ K}^{-1}$ , and  $g \approx 20 \text{ m sec}^{-2}$ ), we obtain  $\delta T \sim 10^{-3} \text{ K}$ , suggesting fractional density perturbations of  $\alpha \delta T \sim 10^{-8}$ . Thus, deviations from an adiabat in the interior should be extremely small. Even objects with large interior heat fluxes, such as brown dwarfs or young giant planets, will have only modest deviations from an adiabat; for example, the above equations suggest that an isolated 1000-K Jupiter-like planet with a heat flux of  $6 \times 10^4 \text{ W m}^{-2}$  would experience deviations from an adiabat in its interior of only  $\sim 0.1 \text{ K}$ .

At sufficiently low pressures in the atmosphere, the opacities become small enough that the outward energy transport transitions from convection to radiation, leading to a temperature profile that in radiative equilibrium is stably stratified and hence suppresses convection. At a minimum, this transition (called the *radiative-convective boundary*) will occur when the gas becomes optically thin to escaping infrared radiation (at pressures less than  $\sim 0.01-1$  bar depending on the opacities). For Jupiter, Saturn, Uranus, and Neptune, this transition occurs at pressures somewhat less than 1 bar. However, in the presence of intense stellar irradiation, the absorbed stellar energy greatly exceeds the energy loss from the interior; thus, the mean photospheric temperature only slightly exceeds the temperature that would exist

<sup>20</sup>This occurs because mass continuity requires that, in a time average, there be no net north-south mass transport, hence no net east-west Coriolis acceleration.

<sup>21</sup>Compositional gradients that force the interior density structures to deviate from a uniform adiabat could exist in Uranus and some giant exoplanets (Podolak et al. 1991; Chabrier and Baraffe 2007).

in thermal equilibrium with the star. In this case, cooling of the interior adiabat can only continue by development of a thick, stably stratified layer that penetrates downward from the surface and deepens with increasing age. Thus, for old, heavily irradiated planets, the radiative-convective boundary can instead occur at large optical depth, at pressures of  $\sim 100$ – $1000$  bars depending on age (see §4.3 and Fortney et al. 2009, this volume).

To what extent can large horizontal temperature differences develop in the observable atmosphere? This depends greatly on the extent to which the infrared photosphere<sup>22</sup> and radiative-convective boundaries differ in pressure. On Jupiter, Saturn, Uranus, and Neptune, the infrared photospheres lie at  $\sim 300$  mbar, close to the pressure of the radiative-convective boundary. Thus, the convective interiors—with their exceedingly small lateral temperature contrasts—effectively outcrop into the layer where radiation streams into space. On such a planet, lateral temperature contrasts in the observable atmosphere should be small (Ingersoll and Porco 1978), and indeed the latitudinal temperature contrasts are typically only  $\sim 2$ – $5$  K in the upper tropospheres and lower stratospheres of our Solar-System giant planets (Ingersoll 1990).

If instead the radiative-convective boundary lies far deeper than the infrared photosphere—as occurs on hot Jupiters—then large lateral temperature contrasts at the photosphere can potentially develop. Above the radiative-convective boundary, convective mixing is inhibited and thus cannot force vertical air columns in different regions to lie along a single temperature profile. Laterally varying absorption of light from the parent star (or other processes) can thus generate different vertical temperature gradients in different regions, potentially leading to significant horizontal temperature contrasts. In reality, such lateral temperature contrasts lead to horizontal pressure gradients, which generate horizontal winds that attempt to reduce the temperature contrasts. The resulting temperature contrasts thus depend on a competition between radiation and dynamics. These processes will be particularly important when strongly uneven external irradiation occurs, as on hot Jupiters.

Several additional processes can produce meteorologically significant temperature perturbations on giant planets. In particular, most giant planets contain trace constituents that are gaseous in the high pressure/temperature conditions of the interiors but condense in the outermost layers. This condensation releases latent heat and changes the mean molecular weight of the air, both of which cause significant density perturbations. On Jupiter and Saturn, ammonia, ammonium hydrosulfide, and water condense at pressures of  $\sim 0.5$ , 2, and 6 bars, causing temperature increases of  $\sim 0.2$ , 0.1, and 2 K, respectively, for solar abundances. For Jupiter, this corresponds to fractional density changes of  $\sim 10^{-3}$  for  $\text{NH}_3$  and  $\text{NH}_4\text{SH}$  and  $\sim 10^{-2}$  for

$\text{H}_2\text{O}$ . At deep levels ( $\sim 2000$  K, which occurs at pressures of  $\sim 5000$  bars on Jupiter), iron, silicates, and various metal oxides and hydrides condense, with a total latent heating of  $\sim 1$  K and a fractional density perturbation of  $\sim 10^{-3}$ . For Uranus/Neptune, the condensation structure is similar but also includes methane near the tropopause, with a latent heating of  $\sim 0.2$  K and a fractional density change of  $\sim 3 \times 10^{-3}$  at solar abundance. Conversion between ortho and para forms of the  $\text{H}_2$  molecule is also important at temperatures  $< 200$  K and produces a fractional density change of  $\sim 10^{-2}$  (Gierasch and Conrath 1985). Note that methane, and plausibly water and other trace constituents, are enhanced over solar abundances by factors of  $\sim 3$ , 7, and 20–40 for Jupiter, Saturn, and Uranus/Neptune, respectively, so the actual density alterations for these planets likely exceed those listed above by these factors.

The key point is that these fractional density perturbations exceed those associated with dry convection in the interior by orders of magnitude; condensation could thus dominate the meteorology in the region where it occurs. Such moist convection could have several effects. First, if the density contrasts become organized on large scales, then significant vertical shear of the horizontal wind can occur (via the thermal-wind equation) that would otherwise not exist in the outermost part of the convection zone. Second, it can generate a background temperature profile that is stably stratified (e.g. Stevens 2005), allowing wave propagation and various other phenomena. Third, the buoyancy produced by the condensation could act as a powerful driver of the circulation. For example, on Jupiter and Saturn, condensation leads to powerful thunderstorms (Little et al. 1999; Gierasch et al. 2000) that are a leading candidate for driving the global-scale jet streams (§4.2). The cloud formation associated with moist convection can also significantly alter the temperature structure due to its influence in scattering/absorbing radiation.

For giant planets hotter than those in our Solar System, the condensation sequence shifts to lower pressures and the more volatile species disappear from the condensation sequence. Important breakpoints occur for giant exoplanets with effective temperatures exceeding  $\sim 150$  and  $\sim 300$ – $500$  K, above which ammonia and water, respectively, no longer condense, thus removing the effects of their condensation from the meteorology. The latter breakpoint will be particularly significant due to the overriding dominance of the fractional density change associated with water condensation. Nevertheless, condensation of iron, silicates, and metal oxides and hydrides will collectively constitute an important source of buoyancy production even for hot giant exoplanets, as long as such condensation occurs within the convection zone, where its buoyancy dominates over that associated with dry convection (Eq. 44). For hot Jupiters, however, evolution models predict the existence of a quasi-isothermal radiative zone extending down to pressures of  $\sim 100$ – $1000$  bars (Guillot 2005; Fortney et al. 2009). Latent heating occurring within this zone is less likely to be important, simply because the  $\sim 1$  K potential temperature change

<sup>22</sup>We define the infrared photosphere as the pressure at which the bulk of the planet's infrared radiation escapes to space.

associated with silicate condensation is small compared to the probable vertical and horizontal potential temperature variations associated with the global circulation (§4.3). For example, in the vertically isothermal radiative zone of a hot Jupiter, a vertical displacement of air by only  $\sim 0.5$  km would produce a temperature perturbation (relative to the background) of  $\sim 1$  K, similar to the magnitude of thermal variation caused by condensation.

#### 4.2. Circulation of giant planets: general considerations

We now turn to the global-scale atmospheric circulation. As yet, few observational constraints exist regarding the circulation of exoplanets. Infrared light curves of several hot Jupiters indirectly suggest the presence of fast winds able to advect the temperature pattern (Knutson et al. 2007; Cowan et al. 2007; Knutson et al. 2009b), and searches for variability in brown dwarfs are being made (e.g., Morales-Calderón et al. 2006; Goldman et al. 2008). But, at present, our local Solar-System giant planets represent the best proxies to guide our thinking about the circulation on a wide class of rapidly rotating giant exoplanets. We consider basic issues here and take up specific models of hot Jupiters in §4.3.

In the observable atmosphere, the global-scale circulation on Jupiter, Saturn, Uranus, and Neptune is dominated by numerous east-west jet streams (Fig. 6). Jupiter and Saturn each exhibit  $\sim 20$  jet streams whereas Uranus and Neptune exhibit three jets each. Peak speeds range from  $\sim 150$  m sec $^{-1}$  for Jupiter to over 400 m sec $^{-1}$  for Saturn and Neptune. The winds are determined by tracking the motion of small cloud features, which occur at pressures of  $\sim 0.5$ –4 bars, over periods of hours. The jet streams modulate the patterns of ascent and descent, leading to a banded cloud pattern that can be seen in Fig. 6.

*Constraints from balance arguments:* For giant exoplanets and Solar-System giant planets alike, the dynamical link between temperatures and winds encapsulated by the thermal-wind equation allows plausible scenarios for the vertical structure of the winds to be identified. The likelihood that giant planets lose their internal energy by convection suggests that the interior entropy is nearly homogenized and hence that the interiors are close to a barotropic state (§3.3). This would lead to the Taylor-Proudman theorem (Eqs. 25–27), which states that the winds are constant on cylinders parallel to the planetary rotation axis. This scenario, first suggested by Busse (1976) for Jupiter, Saturn, Uranus, and Neptune, postulates that the jets observed in the cloud layer would simply represent the intersection with the surface of eastward- and westward-moving Taylor columns that penetrate throughout the molecular envelope.

How closely will the molecular interior of a giant planet follow the Taylor-Proudman theorem? It might not apply if geostrophy does not hold on the length scale of the jets (i.e. Rossby number  $\gtrsim 1$ ), but this is unlikely, at least for the rapidly rotating giant planets of our Solar System (Liu et al. 2008). However, for giant exoplanets, geostrophy could

break down if the interior wind speeds are sufficiently fast, planetary rotation rate is sufficiently low, the interior heat flux is sufficiently large (so that convective buoyancy forces exceed Coriolis forces  $\Omega u$  associated with the jets, for example), or magnetic effects dominate. Alternately, even if the interior exhibits geostrophic columnar behavior, the interior could exhibit a shear of the wind along the Taylor columns if density variations on isobars in the interior are sufficiently large. To illustrate how this might work, we cast Eq. (24) in a cylindrical coordinate system and take the longitudinal component, which gives

$$2\Omega \frac{\partial u}{\partial z_*} = -\frac{\nabla\rho \times \nabla p}{\rho^2} \cdot \hat{\lambda}, \quad (45)$$

where  $u$  is the zonal wind,  $z_*$  is the coordinate parallel to the rotation axis (see §3.3), and  $\hat{\lambda}$  is the unit vector in the longitudinal direction. Suppose that horizontal density variations (on isobars) occur only in latitude. A geometrical argument shows that the magnitude of  $\nabla\rho \times \nabla p$  is then  $|\nabla p|(\partial\rho/\partial y)_p$ , where  $(\partial\rho/\partial y)_p$  is the partial derivative of density with northward distance,  $y$ , on a surface of constant pressure. The magnitude of the pressure gradient is dominated by the hydrostatic component,  $-\rho g$ , and thus we can write

$$2\Omega \frac{\partial u}{\partial z_*} \approx \frac{g}{\rho} \left( \frac{\partial\rho}{\partial y} \right)_p, \quad (46)$$

which, to order-of-magnitude, implies that the magnitude of zonal-wind variation along a Taylor column can be expressed as

$$\Delta u \sim \frac{g}{L\Omega} \left( \frac{\delta\rho}{\rho} \right)_p \Delta z_*, \quad (47)$$

where  $L$  is the width of the jets in latitude,  $(\delta\rho/\rho)_p$  is the fractional density difference (on isobars) across a jet, and  $\Delta z_*$  is the distance along the Taylor column over which this fractional density difference occurs. In the interior, convection supplies the fractional density contrasts, and as shown in §4.1 these plausibly have extremely small values of  $10^{-6}$ – $10^{-8}$  below the region where condensation can occur. We can obtain a crude order-of-magnitude estimate for the thermal-wind shear along a Taylor column by assuming that these fractional density differences are organized on the jet scale and coherently extend across the full  $\sim 10^4$  km vertical length of a Taylor column. Inserting these values into Eq. (47), along with parameters relevant to a Jupiter-like planet ( $g \approx 20$  m sec $^{-2}$ ,  $L \approx 5000$  km,  $\Omega = 1.74 \times 10^{-4}$  sec $^{-1}$ ) yields  $\Delta u \sim 0.001$ – $0.1$  m sec $^{-1}$ . If this estimate is correct, then Jupiter-like planets would exhibit only small thermal-wind shear along Taylor columns, and the Taylor-Proudman theorem would hold to good approximation in the molecular interior.

However, the above estimate is crude; if the jet-scale horizontal density contrasts were much larger than the density contrasts associated with convective plumes, for example, then the wind shear along Taylor columns could exceed the values estimated above. The quantitative validity of Eq. (44), on which the wind-shear estimates are based,

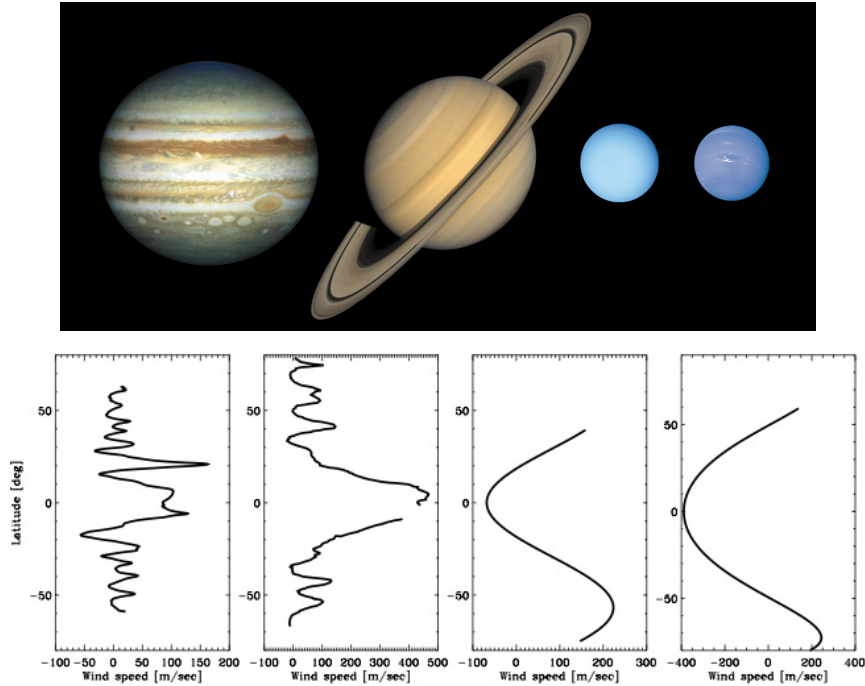


Fig. 6.— *Top:* Jupiter, Saturn, Uranus, and Neptune shown to scale in visible-wavelength images from the Cassini and Voyager spacecraft. *Bottom:* Zonal-mean zonal wind profiles obtained from tracking small-scale cloud features over a period of hours. Jupiter and Saturn have an alternating pattern of  $\sim 20$  east-west jets, whereas Uranus and Neptune have 3 broad jets.

also remains uncertain. To attack the problem more rigorously, Kaspi et al. (2009) performed full 3D numerical simulations of convection in giant-planet interiors, suggesting that the compressibility may play an important role in allowing the generation of thermal-wind shear within giant planets, especially in the outermost layers of their convection zones. Such wind shear is particularly likely to be important for young and/or massive planets with large interior heat fluxes.

Although fast winds could exist throughout the molecular envelope, Lorentz forces probably act to brake the zonal flows in the underlying metallic region at pressures exceeding  $\sim 1\text{--}3$  Mbar (Kirk and Stevenson 1987; Grote et al. 2000; Busse 2002). The winds in the deep, metallic interior are thus often assumed to be weak. The transition between molecular and metallic occurs gradually, and there exists a wide semi-conducting transition zone over which the Taylor-Proudman theorem approximately holds yet the electrical conductivity becomes important. Liu et al. (2008) argued that, if the observed jets on Jupiter and Saturn penetrated downward as Taylor columns, the Ohmic dissipation would exceed the luminosity of Jupiter (Saturn) if the jets extended deeper than 95% (85%) of the planetary radius. The observed jets are thus probably shallower than these depths. However, if the jets extended partly through the molecular envelope, terminating within the semi-conducting zone where the Ohmic dissipation occurs, the shear at the base of the jets must coexist with lateral density contrasts on isobars via the thermal wind relation-

ship (Eq. 46). This is problematic, because, as previously discussed, sufficiently large sources of density contrasts are lacking in the deep interior. Liu et al. (2008) therefore argued that the jets must be weak *throughout* the molecular envelope up to shallow levels where alternate buoyancy sources become available (e.g., latent heating and/or transition to a radiative zone).

In the outermost layers of a giant planet, density variations associated with latent heating and/or a transition to a radiative zone allow significant thermal wind-shear to develop. On Jupiter and Saturn, this so-called “baroclinic” layer begins with condensation of iron, silicates, and various metal oxides and hydrides at pressures of  $\sim 10^4$  bars and continues with condensation of water,  $\text{NH}_4\text{SH}$ , and ammonia (at  $\sim 10$ , 2, and 0.5 bars, respectively), finally transitioning to the stably stratified stratosphere at  $\sim 0.2$  bars. Early models showed that the observed jet speeds can plausibly result from thermal-wind shear within this layer assuming the winds in the interior are zero (Ingersoll and Cuzzi 1969). For example, water condensation could cause a fractional density contrast on isobars of up to  $10^{-2}$ , and if these density differences extend vertically over  $\sim 100$  km (roughly the altitude difference between the water-condensation level and the observed cloud deck), then Eq. (47) implies  $\Delta u \sim 30 \text{ m sec}^{-1}$ , similar to the observed speed of Jupiter’s mid-latitude jets (Fig. 6).

To summarize, current understanding suggests that giant planets should exhibit winds within the convective molecular envelope that exhibit columnar structure parallel to the

rotation axis, transitioning in the outermost layers (pressures less than thousands of bars) to a baroclinic zone where horizontal density contrasts associated with latent heating and/or a radiative zone allow the zonal winds to vary with altitude.

*Constraints from observations:* Few observations yet exist that constrain the deep wind structure in Jupiter, Saturn, Uranus, and Neptune. On Neptune, gravity data from the 1989 *Voyager 2* flyby imply that the fast jets observed in the cloud layers are confined to the outermost few percent or less of the planet's mass, corresponding to pressures less than  $\sim 10^5$  bars (Hubbard et al. 1991). By comparison, only weak constraints currently exist for Jupiter and Saturn. The Galileo Probe, which entered Jupiter's atmosphere at a latitude of  $\sim 7^\circ\text{N}$  in 1995, showed that the equatorial jet penetrates to at least 22 bars, roughly 150 km below the visible cloud deck (Atkinson et al. 1997), and indirect inferences suggest that the jets penetrate to at least  $\sim 5\text{--}10$  bars at other latitudes (e.g. Dowling and Ingersoll 1989; Sánchez-Lavega et al. 2008). In 2016, however, NASA's *Juno* mission will measure Jupiter's gravity field, finally determining whether Jupiter's jets penetrate deeply or are confined to pressures as shallow as thousands of bars or less. These results will have important implications for understanding the deep-wind structure in giant exoplanets generally.

*Jet-pumping mechanisms:* Two scenarios exist for the mechanisms to pump the zonal jets on the giant planets (for a review see Vasavada and Showman 2005). In the “shallow forcing” scenario, the jets are hypothesized to result from moist convection (e.g., thunderstorms), baroclinic instabilities, or other turbulence-generating processes in the baroclinic layer in the outermost region of the planet. Two-dimensional and shallow-water models of this process, where random turbulence is injected as an imposed forcing (or alternately added as a turbulent initial condition), show success in producing alternating zonal jets through the Rhines effect (§3.6). For appropriately chosen forcing and damping parameters (or for appropriate initial velocities when the turbulence is added as an initial condition), such models typically exhibit jets of approximately the observed speed and spacing (Williams 1978; Cho and Polvani 1996a; Huang and Robinson 1998; Scott and Polvani 2007; Showman 2007; Sukoriansky et al. 2007). Most models of this type produce an equatorial jet that flows westward rather than eastward as on Jupiter and Saturn, though robust eastward equatorial flow has been obtained in a recent shallow-water study (Scott and Polvani 2008). Three-dimensional models of this process can explicitly resolve the turbulent energy generation and therefore need not inject turbulence by hand. These models likewise exhibit multiple zonal jets via the Rhines effect, in some cases spontaneously producing an eastward equatorial jet as on Jupiter and Saturn (e.g. Williams 1979, 2003; Lian and Showman 2008, 2009; Schneider and Liu 2009). Figure 7, for example, illustrates 3D simulations from Lian and Showman (2009) where the

circulation is driven by latent heating associated with condensation of water vapor; the condensation produces turbulent eddies that interact with the planetary rotation (i.e., non-zero  $\beta$ ) to generate jets. Globes show the zonal wind for a Jupiter case (top row), Saturn case (middle), and a case representing Uranus/Neptune (bottom row). The Jupiter and Saturn cases develop  $\sim 20$  jets, including an eastward equatorial jet, whereas the Uranus/Neptune case develops a 3-jet structure with a broad westward equatorial flow—qualitatively similar to the observed jet patterns on these planets (Fig. 6). Note that shallow *forcing* need not imply shallow *jets*; because the atmosphere's response to a perturbation is nonlocal, deep jets (penetrating many scale heights below the clouds) can result from jet pumping confined to the cloud layer if the frictional damping in the interior is sufficiently weak (Showman et al. 2006; Lian and Showman 2008).

In the “deep forcing” scenario, convection throughout the molecular envelope is hypothesized to drive the jets. To date, most studies of this process involve 3D numerical simulations of convection in a self-gravitating spherical shell excluding the effects of magnetohydrodynamics (e.g., Aurnou and Olson 2001; Christensen 2001, 2002; Heimpel et al. 2005). The boundaries are generally taken as free-slip impermeable spherical surfaces with an outer boundary at the planetary surface and an inner boundary at a radius of 0.5 to 0.9 planetary radii. Most of these studies assume the mean density, thermal expansivity, and other fluid properties are constant with radius. These studies generally produce jets penetrating through the shell as Taylor columns. When the shell is thick (inner radius  $\leq 0.7$  of the outer radius), only  $\sim 3\text{--}5$  jets form (Aurnou and Olson 2001; Christensen 2001, 2002; Aurnou and Heimpel 2004), inconsistent with Jupiter and Saturn. Only when the shell has a thickness  $\sim 10\%$  or less of the planetary radius do such simulations produce a Jupiter- or Saturn-like profile with  $\sim 20$  jets (Heimpel et al. 2005). However, on giant planets, the density and thermal expansivity each vary by several orders of magnitude from the photosphere to the deep interior, and this might have a major effect on the dynamics. Only recently has this effect been included in detailed numerical models of the convection (Glatzmaier et al. 2009; Kaspi et al. 2009), and these studies show that the compressibility can exert a significant influence on the jet structure. A difficulty in interpreting all the convective simulations described here is that, to integrate in reasonable times, they must adopt viscosities and heat fluxes orders of magnitude too large.

The fast interior jets in these convection simulations imply the existence of strong horizontal pressure contrasts, which in these models are supported by the impermeable upper and lower boundaries. On a giant planet, however, there is no solid surface to support such pressure variations. If these fast winds transitioned to weak winds within the metallic region, significant lateral density variations would be required via the thermal-wind relationship. As discussed previously, however, there exists no obvious source of such

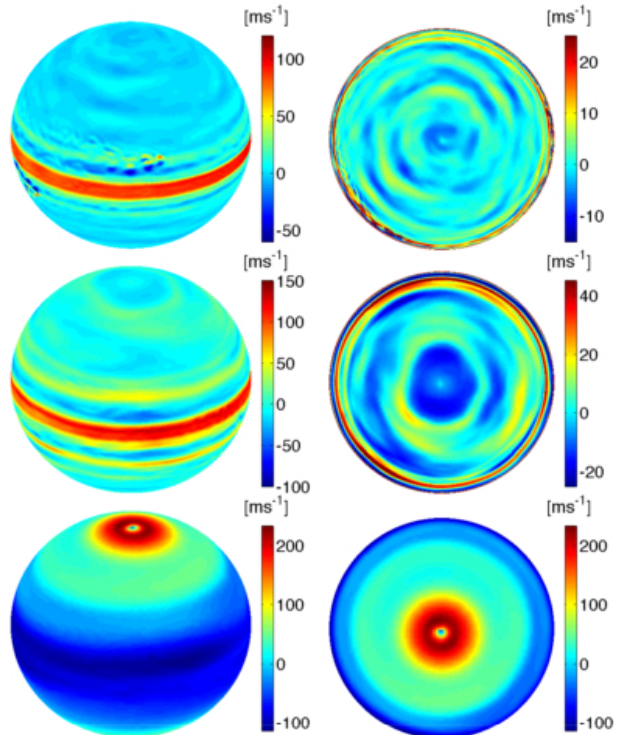


Fig. 7.— Illustration of the effect of latent heating on the circulation of a rapidly rotating giant planet. Shows zonal (east-west) wind from 3D atmospheric simulations of Jupiter (top row), Saturn (middle row), and a case representing Uranus/Neptune (bottom row) where the circulation is driven by condensation of water vapor, with an assumed deep abundance of 3, 5, and 30 times solar for the Jupiter, Saturn, and Uranus/Neptune cases, respectively. Left column shows an oblique view and right column shows a view looking down over the north pole. Note the development of numerous jets (including superrotating equatorial jets on Jupiter and Saturn), which bear qualitative resemblance to the observed jets in Fig. 6. From Lian and Showman (2009).

density variations (on isobars) within the deep interior. Resolving this issue will require 3D convection simulations that incorporate magnetohydrodynamics and simulate the entire molecular+metallic interior. Several groups are currently making such efforts, so the next decade should see significant advances in this area.

### 4.3. Hot Jupiters and Neptunes

Because of their likelihood of transiting their stars, hot Jupiters (giant planets within 0.1 AU of their primary star) remain the best characterized exoplanets and thus far have been the focus of most work on exoplanet atmospheric circulation. Dayside photometry and/or infrared spectra now exist for a variety of hot Jupiters, constraining the dayside temperature structure. For some planets, such as HD 189733b, this suggests a temperature profile that decreases with altitude from  $\sim 0.01$ –1 bar (Charbonneau et al. 2008; Barman 2008; Swain et al. 2009), whereas other hot Jupiters, such as HD 209458b, TrES-2, TrES-4, and XO-1b (Knutson et al. 2008, 2009a; Machalek et al. 2008), appear to exhibit a thermal inversion layer (i.e., a hot stratosphere) where temperatures rise above 2000 K.

Infrared light curves at 8 and/or 24  $\mu\text{m}$  now exist for HD 189733b, Ups And b, HD 209458b, and several other hot Jupiters (Knutson et al. 2007, 2009b; Harrington et al. 2006; Cowan et al. 2007), placing constraints on the day-night temperature distribution of these planets. Light curves for HD 189733b and HD 209458b exhibit nightside brightness temperatures only modestly ( $\sim 20$ –30%) cooler than the dayside brightness temperatures, suggesting efficient redistribution of the thermal energy from dayside to nightside. On the other hand, Ups And b and HD 179949b exhibit larger day-night phase variations that suggests large (perhaps  $> 500$  K) day-night temperature differences.

These and other observations provide sufficient constraints on the dayside temperature structure and day-night temperature distributions to make comparison with detailed atmospheric circulation models a useful exercise. Here we survey the basic dynamical regime and recent efforts to model these objects (see also Showman et al. 2008b; Cho 2008).

The dynamical regime on hot Jupiters differs from that on Jupiter and Saturn in several important ways. First, because of the short spindown times due to their proximity to their stars, hot Jupiters are expected to rotate nearly synchronously<sup>23</sup> with their orbital periods, implying rotation periods of 1–5 Earth days for most hot Jupiters discovered to date. This is 2–12 times slower than Jupiter’s 10-hour rotation period, implying that, compared to Jupiter, hot Jupiters experience significantly weaker Coriolis forces for a given wind speed. Nevertheless, Coriolis forces can still play a key role: for global-scale flows (length scales  $L \sim 10^8$  m) and wind speeds of 2  $\text{km sec}^{-1}$  (see below), the Rossby number for a hot Jupiter with a 3-day period is

$\sim 1$ , implying a three-way force balance between Coriolis, pressure-gradient, and inertial (i.e. advective) terms in the horizontal equation of motion. Slower winds would imply smaller Rossby numbers, implying greater rotational dominance.

Second, hot Jupiters receive enormous energy fluxes ( $\sim 10^4$ – $10^6 \text{ W m}^{-2}$  on a global average) from their parent stars, in contrast to the  $\sim 10 \text{ W m}^{-2}$  received by Jupiter and  $1 \text{ W m}^{-2}$  for Neptune. The resulting high temperatures lead to short radiative time constants of days or less at pressures  $< 1$  bar (Showman and Guillot 2002; Iro et al. 2005; Showman et al. 2008a, and Eq. (19)), in contrast to Jupiter where radiative time constants are years. Even in the presence of fast winds, these short radiative time constants allow the possibility of large fractional day-night temperature differences, particularly on the most heavily irradiated planets—in contrast to Jupiter where temperatures vary horizontally by only a few percent.

Third, over several Gyr of evolution, the intense irradiation received by hot Jupiters leads to the development of a nearly isothermal radiative zone extending to pressures of  $\sim 100$ –1000 bars (Guillot et al. 1996; Guillot 2005; Fortney et al. 2009). The observable weather in hot Jupiters thus occurs not within the convection zone but within the stably stratified radiative zone. Moreover, as described in §4.1, this separation between the photosphere and the radiative-convective boundary may allow large horizontal temperature differences to develop and support significant thermal-wind shear. For example, assuming that a lateral temperature contrast of  $\Delta T \sim 300$  K extending over several scale heights occurs over a lateral distance of  $10^8$  m, the resulting thermal-wind shear is  $\Delta u \sim 2 \text{ km sec}^{-1}$ . Thus, balance arguments suggest that the existence of significant horizontal temperature contrasts would naturally require fast wind speeds.

The modest rotation rates, large stable stratifications, and possible fast wind speeds suggest that the Rossby deformation radius and Rhines scale are large on hot Jupiters. On Jupiter, the deformation radius is  $\sim 2000$  km and the Rhines scale is  $\sim 10^4$  km (much smaller than the planetary radius of 71,400 km), which helps explain why Jupiter and Saturn have an abundant population of small vortices and numerous zonal jets (Figs. 5–6) (Williams 1978; Cho and Polvani 1996a; Vasavada and Showman 2005). In contrast, a hot Jupiter with a rotation period of 3 Earth days and wind speed of 2  $\text{km sec}^{-1}$  has a deformation radius and Rhines scale comparable to the planetary radius. Thus, dynamical structures such as vortices and jets should be more global in scale than occurs on Jupiter and Saturn (Menou et al. 2003; Showman and Guillot 2002; Cho et al. 2003). This scaling argument is supported by detailed nonlinear numerical simulations of the circulation, which generally show the development of only  $\sim 1$ –3 broad jets (Showman and Guillot 2002; Cho et al. 2003, 2008; Dobbs-Dixon and Lin 2008; Langton and Laughlin 2007, 2008a; Showman et al. 2008a, 2009).

A variety of 2D and 3D models have been used to inves-

<sup>23</sup>or pseudo-synchronously in the case of hot Jupiters on highly eccentric orbits

tigate the atmospheric circulation of hot Jupiters. Cho et al. (2003, 2008) performed global numerical simulations of hot Jupiters on circular orbits using the one-layer equivalent barotropic equations (a one-layer model that is mathematically similar to the shallow-water equations described in § 2.3). They initialized the simulations with small-scale balanced turbulence and forced them with a large-scale deflection of the surface to provide a crude representation of the pressure effects of the day-night heating gradient. However, no explicit heating/cooling was included. Together, these effects led to the production of several broad, meandering jets and drifting polar vortices (Fig. 8). The mean wind speed in the final state is to a large degree determined by the mean speed of the initial turbulence, which ranged from 100–800 m sec<sup>-1</sup> in their models. At the large (~planetary-scale) deformation radius relevant to hot Jupiters, the equatorial jet in the final state can flow either eastward or westward depending on the initial condition and other details. The simulations exhibit significant time variability that, if present on hot Jupiters, would lead to detectable orbit-to-orbit variability in light curves and secondary eclipse depths (Cho et al. 2003; Rauscher et al. 2007, 2008).

Langton and Laughlin (2007) performed global, 2D simulations of hot Jupiters on circular orbits using the shallow-water equations with a mass source on the dayside and mass sink on the nightside to parameterize the effects of dayside heating and nightside cooling. When the obliquity is assumed zero and the mass sources/sinks are sufficiently large, their forced flows quickly reach a steady state with wind speeds of  $\sim 1$  km sec<sup>-1</sup> and order-unity lateral variations in the thickness of the shallow-water layer. On the other hand, Langton and Laughlin (2008a) numerically solved the 2D fully compressible equations for the horizontal velocity and temperature of hot Jupiters on eccentric orbits and obtained very turbulent, time-varying flows. Apparently, in this case, the large-scale heating patterns produced hemisphere-scale vortices that were dynamically unstable, leading to the breakdown of these eddies into small-scale turbulence.

Several authors have also performed 3D numerical simulations of hot Jupiters. Showman and Guillot (2002), Cooper and Showman (2005, 2006), Showman et al. (2008a), and Menou and Rauscher (2009) performed global simulations with the 3D primitive equations where the dayside heating and nightside cooling was parameterized with a Newtonian heating/cooling scheme, which relaxes the temperatures toward a prescribed radiative-equilibrium temperature profile (hot on the dayside, cold on the nightside) over a prescribed radiative timescale. Dobbs-Dixon and Lin (2008) performed simulations with the fully compressible equations in a limited-area domain, consisting of the equatorial and mid-latitudes but with the poles cut off. Like the studies listed above, they also adopted a simplified method for forcing their flow, in this case using a radiative diffusion scheme. Showman et al. (2009) coupled their global 3D dynamical solver to a state-of-the-art, non-gray, cloud-free radiative transfer scheme with opacities calculated assum-

ing local chemical equilibrium (Figs. 9 and 10). The above models all generally obtain wind structures with  $\sim 1$ –3 broad jets with speeds of  $\sim 1$ –4 km sec<sup>-1</sup>.

Despite the diversity in modeling approaches, the studies described above agree in several key areas.

- First, most of the above studies generally produce peak wind speeds similar to within a factor of 2–3, in the range of one to several km sec<sup>-1</sup>.<sup>24</sup> This similarity is not a coincidence but results from the force balances that occur for a global-scale flow in the presence of large fractional temperature differences. Consider the longitudinal force balance at the equator, for example, and suppose the day-night heating gradient produces a day-night temperature difference  $\Delta T_{\text{horiz}}$  that extends vertically over a range of log-pressure  $\Delta \ln p$ . This temperature difference causes a day-night horizontal pressure-gradient acceleration which, to order-of-magnitude, can be written  $R\Delta T_{\text{horiz}}\Delta \ln p/a$ , where  $a$  is the planetary radius. At high latitudes, this could be balanced by the Coriolis force arising from a north-south flow, but the horizontal Coriolis force is zero at the equator. At the equator, such a force instead tends to cause acceleration of the flow in the east-west direction. Balancing the pressure-gradient acceleration by  $\mathbf{v} \cdot \nabla \mathbf{v}$ , which to order-of-magnitude is  $U^2/a$  for a global-scale flow, we have

$$U \sim \sqrt{R\Delta T_{\text{horiz}}\Delta \ln p} \quad (48)$$

This should be interpreted as the characteristic variation in zonal wind speed along the equator. For  $R = 3700 \text{ J kg}^{-1} \text{ K}^{-1}$ ,  $\Delta T_{\text{horiz}} \sim 400 \text{ K}$ , and  $\Delta \ln p \sim 3$  (appropriate to a temperature difference extending vertically over three scale heights), this yields  $U \sim 2 \text{ km sec}^{-1}$ .

Likewise, consider the latitudinal force balance in the mid-latitudes. To order-of-magnitude, the latitudinal pressure-gradient acceleration is again given by  $R\Delta T_{\text{horiz}}\Delta \ln p/a$ , where here  $\Delta T_{\text{horiz}}$  is the latitudinal temperature contrast (e.g., from equator to pole) that extends vertically over  $\Delta \ln p$ . If  $Ro \gg 1$ , this is balanced by the advective acceleration  $U^2/a$ , whereas if  $Ro \ll 1$ , it would instead be balanced by the Coriolis acceleration  $fU$ , where  $f$  is the Coriolis parameter (§3.3). The former case recovers Eq. (48), whereas the latter case yields

$$U \sim \frac{R\Delta T_{\text{horiz}}\Delta \ln p}{fa} \quad (49)$$

Here,  $U$  is properly interpreted as the characteristic difference in horizontal wind speed vertically across  $\Delta \ln p$ . Inserting  $R = 3700 \text{ J kg}^{-1} \text{ K}^{-1}$ ,  $\Delta T_{\text{horiz}} \sim$

<sup>24</sup>In intercomparing studies, one must be careful to distinguish mean versus peak speeds and, in the case of 3D models, the pressure level at which those speeds are quoted; such quantities can differ by a factor of several in a single model.

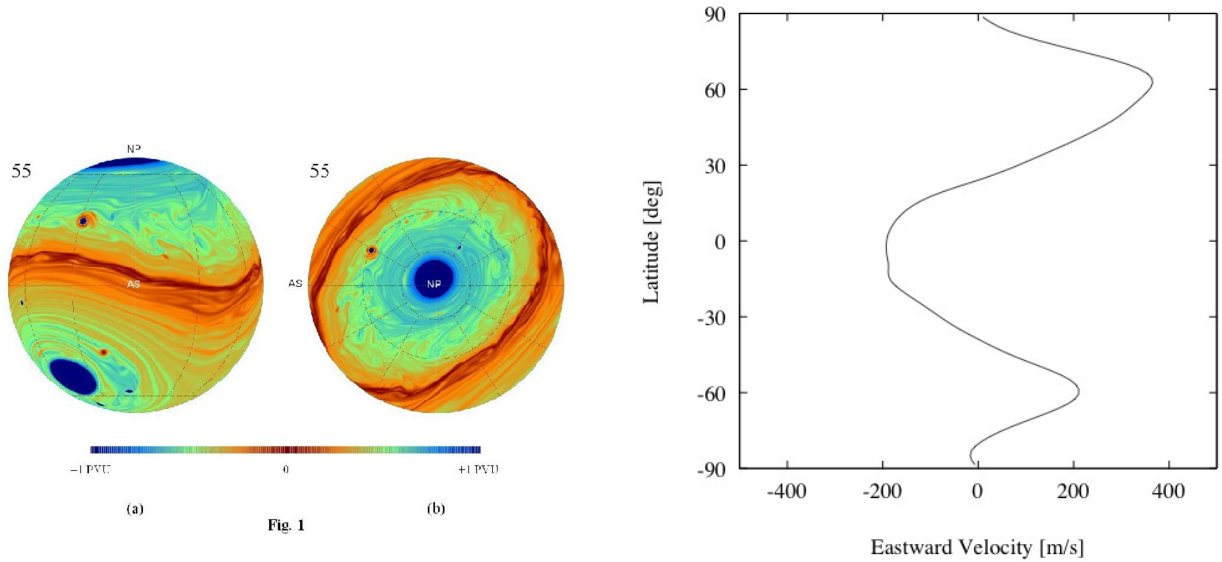


**Fig. 1**

Fig. 8.— One-layer, global equivalent barotropic simulation of the hot Jupiter HD 209458b from Cho et al. (2003). Globes show equatorial (left) and polar (right) views of the potential vorticity (see §2); note the development of large polar vortices and small-scale turbulent structure, which result from a combination of the turbulent initial condition and large-scale “topographic” forcing intended to qualitatively represent the day-night heating contrast. Plot shows zonal-mean zonal wind versus latitude, illustrating the 3-jet structure that develops.

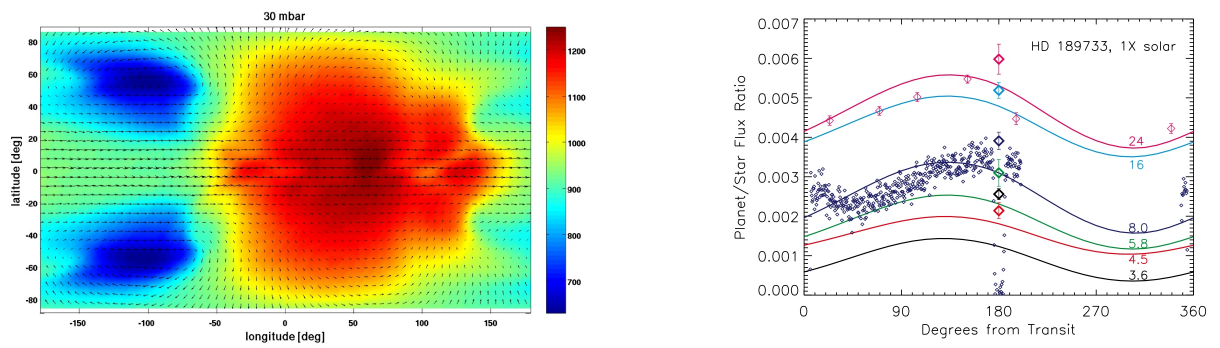


Fig. 9.— Results from a 3D simulation of the hot Jupiter HD 189733b from Showman et al. (2009). The dynamics are coupled to a realistic representation of cloud-free, non-gray radiative transfer assuming solar abundances. *Left:* Temperature (colorscale, in K) and winds (arrows) at the 30 mbar pressure, which is the approximate level of the mid-IR photosphere. A strong eastward equatorial jet develops that displaces the hottest regions eastward from the substellar point (which lies at  $0^\circ$  longitude,  $0^\circ$  latitude). *Right:* Light curves in *Spitzer* bandpasses calculated from the simulation (curves; labels show wavelength in  $\mu\text{m}$ ) in comparison to observations (points) from Knutson et al. (2007, 2009b), Charbonneau et al. (2008), and Deming et al. (2006).

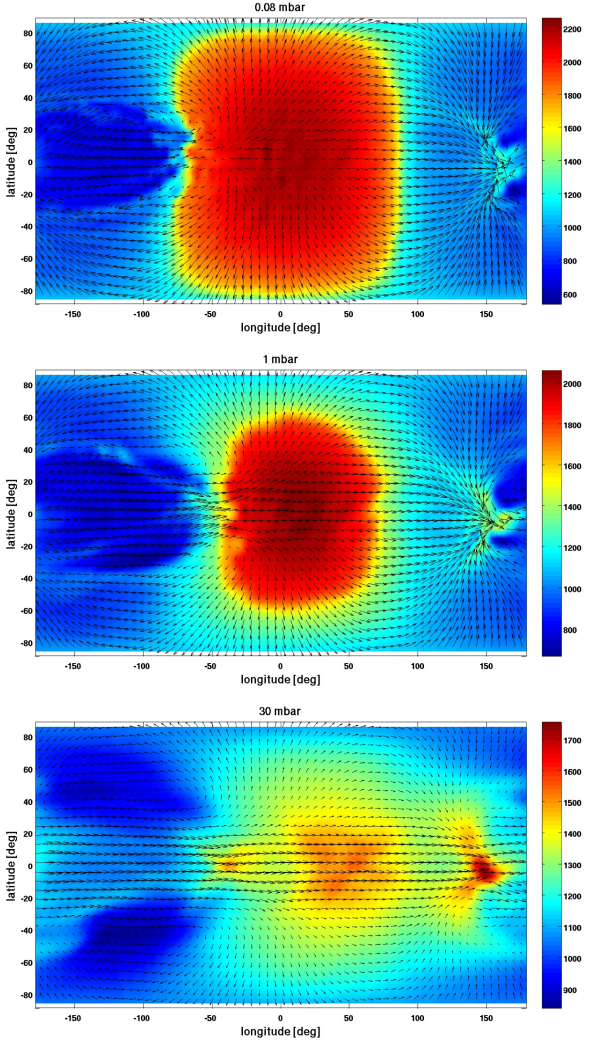


Fig. 10.— 3D simulation of HD 209458b, including realistic cloud-free, non-gray radiative transfer, illustrating development of a dayside stratosphere when opacity from visible-absorbing species (in this case TiO and VO) are included. Such stratospheres are relevant to explaining *Spitzer* data of HD 209458b, TrES-2, TrES-4, XO-1b, and other hot Jupiters. Here, the stratosphere (shown in red) begins at pressures of  $\sim 10$  mbar and widens with altitude until it covers most of the dayside at pressures of  $\sim 0.1$  mbar. Panels show temperature (colorscale, in K) and winds (arrows) at the 0.08, 1, and 30 mbar levels from top to bottom, respectively. Substellar longitude and latitude are  $(0^\circ, 0^\circ)$ . From Showman et al. (2009).

400 K,  $\Delta \ln p \sim 3$ ,  $f \sim 2 \times 10^{-5}$  (appropriate in mid-latitudes to a hot Jupiter with a 3-day period), and  $a \approx 10^8$  m, we again obtain  $U \sim 2 \text{ km sec}^{-1}$ .<sup>25</sup>

While not minimizing the real differences in the numerical results obtained in the various studies, the above estimates show that the existence of wind speeds of a few  $\text{km sec}^{-1}$  in the various numerical studies is a basic outcome of force balance in the presence of lateral temperature contrasts of hundreds of K.

- Second, the various numerical studies all produce a small number ( $\sim 1\text{--}4$ ) of broad jets. This was first pointed out by Showman and Guillot (2002), Menou et al. (2003), and Cho et al. (2003) and, as described previously, results from the fact that the Rossby deformation radius and Rhines scale are comparable to a planetary radius for conditions relevant to typical hot Jupiters. At least two specific mechanisms seem to be relevant. When the deformation radius is close to the planetary radius, the day-night forcing tends to inject energy at horizontal scales comparable to the planetary radius; the  $\beta$  effect then anisotropizes this energy into zonal jets whose widths are the order of a planetary radius. Alternately, if the energy injection occurs primarily at small horizontal scales, an inverse cascade can reorganize the energy into planetary-scale jets if the planetary rotation is sufficiently slow and friction sufficiently weak (allowing fast winds and a large Rhines scale). Follow-up studies are consistent with these general expectations (Cooper and Showman 2005; Cho et al. 2008; Langton and Laughlin 2007, 2008a; Dobbs-Dixon and Lin 2008; Showman et al. 2008a, 2009), but additional work to clarify the relative roles of  $L_D$  and  $L_\beta$  in setting the jet widths would be beneficial.

Despite these similarities, there remain some key differences in the numerical results obtained by the various groups so far. These include the following:

- As yet, little agreement exists on whether hot Jupiters should exhibit significant temporal variability on the global scale. The 2D simulations of Cho et al. (2003, 2008) and Langton and Laughlin (2008a) produce highly turbulent, time-variable flows, whereas the shallow-water study of Langton and Laughlin (2007) and most of the 3D studies (Showman and Guillot 2002; Cooper and Showman 2005; Dobbs-Dixon and Lin 2008; Showman et al. 2008a, 2009) exhibit relatively steady flow patterns with only modest time variability for zero-obliquity, zero-eccentricity hot

<sup>25</sup>The similarity of the numerical estimates from Eq. (48) and (49) results from the fact that we assumed the same horizontal temperature differences in longitude and latitude and that  $Ro \sim 1$  for the parameter regime explored here.

Jupiters. The Cho et al. simulations essentially guarantee a time-variable outcome because of the turbulent initial condition, although breaking Rossby waves and dynamical instabilities during the simulations also play a large role; the Langton and Laughlin (2008a) simulations were initialized from rest and naturally develop turbulence via dynamical instability throughout the course of the simulation.

Time variability can result from several mechanisms, including dynamical (e.g., barotropic or baroclinic) instabilities, large-scale oscillations, and modification of the jet pattern by atmospheric waves. If the jet pattern is dynamically stable (or, more rigorously, if relevant instability growth times are significantly longer than the characteristic atmospheric heating/cooling times), then this mechanism for producing variability would be inhibited; on the other hand, if the jet pattern is unstable (with instability growth rates comparable to or less than the heating/cooling times), the jets will naturally break up and produce a wide range of turbulent eddies. In this regard, it is crucial to carefully distinguish between 2D and 3D models, because they exhibit very different stability criteria (e.g., Dowling 1995). For example, in a 2D, nondivergent model, theoretical and numerical work shows that jets are guaranteed stable only if

$$\frac{\partial^2 u}{\partial y^2} < \beta \quad (50)$$

a relationship called the *barotropic stability criterion*. Numerical simulations show that 2D, nondivergent fluids initialized with jets violating Eq. (50) generally develop instabilities that rob energy from the jets until the jets no longer violate the equation. However, jets in a 3D fluid can in some cases strongly violate Eq. (50) while remaining stable; Jupiter and Saturn, for example, have several jets where  $\partial^2 u / \partial y^2$  exceed  $\beta$  by a factor of 2–3 (Ingersoll et al. 1981; Sanchez-Lavega et al. 2000), and yet the jet pattern has remained almost unchanged over multi-decade time scales. This may simply imply that the barotropic stability criterion is irrelevant for a 3D fluid (Dowling 1995; Vasavada and Showman 2005). Thus, it is *a priori* unsurprising that 2D and 3D models would make different predictions for time variability.

However, a recent study by Menou and Rauscher (2009) shows that the issue is not only one of 2D versus 3D. Making straightforward extensions to an Earth model, they performed forced 3D shallow simulations initialized from rest that developed highly turbulent, time variable flows on the global scale, showing that time variability from the emergence of horizontal shear instability may occur in 3D under some conditions relevant to hot Jupiters. Like several previous studies, they forced their flows with a Newtonian heating/cooling scheme that generates a day-

night temperature difference. However, their forcing set-up differs significantly from those of previous studies. They place an impermeable surface at 1 bar and apply their maximum day/night forcing immediately above the surface; the day-night radiative-equilibrium temperature difference decreases with altitude and reaches zero near the top of their model. This is the reverse of the set-up used in Cooper and Showman (2005, 2006) and Showman et al. (2008a, 2009) where the forcing amplitude peaks near the top of the domain and decreases with depth, and where the surface is placed significantly deeper than the region of atmospheric heating/cooling to minimize its interaction with the circulation in the observable atmosphere. The differences in the forcing schemes and position of the surface presumably determine whether or not a given 3D simulation develops global-scale instability and time variability. Further work will be necessary to identify the specific forcing conditions that lead to time-variable or quasi-steady conditions at the global scale.

It is also worth remembering that hot Jupiters themselves exhibit huge diversity; among the known transiting planets, for example, incident stellar flux varies by a factor of  $\sim 150$ , gravities range over a factor of  $\sim 70$ , and expected rotation rates vary over nearly a factor of 10 (e.g., Table 1). Given this diversity, it is reasonable to expect that some hot Jupiters will exhibit time-variable conditions while others will exhibit relatively steady flow patterns.

- Another area of difference between models regards the direction of the equatorial jet. The shallow-water and equivalent barotropic models can produce either eastward or westward equatorial jets, depending on the initial conditions and other modeling details (Cho et al. 2003, 2008; Langton and Laughlin 2007, 2008a). In contrast, all of the 3D models published to date for synchronously rotating hot Jupiters with zero obliquity and eccentricity have produced robust eastward equatorial jets (Showman and Guillot 2002; Cooper and Showman 2005, 2006; Showman et al. 2008a, 2009; Dobbs-Dixon and Lin 2008; Menou and Rauscher 2009). The mechanisms responsible for generating the eastward jets in these 3D models remain to be diagnosed in detail but presumably involve the global-scale eddies generated by the day-night heating contrast.

To date, most work on hot-Jupiter atmospheric circulation has emphasized planets on circular orbits. However, several transiting hot Jupiters and Neptunes have eccentric orbits, including GJ 436b, HAT-P-2b, HD 17156b, and HD 80606b, whose orbital eccentricities are 0.15, 0.5, 0.67, and 0.93, respectively. When the eccentricity is large, the incident stellar flux varies significantly throughout the orbit—HAT-P-2b, for example, receives  $\sim 9$  times more flux at pe-

riapse than at apoapse, while for HD 80606b, the maximum incident flux exceeds the minimum incident flux by a factor of over 800! These variations dwarf those experienced in our Solar System and constitute an uncharted regime of dynamical forcing for a planetary atmosphere. An 8- $\mu\text{m}$  light curve of HD 80606b has recently been obtained with the *Spitzer Space Telescope* during a 30-hour interval surrounding periape passage (Laughlin et al. 2009), which shows the increase in planetary flux that presumably accompanies the flash heating as the planet passes by its star. 2D and 3D numerical simulations suggest that these planets may exhibit dynamic, time-variable flows and show that the planet's emitted infrared flux can peak hours to days after periape passage (Langton and Laughlin 2008a,b; Lewis et al. 2009).

#### 4.4. Chemistry as a probe of the meteorology

Chemistry can provide important constraints on the meteorology of giant planets. On Jupiter, for example, gaseous CO, PH<sub>3</sub>, GeH<sub>4</sub>, and AsH<sub>3</sub> have been detected in the upper troposphere ( $p < 5$  bars) with mole fractions of  $\sim 0.8$ , 0.2, 0.6, and 0.5–1 ppb, respectively. None of these compounds are thermochemically stable in the upper troposphere—the chemical equilibrium mole fractions are  $< 10^{-14}$  for AsH<sub>3</sub> and  $< 10^{-20}$  for the other three species (Fegley and Lodders 1994). However, the equilibrium abundances of all four species rise with depth, exceeding 1 ppb at pressures greater than 500, 400, 160, and 20 bars for CO, PH<sub>3</sub>, GeH<sub>4</sub>, and AsH<sub>3</sub>, respectively. Thus, the high abundances of these species in the upper troposphere appear to result from rapid convective mixing from the deep atmosphere.<sup>26</sup> Kinetic reaction times are rapid at depth but plummet with decreasing temperature and pressure, allowing these species to persist in disequilibrium (i.e., “quench”) in the low-pressure and temperature conditions of the upper troposphere. Knowledge of the chemical kinetic rate constants allows quantitative estimates to be made of the vertical mixing rate needed to explain the observed abundances. For all four of the species listed above, the required vertical mixing rates yield order-of-magnitude matches with the mixing rate expected from thermal convection at Jupiter’s known heat flux (e.g. Prinn and Barshay 1977; Fegley and Lodders 1994; Bézard et al. 2002). Thus, the existence of these disequilibrium species provides evidence that the deep atmosphere is indeed convective.

Given the difficulty of characterizing the meteorology of exoplanets with spatially resolved observations, these types of chemical constraints will likely play an even more important role in our understanding of exoplanets than is the case for Jupiter. Several brown dwarfs, including Gl 229b, Gl 570d, and 2MASS J0415-0935, show evidence for disequilibrium abundances of CO and/or NH<sub>3</sub> (e.g., Noll et al. 1997; Saumon et al. 2000, 2006, 2007). These observations can also plausibly be explained by vertical mixing. For

<sup>26</sup>Jupiter also has a high stratospheric CO abundance that is inferred to result from exogenous sources (Bézard et al. 2002).

these objects,  $\text{NH}_3$  is quenched in the convection zone, but CO is quenched in the overlying radiative zone where vertical mixing must result from some combination of small-scale turbulence (due, for example, to the breaking of vertically propagating gravity waves) and vertical advection due to the large-scale circulation (§3.7). Current models suggest that such mixing corresponds to an eddy diffusivity in the radiative zone of  $\sim 1\text{--}10 \text{ m}^2 \text{ sec}^{-1}$  for Gl 229b and  $10\text{--}100 \text{ m}^2 \text{ sec}^{-1}$  for 2MASS J0415-0935 (Saumon et al. 2007). These inferences on vertical mixing rate provide constraints on the atmospheric circulation that would be difficult to obtain in any other way.

Several hot Jupiters likewise reside in temperature regimes where  $\text{CH}_4$  is the stable form in the observable atmosphere and CO is the stable form at depth, or where  $\text{CH}_4$  is the stable form on the nightside and CO is the stable form on the dayside. The abundance and spatial distribution of CO and  $\text{CH}_4$  on these objects could thus provide important clues about the wind speeds and other aspects of the meteorology.  $\text{CH}_4$  has been detected via transmission spectroscopy on HD 189733b (Swain et al. 2008) and CO has been indirectly inferred from the shape of the dayside emission spectrum (Barman 2008), although further observations and radiative-transfer models are needed to determine their abundances and spatial variability (if any). Cooper and Showman (2006) coupled a simple model for CO/ $\text{CH}_4$  interconversion kinetics to their 3D dynamical model of hot Jupiters to demonstrate that CO and  $\text{CH}_4$  should be quenched in the observable atmosphere, where thermochemical  $\text{CO} \leftrightarrow \text{CH}_4$  interconversion times are orders of magnitude longer than plausible dynamical times. If so, one would expect CO and  $\text{CH}_4$  to have similar abundances on the dayside and nightside of hot Jupiters, in contrast to the chemical-equilibrium situation where  $\text{CH}_4$  would be much more prevalent on the nightside (note, however, that their models neglect photochemistry, which could further modify the abundances of both species). For temperatures relevant to objects like HD 209458b and HD 189733b, Cooper and Showman (2006) found that the quenching occurs at pressures of  $\sim 1\text{--}10$  bars, and that the quenched abundance depends primarily on the temperatures and vertical velocities in this pressure range.

Thus, future observational determination of CO and  $\text{CH}_4$  abundances and comparison with detailed 3D models may allow constraints on the temperatures and vertical velocities in the deep ( $1\text{--}10$  bar) atmospheres of hot Jupiters to be obtained. Such constraints probe significantly deeper than the expected visible and infrared photospheres of hot Jupiters and hence would nicely complement the characterization of hot-Jupiter thermal structure via light curves and secondary-eclipse spectra. Note also that an analogous story involving  $\text{N}_2$  and  $\text{NH}_3$  interconversion may occur on even cooler objects ( $T_{\text{eff}} \sim 700 \text{ K}$  “warm” Jupiters).

## 5. CIRCULATION REGIMES: TERRESTRIAL PLANETS

With current groundbased searches and spacecraft such as NASA’s *Kepler* mission, terrestrial planets are likely to be discovered around main-sequence stars within the next five years, and basic characterization of their atmospheric composition and temperature structure should follow over the subsequent decade. At base, we wish to understand not only whether such planets exist but whether they have atmospheres, what their atmospheric composition, structure and climate may be, and whether they can support life. Addressing these issues will require a consideration of relevant physical and chemical climate feedbacks as well as the plausible circulation regimes in these planets’ atmospheres.

The study of terrestrial exoplanet atmospheres is just beginning, and only a handful of papers have specifically investigated the possible circulation regimes on these objects. However, a vast literature has developed to understand the climate and circulation of Venus, Titan, Mars, and especially Earth, and many of the insights developed for understanding these planets may be generalizable to exoplanets. Our goal here is to provide conceptual and theoretical guidance on the types of climate and circulation processes that exist in terrestrial planet atmospheres and discuss how those processes vary under diverse planetary conditions. In §5.1 we survey basic issues in climate. The following sections, §5.2–§5.5, address basic circulation regimes on terrestrial planets, emphasizing those aspects (e.g., processes that determine the horizontal temperature contrasts) relevant to future exoplanet observations. §5.6 discusses regimes of exotic forcing associated with synchronous rotation, large obliquities, and large orbital eccentricities.

### 5.1. Climate

Climate can be defined as the mean condition of a planet’s atmosphere/ocean system—the temperatures, pressures, winds, humidities, and cloud properties—averaged over time intervals longer than the timescale of typical weather events. The climate on the terrestrial planets results from a wealth of interacting physical, chemical, geological, and (when relevant) biological effects, and even on Earth, understanding the past and present climate has required a multi-decade interdisciplinary research effort. In this section, we provide only a brief sampling of the subject, touching only on the most basic physical processes that help to determine a planet’s global-mean conditions.

The mean temperatures at which a planet radiates to space depend primarily on the incident stellar flux and the planetary albedo. Equating emitted infrared energy (assumed blackbody) with absorbed stellar flux yields a planet’s global-mean effective temperature at radiative equilibrium:

$$T_{\text{eff}} = \left[ \frac{F_*(1 - A_B)}{4\sigma} \right]^{1/4} \quad (51)$$

where  $F_*$  is the incident stellar flux,  $A_B$  is the planet’s

global-mean bond albedo<sup>27</sup>, and  $\sigma$  is the Stefan-Boltzmann constant. The factor of 4 results from the fact that the planet intercepts a stellar beam of area  $\pi a^2$  but radiates infrared from its full surface area of  $4\pi a^2$ .

Given an incident stellar flux, a variety of atmospheric processes act to determine the planet's surface temperature. First, the circulation and various atmospheric feedbacks can play a key role in determining the planetary albedo. Bare rock is fairly dark, and for terrestrial planets the albedo is largely determined by the distribution of clouds and surface ice. The Moon, for example, has bond albedo of 0.11, yielding an effective temperature of 274 K. In contrast, Venus has a bond albedo of 0.75 because of its global cloud cover, yielding an effective temperature of 232 K. With partial cloud and ice cover, Earth is an intermediate case, with a bond albedo of 0.31 and an effective temperature of 255 K. These examples illustrate that the circulation, via its effect on clouds and surface ice, can have a major influence on mean conditions—Venus' effective temperature is less than that of the Earth and Moon despite receiving nearly double the Solar flux!

Second,  $T_{\text{eff}}$  is not the surface temperature but the mean blackbody temperature at which the planet radiates to space. The surface temperatures can significantly exceed  $T_{\text{eff}}$  through the *greenhouse effect*. Planets orbiting Sun-like stars receive most of their energy in the visible, but they tend to radiate their energy to space in the infrared. Most gases tend to be relatively transparent in the visible, but  $\text{H}_2\text{O}$ ,  $\text{CO}_2$ ,  $\text{CH}_4$ , and other molecules absorb significantly in the infrared. On a planet like Earth or Venus, a substantial fraction of the sunlight therefore reaches the planetary surface, but infrared emission from the surface is mostly absorbed in the atmosphere and cannot radiate directly to space. In turn, the atmosphere radiates both up (to space) and down (to the surface). The surface therefore receives a double whammy of radiation from both the Sun and the atmosphere; to achieve energy balance, the surface temperature becomes elevated relative to the effective temperature. This is the greenhouse effect. Contrary to popular descriptions, the greenhouse effect should *not* be thought of as a situation where the heat is “trapped” or “cannot escape.” Indeed, the planet as a whole resides in a near-balance where infrared emission to space (mostly from the atmosphere when the greenhouse effect is strong) almost equals absorbed sunlight.

To have a significant greenhouse effect, a planet must have a massive-enough atmosphere to experience pressure broadening of the spectral lines. Mars, for example, has  $\sim 15$  times more  $\text{CO}_2$  per area than Earth, yet its greenhouse effect is significantly weaker because its surface pressure is only 6 mbar.

The climate is influenced by numerous feedbacks that can affect the mean state and how the atmosphere responds to perturbations. Some of the more important feedbacks

are as follows:

- *Thermal feedback:* Increases or decreases in the temperature at the infrared photosphere lead to enhanced or reduced radiation to space, respectively. This is a negative feedback that allows planets to reach a stable equilibrium with absorbed starlight.
- *Ice-albedo feedback:* Surface ice can form on planets exhibiting trace gases that can condense to solid form. Because of the brightness of ice and snow, an increase in snow/ice coverage decreases the absorbed starlight, promoting colder conditions and growth of even more ice. Conversely, melting of surface ice increases the absorbed starlight, promoting warmer conditions and continued melting. This is a positive feedback.

Simple models of the ice-albedo feedback show that, over a range of  $F_*$  values (depending on the strength of the greenhouse effect), an Earth-like planet can exhibit two stable equilibrium states for a given value of  $F_*$ : a warm, ice-poor state with a low albedo and a cold, ice-covered state with a high albedo (e.g., North et al. 1981). Geologic evidence suggests that  $\sim 0.6\text{--}2.4$  Gyr ago Earth experienced several multi-Myr-long glaciations with global or near-global ice cover (dubbed “snowball Earth” events; Hoffman and Schrag 2002), suggesting that Earth has flipped back and forth between these equilibria. The susceptibility of a planet to entering such a snowball state is highly sensitive to the strength of latitudinal heat transport (Spiegel et al. 2008), thereby linking this feedback to the global circulation.

- *Condensable-greenhouse-gas feedback:* When an atmospheric constituent is a greenhouse gas that also exists in condensed form on the surface, the atmosphere can experience a positive feedback that affects the temperature and the distribution of this constituent between the atmosphere and surface. An increase in surface temperature increases the constituent's saturation vapor pressure, hence the atmospheric abundance and therefore the greenhouse effect. A decrease in surface temperature decreases the saturation vapor pressure, reducing the atmospheric abundance and therefore the greenhouse effect. Thermal perturbations are therefore amplified. For Earth, this process occurs with water vapor (Earth's most important greenhouse gas) and is called the “water-vapor feedback” in the Earth climate literature (Held and Soden 2000). The water-vapor feedback will play a major role in determining how Earth responds to anthropogenic increases in carbon dioxide over the next century.

In some circumstances, this positive feedback is so strong that it can trigger a runaway that shifts the atmosphere into a drastically different state. In

<sup>27</sup>The bond albedo is the fraction of light incident upon a planet that is scattered back to space, integrated over all wavelengths and directions.

the case of warming, this would constitute a *runaway greenhouse* that leads to the complete evaporation/sublimation of the condensable constituent from the surface. If early Venus had oceans, for example, they might have experienced runaway evaporation, leading to a monstrous early water vapor atmosphere (Ingersoll 1969; Kasting 1988) that would have had major effects on subsequent planetary evolution.

In the case of cooling, such a runaway would remove most of the condensable constituent from the atmosphere, and if the relevant gas dominates the atmosphere, this could lead to *atmospheric collapse*. For example, if a Venus-like planet (with its  $\sim 500$ -K greenhouse effect) were moved sufficiently far from the Sun, CO<sub>2</sub> condensation would initiate, potentially collapsing the atmosphere to a Mars-like state with most of the CO<sub>2</sub> condensed on the ground, a cold, thin CO<sub>2</sub> atmosphere in vapor-pressure equilibrium with the surface ice, and minimal greenhouse effect. The CO<sub>2</sub> cloud formation that precedes such a collapse is often used to define the outer edge of the classical habitable zone for terrestrial planets whose greenhouse effect comes primarily from CO<sub>2</sub> (Kasting et al. 1993).

Because CO<sub>2</sub> condensation naturally initiates in the coldest regions (the poles for a rapidly rotating planet; the nightside for a synchronous rotator), the conditions under which atmospheric collapse initiates depend on the atmospheric circulation. Weak equator-to-pole (or day-night) heat transport leads to colder polar (or nightside) temperatures for a given solar flux, promoting atmospheric collapse. These dynamical effects have yet to be fully included in climate models.

- *Clouds:* Cloud coverage increases the albedo, lessening the absorption of starlight and promoting cooler conditions. On the other hand, because the tropospheric temperatures generally decrease with altitude, cloud tops are typically cooler than the ground and therefore radiate less infrared energy to space, promoting warmer conditions (an effect that depends sensitively on cloud altitude and latitude). These effects compete with each other. By determining the detailed properties of clouds (e.g., fractional coverage, latitudes, altitudes, and size-particle distributions), the atmospheric circulation therefore plays a major role in determining the mean surface temperature.

To the extent that cloud properties depend on atmospheric temperature, clouds can act as a feedback that affects the mean state and amplifies or reduces a thermal perturbation to the climate system. However, because the sensitivity of cloud properties to the global circulation and mean climate is extremely difficult to predict, the net sign of this feedback (positive or neg-

ative) remains unknown even for Earth. For exoplanets, clouds could plausibly act as a positive feedback in some cases and negative feedback in others.

- *Long-term atmosphere/geology feedbacks:* On geological timescales, terrestrial planets can experience significant exchange of material between the interior and atmosphere. An example that may be particularly relevant for Earth-like (i.e. ocean and continent-bearing) exoplanets is the carbonate-silicate cycle, which can potentially buffer atmospheric CO<sub>2</sub> in a temperature-dependent way that tends to stabilize the atmospheric temperature against variations in solar flux (see, e.g. Kasting and Catling 2003). Such feedbacks, while beyond the scope of this chapter, may be critical in determining the mean composition and temperature of terrestrial exoplanets.

In addition to the major feedbacks outlined above, there exist dozens of additional interacting physical, chemical, and biological feedbacks that can influence the mean climate and its sensitivity to perturbations. Hartmann and coauthors (2003) provide a thorough assessment for the Earth's current climate; although the details will be different for other planets, this gives a flavor for the complexity that can be expected.

## 5.2. Global circulation regimes

For atmospheres with radiative time constants greatly exceeding the planet's solar day, the atmosphere cannot respond rapidly to day-night variations in stellar heating and instead responds primarily to the daily-mean insolation, which is a function of latitude. This situation applies to most planets in the Solar System, including the (lower) atmospheres of Venus, Earth, Titan, Jupiter, Saturn, Uranus, and Neptune.<sup>28</sup> The resulting patterns of temperature and winds vary little with longitude in comparison to their variation in latitude and height. In such an atmosphere, the primary task of the atmospheric circulation is to transport thermal energy not from day to night but between the equator and the poles.<sup>29</sup> On the other hand, when the atmosphere's radiative time constant is much shorter than the solar day, the day-night heating gradient will be paramount and day-night temperature variations at the equator could potentially rival temperature variations between the equator and poles.

In the next several subsections we survey our understanding of global atmospheric circulations for these two regimes. Because the first situation applies to most Solar-System atmospheres, it has received the vast majority of work and remains better understood. This regime, which

---

<sup>28</sup>Mars is a transitional case, with a radiative time constant  $\sim 2\text{--}3$  times its 24.6-hour day.

<sup>29</sup>At low obliquity ( $< 54^\circ$ ), yearly averaged starlight is absorbed primarily at low latitudes, so the circulation transports thermal energy poleward, but at high obliquity ( $> 54^\circ$ ), yearly averaged starlight is absorbed primarily at the poles (Ward 1974), and the yearly averaged energy transport by the circulation is equatorward. At high obliquity, strong seasonal cycles will also occur.

we discuss in §§5.3–5.5, will apply to planets whose orbits are sufficiently far from their stars that the planets have not despun into a synchronously rotating state; it can also apply to atmosphere-bearing moons of hot Jupiters even at small distances from their stars. The latter regime, surveyed in §5.6, prevails for planets exhibiting small enough orbital eccentricities and semi-major axes to become synchronously locked to their stars. This situation probably applies to most currently known transiting giant exoplanets and may also apply to terrestrial planets in the habitable zones of M dwarfs, which are the subject of current observational searches. Despite its current relevance, this novel forcing regime has come under investigation only in the past decade and remains incompletely understood due to a lack of Solar-System analogs.

### 5.3. Axisymmetric flows: Hadley cells

Perhaps the simplest possible idealization of a circulation that transports heat from equator to poles is an axisymmetric circulation—that is, a circulation that is independent of longitude—where hot air rises at the equator, moves poleward aloft, cools, sinks at high latitudes, and returns equatorward at depth (near the surface on a terrestrial planet). Such a circulation is termed a *Hadley cell*, and was first envisioned by Hadley in 1735 to explain Earth’s trade winds. Most planetary atmospheres in our Solar System, including those of Venus, Earth, Mars, Titan, and possibly the giant planets, exhibit Hadley circulations.

Hadley circulations on real planets are of course not truly axisymmetric; on the terrestrial planets, longitudinal variations in topography and thermal properties (e.g., associated with continent-ocean contrasts) induce asymmetry in longitude. Nevertheless, the fundamental idea is that the longitudinal variations are not *crucial* for driving the circulation. This differs from the circulation in midlatitudes, whose longitudinally averaged properties are fundamentally controlled by the existence of non-axisymmetric baroclinic eddies that are inherently three-dimensional (see §3.7).

Planetary rotation generally prevents Hadley circulations from extending all the way to the poles. Because of planetary rotation, equatorial air contains considerable angular momentum about the planetary rotation axis; to conserve angular momentum, equatorial air would accelerate to unrealistically high speeds as it approached the pole, a phenomenon which is dynamically inhibited. To illustrate, the specific angular momentum about the rotation axis on a spherical planet is  $M = (\Omega a \cos \phi + u)a \cos \phi$ , where the first and second terms represent angular momentum due to planetary rotation and winds, respectively (recall that  $\Omega$ ,  $a$ , and  $\phi$  are planetary rotation rate, planetary radius, and latitude). If  $u = 0$  at the equator, then  $M = \Omega a^2$ , and an angular-momentum conserving circulation would then exhibit winds of

$$u = \Omega a \frac{\sin^2 \phi}{\cos \phi} \quad (52)$$

Given Earth’s radius and rotation rate, this equation im-

plies zonal-wind speeds of  $134 \text{ m sec}^{-1}$  at  $30^\circ$  latitude,  $700 \text{ m sec}^{-1}$  at  $60^\circ$  latitude, and  $2.7 \text{ km sec}^{-1}$  at  $80^\circ$  latitude. Such high-latitude wind speeds are unrealistically high and would furthermore be violently unstable to 3D instabilities. On Earth, the actual Hadley circulations extend to  $\sim 30^\circ$  latitude.

The Hadley circulation exerts strong control over the wind structure, latitudinal temperature contrast, and climate. Hadley circulations transport thermal energy by the most efficient means possible, namely straightforward advection of air from one latitude to another. As a result, the latitudinal temperature contrast across a Hadley circulation tends to be modest; the equator-to-pole temperature contrast on a planet will therefore depend strongly on the width of the Hadley cell. Moreover, on planets with condensable gases, Hadley cells exert control over the patterns of cloudiness and rainfall. On Earth, the rising branch of the Hadley circulation leads to cloud formation and abundant rainfall near the equator, helping to explain for example the prevalence of tropical rainforests in Southeast Asia/Indonesia, Brazil, and central Africa.<sup>30</sup> On the other hand, because condensation and rainout dehydrates the rising air, the descending branch of the Hadley cell is relatively dry, which explains the abundances of arid climates on Earth at  $20$ – $30^\circ$  latitude, including the deserts of the African Sahara, South Africa, Australia, central Asia, and the southwestern United States. The Hadley cell can also influence the mean cloudiness, hence albedo and thereby the mean surface temperature. Venus’s slow rotation rate leads to a global equator-to-pole Hadley cell, with a broad ascending branch in low latitudes. Coupled with the presence of trace condensable gases, this widespread ascent contributes to a near-global cloud layer that helps generate Venus’ high bond albedo of 0.75. Different Hadley cell patterns would presumably cause different cloudiness patterns, different albedos, and therefore different global-mean surface temperatures. On exoplanets, Hadley circulations will also likewise help control latitudinal heat fluxes, equator-to-pole temperature contrasts, and climate.

A variety of studies have been carried out using fully nonlinear, global 3D numerical circulation models to determine the sensitivity of the Hadley cell to the planetary rotation rate and other parameters (e.g. Hunt 1979; Williams and Holloway 1982; Williams 1988a,b; Del Genio and Suozzo 1987; Navarra and Boccaletti 2002; Walker and Schneider 2005, 2006). These studies show that as the rotation rate is decreased the width of the Hadley cell increases, the equator-to-pole heat flux increases, and the equator-to-pole temperature contrast decreases. Figs. 11–12 illustrates examples from Navarra and Boccaletti (2002) and Del Genio and Suozzo (1987). For Earth parameters, the circulation exhibits mid-latitude eastward jet streams that peak in the upper troposphere ( $\sim 200$  mbar pressure), with weaker wind at the equator (Fig. 11). The Hadley cells extend from the equator to the equatorward flanks of the mid-latitude

---

<sup>30</sup>Regional circulations, such as monsoons, also contribute.

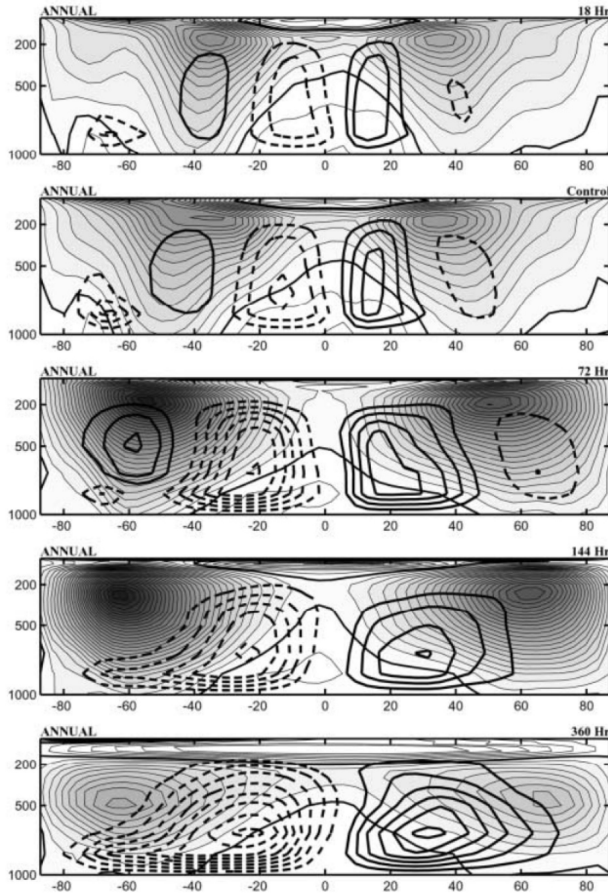


Fig. 11.— **Left:** Zonal-mean circulation versus latitude in degrees (abscissa) and pressure in mbar (ordinate) in a series of Earth-based GCM experiments from Navarra and Boccaletti (2002) where the rotation period is varied from 18 hours (top) to 360 hours (bottom). Greyscale and thin grey contours depict zonal-mean zonal wind,  $\bar{u}$ , and thick black contours denote streamfunction of the circulation in the latitude-height plane (the so-called “meridional circulation”), with solid being clockwise and dashed being counterclockwise. The meridional circulation flows parallel to the streamfunction contours, with greater mass flux when contours are more closely spaced. The two cells closest to the equator correspond to the Hadley cell. As rotation period increases, the jets move poleward and the Hadley cell widens, becoming nearly global at the longest rotation periods.

jets. As the rotation rate decreases, the Hadley cells widen and the jets shift poleward. At first, the jet speeds increase with decreasing rotation rate, which results from the fact that as the Hadley cells extend poleward (i.e., closer to the rotation axis) the air can spin-up faster (cf Eq. 52). Eventually, once the Hadley cells extend almost to the pole (at rotation periods exceeding  $\sim 5\text{--}10$  days for Earth radius, gravity, and vertical thermal structure), further decreases in rotation rate reduce the mid-latitude jet speed.

Perhaps more interestingly for exoplanet observations, these changes in the Hadley cell significantly influence the planetary temperature structure. This is illustrated in Fig. 12 from a series of simulations by Del Genio and Suozzo (1987). Because the Hadley cells transport heat extremely efficiently, the temperature remains fairly constant across the width of the Hadley cells. Poleward of the Hadley cells, however, the heat is transported in latitude by baroclinic instabilities (§§3.7 and 5.4), which are less efficient, so a large latitudinal temperature gradient exists within this so-called “baroclinic zone.” The equator-to-pole temperature contrast depends strongly on the width of the Hadley cell.

Despite the value of the 3D circulation models described above, the complexity of these models tends to obscure the physical mechanisms governing the Hadley circulation’s strength and latitudinal extent and cannot easily be extrapolated to different planetary parameters. A conceptual theory for the Hadley cell, due to Held and Hou (1980), provides considerable insight into Hadley cell dynamics and allows estimates of how, for example, the width of the Hadley cell should scale with planetary size and rotation rate [see reviews in James (1994, pp. 80–92), Vallis (2006, pp. 457–466), and Schneider (2006)]. Stripped to its basics, the scheme envisions an axisymmetric two-layer model, where the lower layer represents the equatorward flow near the surface and the upper layer represents the poleward flow in the upper troposphere. For simplicity, Held and Hou (1980) adopted a basic-state density that is constant with altitude. Absorption of sunlight and loss of heat to space generate a latitudinal temperature contrast that drives the circulation; for concreteness, let us parameterize the radiation as a relaxation toward a radiative-equilibrium potential temperature profile that varies with latitude as  $\theta_{\text{rad}} = \theta_0 - \Delta\theta_{\text{rad}} \sin^2 \phi$ , where  $\theta_0$  is the radiative-equilibrium potential temperature at the equator and  $\Delta\theta_{\text{rad}}$  is the equator-to-pole difference in radiative-equilibrium potential temperature. If we make the small-angle approximation for simplicity (valid for a Hadley cell that is confined to low latitudes), we can express this as  $\theta_{\text{rad}} = \theta_0 - \Delta\theta_{\text{rad}} \phi^2$ .

In the lower layer, we assume that friction against the ground keeps the wind speeds low; in the upper layer, assumed to occur at an altitude  $H$ , the flow conserves angular momentum. The upper layer flow is then specified by Eq. (52), which is just  $u = \Omega a \phi^2$  in the small-angle limit. We expect that the upper-layer wind will be in thermal-wind

balance with the latitudinal temperature contrast<sup>31</sup>:

$$f \frac{\partial u}{\partial z} = f \frac{u}{H} = -\frac{g}{\theta_0} \frac{\partial \theta}{\partial y} \quad (53)$$

where  $\partial u / \partial z$  is simply given by  $u/H$  in this two-layer model. Inserting  $u = \Omega a \phi^2$  into Eq. (53), approximating the Coriolis parameter as  $f = \beta y$  (where  $\beta$  is treated as constant), and integrating, we obtain a temperature that varies with latitude as

$$\theta = \theta_{\text{equator}} - \frac{\Omega^2 \theta_0}{2ga^2 H} y^4 \quad (54)$$

where  $\theta_{\text{equator}}$  is a constant to be determined.

At this point, we introduce two constraints. First, Held and Hou (1980) assumed the circulation is energetically closed, i.e. that no net exchange of mass or thermal energy occurs between the Hadley cell and higher latitude circulations. Given an energy equation with radiation parameterized using Newtonian cooling,  $d\theta/dt = (\theta_{\text{rad}} - \theta)/\tau_{\text{rad}}$ , where  $\tau_{\text{rad}}$  is a radiative time constant, the assumption that the circulation is steady and closed requires that

$$\int_0^{\phi_H} \theta dy = \int_0^{\phi_H} \theta_{\text{rad}} dy \quad (55)$$

where we are integrating from the equator to the poleward edge of the Hadley cell, at latitude  $\phi_H$ . Second, temperature must be continuous with latitude at the poleward edge of the Hadley cell. In the axisymmetric model, baroclinic instabilities are suppressed, and the regions poleward of the Hadley cells reside in a state of radiative equilibrium. Thus,  $\theta$  must equal  $\theta_{\text{rad}}$  at the poleward edge of the cell. Inserting our expressions for  $\theta$  and  $\theta_{\text{rad}}$  into these two constraints yields a system of two equations for  $\phi_H$  and  $\theta_{\text{equator}}$ . The solution yields a Hadley cell with a latitudinal half-width of

$$\phi_H = \left( \frac{5\Delta\theta_{\text{rad}} g H}{3\Omega^2 a^2 \theta_0} \right)^{1/2} \quad (56)$$

in radians. This solution suggests that the width of the Hadley cell scales as the square root of the fractional equator-to-pole radiative-equilibrium temperature difference, the square root of the gravity, the square root of the height of the cell, and inversely with the rotation rate. Inserting Earth annual-mean values ( $\Delta\theta_{\text{rad}} \approx 70$  K,  $\theta = 260$  K,  $g = 9.8 \text{ m sec}^{-2}$ ,  $H = 15$  km,  $a = 6400$  km, and  $\Omega = 7.2 \times 10^{-5} \text{ sec}^{-1}$ ) yields  $\sim 30^\circ$ .

Redoing this analysis without the small-angle approximation leads to a transcendental equation for  $\phi_H$  (see Eq. (17) in Held and Hou 1980), which can be solved numerically. Figure 13 (*solid curve*) illustrates the solution. As expected,  $\phi_H$  ranges from  $0^\circ$  as  $\Omega \rightarrow \infty$  to  $90^\circ$  as  $\Omega \rightarrow 0$ , and, for planets of Earth radius with Hadley circulations  $\sim 10$  km tall, bridges these extremes between rotation periods of  $\sim 0.5$  and 20 days. Although deviations

<sup>31</sup>This form differs slightly from Eq. (22) because Eq. (53) adopts a constant basic-state density (the so-called “Boussinesq” approximation) whereas Eq. (22) adopts the compressible ideal-gas equation of state.

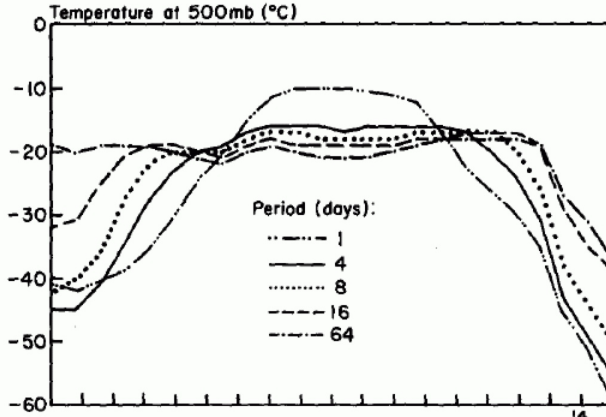


Fig. 12.— Zonally averaged temperature in  $^{\circ}\text{C}$  versus latitude at 500 mbar (in the mid-troposphere) for a sequence of Earth-like GCM runs that vary the planetary rotation period between 1 and 64 Earth days (labelled in the graph). Latitude runs from  $90^{\circ}$  on the left to  $-90^{\circ}$  on the right, with the equator at the center of the horizontal axis. The flat region near the equator in each run results from the Hadley cell, which transports thermal energy extremely efficiently and leads to a nearly isothermal equatorial temperature structure. The region of steep temperature gradients at high latitudes is the baroclinic zone, where the temperature structure and latitudinal heat transport are controlled by eddies resulting from baroclinic instability. Note that the width of the Hadley cell increases, and the equator-to-pole temperature difference decreases, as the planetary rotation period is increased. From Del Genio and Suozzo (1987).

exist, the agreement between the simple Held-Hou model and the 3D GCM simulations are surprisingly good given the simplicity of the Held-Hou model.

Importantly, the Held-Hou model demonstrates that latitudinal confinement of the Hadley cell occurs even in an axisymmetric atmosphere. Thus, the cell's latitudinal confinement does not require (for example) three-dimensional baroclinic or barotropic instabilities associated with the jet at the poleward branch of the cell. Instead, the confinement results from energetics: the twin constraints of angular-momentum conservation in the upper branch and thermal-wind balance specify the latitudinal temperature profile in the Hadley circulation (Eq. 54). This generates equatorial temperatures colder than (and subtropical temperatures warmer than) the radiative equilibrium, implying radiative heating at the equator and cooling in the subtropics. This properly allows the circulation to transport thermal energy poleward. If the cell extended globally on a rapidly rotating planet, however, the circulation would additionally produce high-latitude temperatures *colder* than the radiative equilibrium temperature, which in steady state would require radiative *heating* at high latitudes. This is thermodynamically impossible given the specified latitudinal dependence of  $\theta_{\text{rad}}$ . The highest latitude to which the cell can extend without encountering this problem is simply given by Eq. (55).

The model can be generalized to consider a more realistic treatment of radiation than the simplified Newtonian cooling/heating scheme employed by Held and Hou (1980). Caballero et al. (2008) reworked the scheme using a two-stream, non-grey representation of the radiative transfer with parameters appropriate for Earth and Mars. This leads to a prediction for the width of the Hadley cell that differs from Eq. (56) by a numerical constant of order unity.

Although the prediction of Held-Hou-type models for  $\phi_H$  provides important insight, several failures of these models exist. First, the model underpredicts the strength of the Earth's Hadley cell (e.g., as characterized by the magnitude of the north-south wind) by about an order of magnitude. This seems to result from the lack of turbulent eddies in axisymmetric models; several studies have shown that turbulent three-dimensional eddies exert stresses that act to strengthen the Hadley cells beyond the predictions of axisymmetric models (e.g. Kim and Lee 2001; Walker and Schneider 2005, 2006; Schneider 2006).<sup>32</sup> Second, the Hadley cells on Earth and probably Mars are not energetically closed; rather, mid-latitude baroclinic eddies transport thermal energy out of the Hadley cell into the polar regions. Third, the poleward-moving upper tropospheric branches of the Hadley cells do not conserve angular momentum—although the zonal wind does become eastward as one moves poleward across the cell, for Earth this increase is a factor of  $\sim 2\text{--}3$  less than predicted by Eq. (52). Overcoming these failings requires the inclusion of three-dimensional eddies.

Several studies have shown that turbulent eddies in the mid- to high-latitudes—which are neglected in the Held-Hou and other axisymmetric models—can affect the width of the Hadley circulation and alter the parameter dependences suggested by Eq. (56) (e.g., Del Genio and Suozzo 1987; Walker and Schneider 2005, 2006). Turbulence can produce an acceleration/deceleration of the zonal-mean

<sup>32</sup>Held and Hou (1980)'s original model neglected the seasonal cycle, and it has been suggested that generalization of the Held-Hou axisymmetric model to include seasonal effects could alleviate this failing (Lindzen and Hou 1988). Although this improves the agreement with Earth's observed *annual-mean* Hadley-cell strength, it predicts large solstice/equinox oscillations in Hadley-cell strength that are lacking in the observed Hadley circulation (Dima and Wallace 2003).

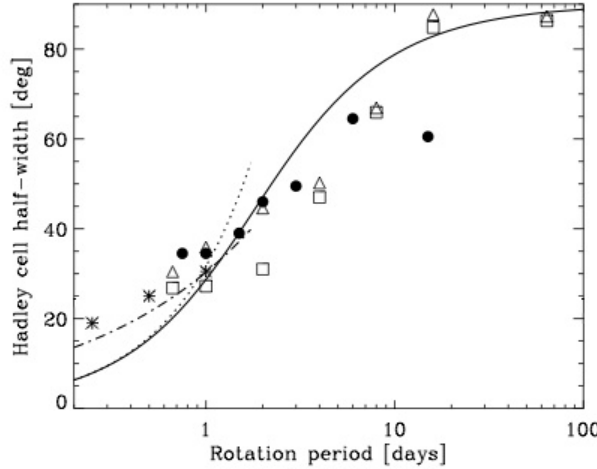


Fig. 13.— Latitudinal width of the Hadley cell from a sequence of Earth-like GCM runs that vary the planetary rotation period (symbols) and comparison to the Held and Hou (1980) theory (solid curve), the small-angle approximation to the Held-Hou theory from Eq. (56) (dotted curve), and the Held (2000) theory from Eq. (57) (dashed-dotted curve). GCM results are from Del Genio and Suozzo (1987) (squares and triangles, depicting northern and southern hemispheres, respectively), Navarra and Boccaletti (2002) (filled circles), and Korty and Schneider (2008) (asterisks; only cases adopting  $\theta_{\text{rad}} \approx 70$  K and their parameter  $\Gamma = 0.7$  are shown). Parameters adopted for the curves are  $g = 9.8$  m sec $^{-2}$ ,  $H = 15$  km,  $\Delta\theta_{\text{rad}} = 70$  K,  $a = 6400$  km,  $\theta_0 = 260$  K, and  $\Delta\theta_v = 30$  K. In the GCM studies, different authors define the width of the Hadley cell in different ways, so some degree of scatter is inevitable.

zonal wind, which breaks the angular-momentum conservation constraint in the upper-level wind, causing  $u$  to deviate from Eq. (52). With a different  $u(\phi)$  profile, the latitudinal dependence of temperature will change (via Eq. 53), and hence so will the latitudinal extent of the Hadley cell required to satisfy Eq. (55). Indeed, within the context of axisymmetric models, the addition of strong drag into the upper-layer flow (parameterizing turbulent mixing with the slower-moving surface air, for example) can lead Eq. (55) to predict that the Hadley cell should extend to the poles even for Earth’s rotation rate (e.g., Farrell 1990).

It could thus be the case that the width of the Hadley cell is strongly controlled by eddies. For example, in the midlatitudes of Earth and Mars, baroclinic eddies generally accelerate the zonal flow eastward in the upper troposphere; in steady state, this is generally counteracted by a westward Coriolis acceleration, which requires an *equatorward* upper tropospheric flow—backwards from the flow direction in the Hadley cell. Such eddy effects can thereby terminate the Hadley cell, forcing its confinement to low latitudes. Based on this idea, Held (2000) suggested that the Hadley cell width is determined by the latitude beyond which the troposphere first becomes baroclinically unstable (requiring isentrope slopes to exceed a latitude-dependent critical value). Adopting the horizontal thermal gradient implied by the angular-momentum conserving wind (Eq. 54), making the small-angle approximation, and utilizing a common two-layer model of baroclinic instability, this yields (Held 2000)

$$\phi_H \approx \left( \frac{gH\Delta\theta_v}{\Omega^2 a^2 \theta_0} \right)^{1/4} \quad (57)$$

in radians, where  $\Delta\theta_v$  is the vertical difference in potential temperature from the surface to the top of the Hadley cell. Note that the predicted dependence of  $\phi_H$  on planetary radius, gravity, rotation rate, and height of the Hadley cell is weaker than predicted by the Held-Hou model. Earth-based GCM simulations suggest that Eq. (57) may provide a better representation of the parameter dependences (Frierson et al. 2007; Lu et al. 2007; Korty and Schneider 2008). Nevertheless, even discrepancies with Eq. (57) are expected since the actual zonal wind does not follow the angular-momentum conserving profile (implying that the actual thermal gradient will deviate from Eq. 54). Substantially more work is needed to generalize these ideas to the full range of conditions relevant for exoplanets.

#### 5.4. High-latitude circulations: the baroclinic zones

For terrestrial planets heated at the equator and cooled at the poles, several studies suggest that the equator-to-pole heat engine can reside in either of two regimes depending on rotation rate and other parameters (Del Genio and Suozzo 1987). When the rotation period is long, the Hadley cells extend nearly to the poles, dominate the equator-to-pole heat transport, and thereby determine the equator-to-pole temperature gradient. Baroclinic instabilities are suppressed because of the small latitudinal thermal gradient and large Rossby deformation radius (at which baroclinic instabilities have maximal growth rates), which exceeds the planetary size for slow rotators such as Titan and Venus. On the other hand, for rapidly rotating planets like Earth and Mars, the Hadley cells are confined to low latitudes; in the absence of eddies the mid- and high-latitudes would relax into a radiative-equilibrium state, leading to minimal

equator-to-pole heat transport and a large equator-to-pole temperature difference. This structure is baroclinically unstable, however, and the resulting baroclinic eddies provide the dominant mechanism for transporting thermal energy from the poleward edges of the Hadley cells ( $\sim 30^\circ$  latitude for Earth) to the poles. This baroclinic heat transport significantly reduces the equator-to-pole temperature contrast in the mid- and high-latitudes. For gravity, planetary radius, and heating rates relevant for Earth, the breakpoint between these regimes occurs at a rotation period of  $\sim 5\text{--}10$  days (Del Genio and Suozzo 1987).

On rapidly rotating terrestrial planets like Earth and Mars, then, the equatorial and high-latitude circulations fundamentally differ: the equatorial Hadley cells, while strongly affected by eddies, do not *require* eddies to exist, nor to transport heat poleward. In contrast, the circulation and heat transport at high latitudes (poleward of  $\sim 30^\circ$  latitude on Earth and Mars) fundamentally depends on the existence of eddies. At high latitudes, interactions of eddies with the mean flow controls the latitudinal temperature gradient, latitudinal heat transport, and structure of the jet streams. This range of latitudes is called the *baroclinic zone*.

The extent to which baroclinic eddies can reduce the equator-to-pole temperature gradient has important implications for the mean climate. Everything else being equal, an Earth-like planet with colder poles will develop more extensive polar ice and be more susceptible to an ice-albedo feedback that triggers a globally glaciated “snowball” state (Spiegel et al. 2008). Likewise, a predominantly CO<sub>2</sub> atmosphere can become susceptible to atmospheric collapse if the polar temperatures become sufficiently cold for CO<sub>2</sub> condensation.

There is thus a desire to understand the extent to which baroclinic eddies can transport heat poleward. General circulation models (GCMs) attack this problem by spatially and temporally resolving the full life of every baroclinic eddy and their effect on the mean state, but this is computationally intensive and often sheds little light on the underlying sensitivity of the process to rotation rate and other parameters.

Two simplified approaches have been advanced that illuminate this issue. Although GCMs for terrestrial exoplanets will surely be needed in the future, simplified approaches can guide our understanding of such GCM results and provide testable hypotheses regarding the dependence of heat transport on planetary parameters. They also may provide guidance for parameterizations of the latitudinal heat transport in simpler energy-balance climate models that do not explicitly attempt to resolve the full dynamics. We devote the rest of this section to discussing these simplified approaches.

The first simplified approach postulates that baroclinic eddies relax the midlatitude thermal structure into a state that is neutrally stable to baroclinic instabilities (Stone 1978), a process called *baroclinic adjustment*. This idea is analogous to the concept of convective adjustment: when

radiation or other processes drive the vertical temperature gradient steeper than an adiabat ( $dT/dz < -g/c_p$  for an ideal gas, where  $z$  is height), convection ensues and drives the temperature profile toward the adiabat, which is the neutrally stable state for convection. If the convective overturn timescales are much shorter than the radiative timescales, then convection overwhelms the ability of radiation to destabilize the environment, and the temperature profile then deviates only slightly from an adiabat over a wide range of convective heat fluxes (see, e.g., §4.1). In a similar way, the concept of baroclinic adjustment postulates that when timescales for baroclinic eddy growth are much shorter than the timescale for radiation to create a large equator-to-pole temperature contrast, the eddies will transport thermal energy poleward at just the rate needed to maintain a profile that is neutral to baroclinic instabilities.

This idea was originally developed for a simplified two-layer system, for which baroclinic instability first initiates when the slope of isentropes exceeds  $\sim H/a$ , where  $H$  is a pressure scale height and  $a$  is the planetary radius. Comparison of this critical isentrope slope with Earth observations shows impressive agreement poleward of  $30\text{--}40^\circ$  latitude, where baroclinic instabilities are expected to be active (Stone 1978). A substantial literature has subsequently developed to explore the idea further (for a review see Zurita-Gotor and Lindzen 2006). The resulting latitudinal temperature gradient is then approximately  $H/a$  times the vertical potential temperature gradient. Interestingly, this theory suggests that otherwise identical planets with different Brunt-Väisälä frequencies (due to differing opacities, vertical heat transport by large-scale eddies, or role for latent heating, all of which can affect the stratification) would exhibit very different midlatitude temperature gradients—the planet with smaller stable stratification (i.e., smaller Brunt-Väisälä frequency; Eq. 6) exhibiting a smaller latitudinal temperature gradient. Moreover, although Earth’s ocean transports substantial heat between the equator and poles, the theory also suggests that the ocean may only exert a modest influence on the latitudinal temperature gradients in the *atmosphere* (Lindzen and Farrell 1980a): in the absence of oceanic heat transport, the atmospheric eddies would simply take up the slack to maintain the atmosphere in the baroclinically neutral state. (There could of course be an indirect effect on latitudinal temperature gradients if removing/adding the oceans altered the tropospheric stratification.) Finally, the theory suggests that the latitudinal temperature gradient in the baroclinic zone does not depend on planetary rotation rate except indirectly via the influence of rotation rate on static stability. It is worth emphasizing, however, that even if the latitudinal temperature gradient in the *baroclinic zone* were constant with rotation rate, the total equator-to-pole temperature difference would still decrease with decreasing rotation rate because, with decreasing rotation rate, the Hadley cell occupies a greater latitude range and the baroclinically adjusted region would be compressed toward the poles (see Fig.12).

Despite Stone (1978)’s encouraging results, several

complicating factors exist. First, the time-scale separation between radiation and dynamics is much less obvious for baroclinic adjustment than for convective adjustment. In an Earth or Mars-like context, the convective instability timescales are  $\sim 1$  hour, the baroclinic instability timescales are days, and the radiation timescale is  $\sim 20$  days (Earth) or  $\sim 2$  days (Mars). The ability of baroclinic eddies to adjust the environment to a baroclinically neutral state may thus be marginal, especially for planets with short radiative time constants (such as Mars). Second, the neutrally stable state in the two-layer model—corresponding to an isentrope slope of  $\sim H/a$ —is an artefact of the vertical discretization in that model. When a multi-layer model is used, the critical isentrope slope for initiating baroclinic instability decreases as the number of layers increases, and it approaches zero in a vertically continuous model. One might then wonder why a baroclinic zone can support *any* latitudinal temperature contrast (as it obviously does on Earth and Mars). The reason is that the instability growth timescales are long at small isentropic slopes (Lindzen and Farrell 1980b); the instabilities only develop a substantial ability to affect the mean state when isentrope slopes become steep. In practice, then, the baroclinic eddies are perhaps only able to relax the atmosphere to a state with isentrope slopes of  $\sim H/a$  rather than something significantly shallower.

The second simplified approach to understanding equator-to-pole temperature contrasts on terrestrial planets seeks to describe the poleward heat transport by baroclinic eddies as a diffusive process (Held 1999). This approach is based on the idea that baroclinic eddies have maximal growth rates at scales close to the Rossby radius of deformation,  $L_D$  (see Eq. 23), and if the baroclinically unstable zone has a latitudinal width substantially exceeding  $L_D$  then there will be scale separation between the mean flow and the eddies.<sup>33</sup> The possible existence of a scale separation in the baroclinic instability problem implies that representing the heat transport as a function of *local* mean-flow quantities (such as the mean latitudinal temperature gradient) is a reasonable prospect. Still, caution is warranted, since an inverse energy cascade (§3.6) could potentially transfer the energy to scales larger than  $L_D$ , thereby weakening the scale separation.

The diffusive approach is typically cast in the context of a 1D energy-balance model that seeks to determine the variation with latitude of the zonally averaged surface temperature. This approach has a long history for Earth climate studies (see review in North et al. 1981), Solar-System planets (e.g. Hoffert et al. 1981), and even in preliminary studies of the climates and habitability of terrestrial exoplanets (Williams and Kasting 1997; Williams and Pollard 2003;

Spiegel et al. 2008, 2009). In its simplest form, the governing equation reads

$$c \frac{\partial T}{\partial t} = \nabla \cdot (c D \nabla T) + S(\phi) - I \quad (58)$$

where  $T$  is surface temperature,  $D$  ( $\text{m}^2 \text{ sec}^{-1}$ ) is the diffusivity associated with heat transport by baroclinic eddies,  $S(\phi)$  is the absorbed stellar flux as a function of latitude, and  $I$  is the emitted thermal flux, which is a function of temperature. In the simplest possible case,  $I$  is represented as a linear function of temperature,  $I = A + BT$  (North et al. 1981), where  $A$  and  $B$  are positive constants. In Eq. (58),  $c$  is a heat capacity (with units  $\text{J m}^{-2} \text{ K}^{-1}$ ) that represents the atmosphere and oceans (if any). The steady-state solution in the absence of transport ( $D = 0$ ) is  $T = [S(\phi) - A]/B$ . On the other hand, when transport dominates ( $D \rightarrow \infty$ ), the solution yields constant  $T$ .

The term  $S(\phi)$  includes the effect of latitudinally varying albedo (e.g., due to ice cover), but if albedo is constant with latitude, then  $S$  represents the latitudinally varying insolation. To schematically illustrate the effect of heat transport on the equator-to-pole temperature gradient, parameterize  $S$  as a constant plus a term proportional to the Legendre polynomial  $P_2(\cos \phi)$ . In this case, and if  $D$  and  $c$  are constant, the equation has a steady analytic solution with an equator-to-pole temperature difference given by (Held 1999)

$$\Delta T_{\text{eq-pole}} = \frac{\Delta T_{\text{rad}}}{1 + 6 \frac{cD}{Ba^2}} \quad (59)$$

where  $a$  is the planetary radius and  $\Delta T_{\text{rad}}$  is the equator-to-pole difference in radiative-equilibrium temperature. The equation implies that atmospheric heat transport significantly influences the equator-to-pole temperature difference when the diffusivity exceeds  $\sim Ba^2/(6c)$ . For Earth,  $B \approx 2 \text{ W m}^{-2} \text{ K}^{-1}$ ,  $a = 6400 \text{ km}$ , and  $c \approx 10^7 \text{ J m}^{-2} \text{ K}^{-1}$ , suggesting that atmospheric transport becomes important when  $D \gtrsim 10^6 \text{ m}^2 \text{ sec}^{-1}$ .

The question comes down to how to determine the diffusivity,  $D$ . In Earth models,  $D$  is typically chosen by tuning the models to match the current climate, and then that value of  $D$  is used to explore the regimes of other climates (e.g. North 1975). However, that approach sidesteps the underlying physics and prevents an extrapolation to other planetary environments.

Motivated by an interest in understanding the feedback between baroclinic instabilities and the mean state, substantial effort has been devoted to determining the dependence of the diffusivity on control parameters such as rotation rate and latitudinal thermal gradient (for a review see Held 1999). This work can help guide efforts to understand the temperature distribution on rapidly rotating exoplanets. We expect that the diffusivity will scale as

$$D \approx u_{\text{eddy}} L_{\text{eddy}} \quad (60)$$

where  $u_{\text{eddy}}$  and  $L_{\text{eddy}}$  are the characteristic velocities and horizontal sizes of the heat-transporting eddies. Because baroclinic eddies will be in near-geostrophic balance

<sup>33</sup>As pointed out by Held (1999), this differs from many instability problems in fluid mechanics, such as shear instability in pipe flow or convection in a fluid driven by a heat flux between two plates, where maximal growth rates occur at length scales comparable to the domain size and no eddy/mean-flow scale separation occurs.

(Eq. 21) on a rapidly rotating planet, the characteristic eddy velocities,  $u_{\text{eddy}}$ , will relate to characteristic eddy potential-temperature perturbations  $\theta'_{\text{eddy}}$  via the thermal-wind relation, giving  $u_{\text{eddy}} \sim g\theta'_{\text{eddy}}h_{\text{eddy}}/(fL_{\text{eddy}})$ , where  $h_{\text{eddy}}$  is the characteristic vertical thickness of the eddies. Under the assumption that the ratio of vertical to horizontal scales is  $h_{\text{eddy}}/L_{\text{eddy}} \sim f/N$  (Charney 1971; Haynes 2005), this yields  $u_{\text{eddy}} \approx g\theta'_{\text{eddy}}/(\theta_0 N)$  (where  $N$  is Brunt-Väisälä frequency), which simply states that eddies with larger thermal perturbations will also have larger velocity perturbations. Under the assumption that the thermal perturbations scale as  $\theta'_{\text{eddy}} \approx L_{\text{eddy}}\partial\bar{\theta}/\partial y$ , we then have

$$D \approx L_{\text{eddy}}^2 \frac{g}{N\theta_0} \frac{\partial\bar{\theta}}{\partial y}. \quad (61)$$

Greater thermal gradients and eddy-length scales lead to greater diffusivity and, importantly, the diffusivity depends on the *square* of the eddy size.

Several proposals for the relevant eddy size have been put forward, which we summarize in Table 2. Based on the idea that baroclinic instabilities have the greatest growth rates for lengths comparable to the deformation radius, Stone (1972) suggested that  $L_{\text{eddy}}$  is the deformation radius,  $NH/f$ . On the other hand, baroclinic eddies could energize an inverse cascade, potentially causing the dominant heat-transporting eddies to have sizes exceeding  $L_D$ . In the limit of this process (Green 1970), the eddies would reach the width of the baroclinic zone,  $L_{\text{zone}}$  (potentially close to a planetary radius for a planet with a narrow Hadley cell). This simply leads to Eq. (61) with  $L_{\text{eddy}} = L_{\text{zone}}$ . In contrast, Held and Larichev (1996) argued that the inverse cascade would produce an eddy scale not of order  $L_{\text{zone}}$  but instead of order the Rhines scale,  $(u_{\text{eddy}}/\beta)^{1/2}$ . Finally, Barry et al. (2002) used heat-engine arguments to propose that

$$D \approx \left( \frac{eaq}{\theta_0} \frac{\partial\bar{\theta}}{\partial y} \right)^{3/5} \left( \frac{2}{\beta} \right)^{4/5} \quad (62)$$

where  $\dot{q}_{\text{net}}$  is the net radiative heating/cooling per mass that the eddy fluxes are balancing,  $a$  is the planetary radius, and  $e$  is a constant of order unity. Equation 62 is probably most robust for the dependences on heating rate  $\dot{q}_{\text{net}}$  and thermal gradient  $\partial\bar{\theta}/\partial y$ , which they varied by factors of  $\sim 200$  and 6, respectively; planetary radius and rotation rates were varied by only  $\sim 70\%$ , so the dependences on those parameters should be considered tentative.

As can be seen in Table 2, these proposals have divergent implications for the dependence of diffusivity on background parameters. Stone (1972)'s diffusivity is proportional to the latitudinal temperature gradient and, because of the variation of  $L_D$  with rotation rate, inversely proportional to the square of the planetary rotation rate. Green (1970)'s diffusivity likewise scales with the latitudinal temperature gradient; it contains no explicit dependence on the planetary rotation rate, but a rotation-rate dependence could enter because the Hadley cell shrinks and  $L_{\text{zone}}$  increases with increasing rotation rate. Held and Larichev (1996)'s

diffusivity has the same rotation-rate dependence as that of Stone (1972), but it has a much stronger dependence on gravity and temperature gradient [ $g^3$  and  $(\partial\bar{\theta}/\partial y)^3$ ]. Moreover, it increases with decreasing static stability as  $N^{-3}$ , unlike Stone's diffusivity that scales with  $N$ .<sup>34</sup> Finally, Barry et al. (2002)'s diffusivity suggests a somewhat weaker dependence, scaling with  $(\partial\bar{\theta}/\partial y)^{3/5}$  and  $\Omega^{-3/5}$ . Note that the rotation-rate dependences described above should be treated with caution, because altering the rotation rate or gravity could change the circulation in a way that alters the Brunt-Väisälä frequency, leading to additional changes in the diffusivity.

Additional work is needed to determine which of these schemes (if any) is valid over a wide range of parameters relevant to terrestrial exoplanets. Most of the work performed to test the schemes of Green (1970), Stone (1972), Held and Larichev (1996) and others has adopted simplified two-layer quasi-geostrophic models<sup>35</sup> under idealized assumptions such as planar geometry with constant Coriolis parameter (a so-called “f-plane”). Because variation of  $f$  with latitude alters the properties of baroclinic instability, schemes developed for constant  $f$  may not translate directly into a planetary context. More recently, two-layer planar models with non-zero  $\beta$  have been explored by Thompson and Young (2007) and Zurita-Gotor and Vallis (2009), while full three-dimensional GCM calculations on a sphere (with  $\sim 30$  layers) investigating the latitudinal heat flux have been performed by Barry et al. (2002) and Schneider and Walker (2008) under conditions relevant to Earth. Additional simulations in the spirit of Barry et al. (2002) and Schneider and Walker (2008), considering a wider range of planetary and atmospheric parameters, can clarify the true sensitivities of the heat transport rates in three-dimensional atmospheres.

## 5.5. Slowly rotating regime

At slow rotation rates, the GCM simulations shown in Figs. 11–12 develop near-global Hadley cells with high-latitude jets, but the wind remains weak at the equator. In contrast, Titan and Venus (with rotation periods of 16 and 243 days, respectively) have robust ( $\sim 100 \text{ m sec}^{-1}$ ) superrotating winds in their equatorial upper tropospheres. Because the equator is the region of the planet lying farthest from the rotation axis, such a flow contains a local maximum of angular momentum at the equator. Axisymmetric Hadley circulations (§5.3) cannot produce such superrotation; rather, up-gradient transport of momentum by eddies

<sup>34</sup>The  $N^{-3}$  dependence in Held and Larichev (1996)'s gives the impression that the diffusivity becomes unbounded as the atmospheric vertical temperature profile becomes neutrally stable (i.e. as  $N \rightarrow 0$ ), but this is misleading. In reality, one expects the latitudinal temperature gradient and potential energy available for driving baroclinic instabilities to decrease with decreasing  $N$ . Noting that the slope of isentropes is  $m_\theta \equiv (\partial\theta/\partial y)(\partial\theta/\partial z)^{-1}$ , one can re-express Held and Larichev (1996)'s diffusivity as scaling with  $m_\theta N^3$ . Thus, at constant isentrope slope, the diffusivity properly drops to zero as the vertical temperature profile becomes neutrally stable.

<sup>35</sup>That is, models where geostrophic balance is imposed as an external constraint.

TABLE 2  
PROPOSED DIFFUSIVITIES FOR HIGH-LATITUDE HEAT TRANSPORT ON TERRESTRIAL PLANETS

Scheme	$L_{\text{eddy}}$	$D$
Stone (1972)	$L_D$	$\frac{H^2 N g}{f^2 \theta_0} \frac{\partial \bar{\theta}}{\partial y}$
Green (1970)	$L_{\text{zone}}$	$L_{\text{zone}}^2 \frac{g}{N \theta_0} \frac{\partial \bar{\theta}}{\partial y}$
Held and Larichev (1996)	$L_\beta$	$\frac{g^3}{N^3 \beta^2 \theta_0^3} \left( \frac{\partial \bar{\theta}}{\partial y} \right)^3$
Barry et al. (2002)	$L_\beta$	$\left( \frac{ea\dot{q}_{\text{net}}}{\theta_0} \frac{\partial \bar{\theta}}{\partial y} \right)^{3/5} \left( \frac{2}{\beta} \right)^{4/5}$

is required. This process remains poorly understood. One class of models suggests that this transport occurs from high latitudes; for example, the high-latitude jets that result from the Hadley circulation (which can be seen in Fig. 11) experience a large-scale shear instability that pumps eddy momentum toward the equator, generating the equatorial superrotation (Del Genio and Zhou 1996). Alternatively, thermal tide or wave interaction could induce momentum transports that generate the equatorial superrotation (e.g., Fels and Lindzen 1974). Recently, a variety of simplified Venus and Titan GCMs have been developed that show encouraging progress in capturing the superrotation (e.g., Yamamoto and Takahashi 2006; Richardson et al. 2007; Lee et al. 2007; Herrnstein and Dowling 2007).

The Venus/Titan superrotation problem may have important implications for understanding the circulation of synchronously locked exoplanets. All published 3D circulation models of synchronously locked hot Jupiters (§4.3), and even the few published studies of sychrounously locked terrestrial planets (Joshi et al. 1997; Joshi 2003, see §5.6), develop robust equatorial superrotation. The day-night heating pattern associated with synchronous locking should generate thermal tides and, in analogy with Venus and Titan, these could be relevant in driving the superrotation in the 3D exoplanet models. Simplified Earth-based two-layer calculations that include longitudinally varying heating, and which also develop equatorial superrotation, seem to support this possibility (Suarez and Duffy 1992; Saravanan 1993).

### 5.6. Unusual forcing regimes

Our discussion of circulation regimes on terrestrial planets has so far largely focused on annual-mean forcing conditions. On Earth, seasonal variations represent relatively modest perturbations around the annual-mean climate due to Earth's  $23.5^\circ$  obliquity. On longer timescales, the secular evolution of Earth's orbital elements is thought to be responsible for paleoclimatic trends, such as ice ages, according to Milankovitch's interpretation (e.g. Kawamura et al. 2007). While it may be surprising to refer to Earth's seasons

or ice ages as minor events from a human perspective, it is clear that they constitute rather mild versions of the more diverse astronomical forcing regimes expected to occur on extrasolar worlds.

In principle, terrestrial exoplanets could possess large obliquities ( $i \rightarrow 90$  deg) and eccentricities ( $e \rightarrow 1$ ). This would result in forcing conditions with substantial seasonal variations around the annual mean, such as order-of magnitude variations in the global insolation over the orbital period at large eccentricities. Even the annual mean climate can be dramatically affected under unusual forcing conditions, for instance at large obliquities when the poles receive more annual-mean insolation than the planetary equator (for  $i > 54^\circ$ ). Yet another unusual forcing regime occurs if the terrestrial planet is tidally locked to its parent star and thus possesses permanent day and night sides much like the hot Jupiters discussed in §4.3. Relatively few studies of circulation regimes under such unusual forcing conditions have been carried out to date.

Williams and Kasting (1997) and Spiegel et al. (2009) investigated the climate of oblique Earth-like planets with simple, diffusive energy-balance models of the type described by Eq. (58). While seasonal variations were found to be severe at high obliquity, Williams and Kasting (1997) concluded that highly oblique planets could nevertheless remain regionally habitable, especially if they possessed thick CO<sub>2</sub>-enriched atmospheres with large thermal inertia relative to Earth, as may indeed be expected for terrestrial planets in the outermost regions of a system's habitable zone. Spiegel et al. (2009) confirmed these results and highlighted the risks that global glaciation events and partial atmospheric CO<sub>2</sub> collapse constitute for highly oblique terrestrial exoplanets. Williams and Pollard (2003) presented a much more detailed set of three-dimensional climate and circulation models for Earth-like planets at various obliquities. Despite large seasonal variations at extreme obliquities, Williams and Pollard (2003) found no evidence for any runaway greenhouse effect or global glaciation event in their climate models and thus concluded that Earth-like planets should generally be hospitable to life even at high

obliquity.

Williams and Pollard (2002) also studied the climate on eccentric versions of the Earth with a combination of detailed three-dimensional climate models and simpler energy-balance models. They showed that the strong variations in insolation occurring at large eccentricities can be rather efficiently buffered by the large thermal inertia of the atmosphere+ocean climate system. These authors thus argued that the annually averaged insolation, which is an increasing function of  $e$ , may be the most meaningful quantity to describe in simple terms the climate of eccentric, thermally blanketed Earth-like planets. It is presumably the case that terrestrial planets with reduced thermal inertia from lower atmospheric/oceanic masses would be more strongly affected by such variations in insolation.

It should be emphasized that, despite the existing work on oblique or eccentric versions of the Earth, a fundamental understanding of circulation regimes under such unusual forcing conditions is still largely missing. For instance, variations in the Hadley circulation regime or the baroclinic transport efficiency, expected as forcing conditions vary along the orbit, have not been thoroughly explored. Similarly, the combined effects of a substantial obliquity and eccentricity have been ignored. As the prospects for finding and characterizing exotic versions of the Earth improve, these issues should become the subject of increasing scrutiny.

One of the best observational prospects for the next decade is the discovery of tidally locked terrestrial planets around nearby M-dwarfs (e.g., Irwin et al. 2009; Seager et al. 2008). In anticipation of such discoveries, Joshi et al. (1997) presented a careful investigation of the circulation regime on this class of unusually forced planets, with permanent day and night sides. The specific focus of their work was to determine the conditions under which CO<sub>2</sub> atmospheric collapse could occur on the cold night sides of such planets and act as a trap for this important greenhouse gas, even when circulation and heat transport are present. Using a simplified general circulation model, these authors explored the problem's parameter space for various global planetary and atmospheric attributes and included a study of the potential risks posed by violent flares from the stellar host. The unusual circulation regime that emerged from this work was composed of a direct circulation cell at surface levels (i.e. equatorial day to night transport with polar return) and a superrotating wind higher up in the atmosphere. While detrimental atmospheric collapse did occur under some combinations of planetary attributes (e.g., for thin atmospheres), the authors concluded that efficient atmospheric heat transport was sufficient to prevent collapse under a variety of plausible scenarios. More recently, Joshi (2003) revisited some of these results with a much more detailed climate model with explicit treatments of non-gray radiative transfer and a hydrological cycle. It is likely that this interesting circulation regime will be reconsidered in the next few years as the discovery of such exotic worlds is on our horizon.

## 6. RECENT HIGHLIGHTS

Since the first discovery of giant exoplanets around Sun-like stars via the Doppler velocity technique (Mayor and Queloz 1995; Marcy and Butler 1996), exoplanet research has experienced a spectacular series of observational breakthroughs. The first discovery of a transiting hot Jupiter (Charbonneau et al. 2000; Henry et al. 2000) opened the door to a wide range of clever techniques for characterizing such transiting planets. The drop in flux that occurs during secondary eclipse, when the planet passes behind its star, led to direct infrared detections of the thermal flux from the planet's dayside (Deming et al. 2005; Charbonneau et al. 2005). This was quickly followed by the detection of day/night temperature variations (Harrington et al. 2006), detailed phase curve observations (e.g. Knutson et al. 2007, 2009b; Cowan et al. 2007), infrared spectral and photometric measurements (Grillmair et al. 2007, 2008; Richardson et al. 2007; Charbonneau et al. 2008; Knutson et al. 2008) and a variety of transit spectroscopic constraints (Tinetti et al. 2007; Swain et al. 2008; Barman 2008). Collectively, these observations help to constrain the composition, albedo, three-dimensional (3D) temperature structure, and hence the atmospheric circulation regime of hot Jupiters.

The reality of atmospheric circulation on these objects is suggested by exquisite light curves of HD 189733b showing modest day-night infrared brightness temperature variations and displacement of the longitudes of minimum/maximum flux from the antistar/substellar points, presumably the result of an efficient circulation able to distort the temperature pattern (Knutson et al. 2007, 2009b). Dayside photometry also hints at the existence of an atmospheric circulation on this planet (Barman 2008). Nevertheless, other hot Jupiters, such as Ups And b and HD 179949b, apparently exhibit large day-night temperature variations with no discernable displacement of the hot regions from the substellar point (Harrington et al. 2006; Cowan et al. 2007). Secondary-eclipse photometry suggests that some hot Jupiters have dayside temperatures that decrease with altitude, while other hot Jupiters appear to exhibit dayside thermal inversion layers where temperatures increase with altitude. Some authors have suggested that these two issues are linked (Fortney et al. 2008), although substantial additional observations are needed for a robust assessment. Understanding the dependence of infrared phase variations and dayside temperature profiles on planetary orbital and physical properties remains an ongoing observational challenge for the coming decade.

In parallel, this observational vanguard has triggered a growing body of theoretical and modeling studies to investigate plausible atmospheric circulation patterns on hot Jupiters. The models agree on some issues, such as that synchronously rotating hot Jupiters on  $\sim$  3-day orbits should exhibit fast winds with only a few broad zonal jets. On the other hand, the models disagree on other issues, such as the details of the 3D flow patterns and the extent to which sig-

nificant global-scale time variability is likely. The effect of stellar flux, planetary rotation rate, obliquity, atmospheric composition, and orbital eccentricity on the circulation have barely been explored. Further theoretical work and comparison with observations should help move our understanding onto a firmer foundation.

## 7. FUTURE PROSPECTS

Over the next decade, the observational characterization of hot Jupiters and Neptunes will continue apace, aided especially by the warm *Spitzer* mission and subsequently *JWST*. Equally exciting, NASA's *Kepler* mission and groundbased surveys (e.g., MEarth; see Irwin et al. 2009) may soon lead to the discovery of not only additional super-Earths but Earth-sized terrestrial exoplanets, including "hot Earths" as well as terrestrial planets cool enough to lie within the habitable zones of their stars. If sufficiently favorable systems are discovered, follow-up by *JWST* may allow basic characterization of their spectra and light curves (albeit at significant resources per planet), providing constraints on their atmospheric properties including their composition, climate, circulation, and the extent to which they may be habitable. Finally, over the next decade, significant opportunities exist for expanding our understanding of basic dynamical processes by widening the parameters adopted in circulation models beyond those typically explored in the study of Solar-System planets.

To move the observational characterization of exoplanet atmospheric circulation into the next generation, we recommend full-orbit light curves for a variety of hot Jupiters and Neptunes (and eventually terrestrial planets). Target objects should span a range of incident stellar fluxes, planetary masses, and orbital periods and eccentricities (among other parameters) to characterize planetary diversity. To constrain the planetary thermal-energy budgets, light curves should sample the blackbody peaks at several wavelengths, including both absorption bands and low-opacity windows as expected from theoretical models; this will provide constraints on the day-night temperature contrasts—and hence day-night heat transport—at a range of atmospheric pressure levels. Dayside infrared spectra obtained from secondary-eclipse measurements, while not necessarily diagnostic of the atmospheric circulation in isolation, will provide crucial constraints when combined with infrared light curves. By providing constraints on atmospheric composition, transit spectroscopy will enable much better interpretation of light curves and secondary-eclipse spectra. Secondary eclipses (or full light curves) that are observed repeatedly will provide powerful constraints on global-scale atmospheric variability. *Kepler* may prove particularly useful in this regard, with its ability to observe hundreds of secondary eclipses of hot Jupiters (such as HAT-P-7b; Borucki and colleagues 2009) in its field of view. Such an extensive temporal dataset could provide information on the frequency spectrum of atmospheric variability (if any), which would help to identify the mechanisms of variability as well as the

background state of the mean circulation. Other novel techniques, such as the possibility of separately measuring transit spectra on the leading and trailing limbs and the possibility of detecting the Doppler shifts associated with planetary rotation and/or winds, should be considered.

Specific research questions for the next decade include but are not limited to the following:

- How warm are the nightsides of hot Jupiters? How does this depend on the stellar flux, atmospheric composition, and other parameters?
- What are the dynamical mechanisms for shifting the hot and cold points away from the substellar and antistar points, respectively? Why does HD 189733b appear to have both its hottest and coldest points on the same hemisphere?
- What is the observational and physical relationship (if any) between the amplitude of the day-night temperature contrast and existence or absence of a day-side temperature inversion that has been inferred on some hot Jupiters?
- How does the expected atmospheric circulation regime depend on planetary size, rotation rate, gravity, obliquity, atmospheric composition, and incident stellar flux?
- What are the important dissipation mechanisms in the atmospheres of hot Jupiters? What are the relative roles of turbulence, shocks, and magnetohydrodynamic processes in frictionally braking the flows?
- How coupled are the atmospheric flows on hot Jupiters to convection in the planetary interior? How are momentum, heat, and constituents transported across the deep radiative zone in hot Jupiters?
- Does the atmospheric circulation influence the long-term evolution of hot Jupiters? Can downward transport of atmospheric energy into the interior help explain the radii of some anomalously large hot Jupiters?
- What is the mechanism for equatorial superrotation that occurs in most 3D models of synchronously rotating hot Jupiters? Does such superrotation exist on real hot Jupiters?
- Are the atmospheres of hot Jupiters strongly time variable on the global scale, and if so, what is the mechanism for the variability?
- How does the circulation regime of planets in highly eccentric orbits differ from that of planets in circular orbits?
- To what extent can obliquity, rotation rate, atmospheric mass, and atmospheric circulation properties be inferred from disk-integrated spectra or light curves?

- To what extent, if any, does the atmospheric circulation influence the escape of an atmosphere to space?
- Do the deep molecular envelopes of giant planets differentially rotate?
- What controls the wind speeds on giant planets? Why are Neptune's winds faster than Jupiter's, and what can this teach us about strongly irradiated planets?
- What can observations of chemical disequilibrium species tell us about the atmospheric circulation of giant planets and brown dwarfs?
- What is the role of clouds in affecting the circulation, climate, evolution, and observable properties of exoplanets?
- For terrestrial planets, how does the atmospheric circulation affect the boundaries of the classical habitable zone?
- What is the role of the atmospheric circulation in affecting the ice-albedo feedback, atmospheric collapse, runaway greenhouse, and other climate feedbacks?
- Can adequate scaling theories be developed to predict day-night or equator-to-pole temperature contrasts as a function of planetary and atmospheric parameters?
- What is the dynamical role of a surface (i.e. the ground) in the atmospheric circulation? For super-Earths, is there a critical atmospheric mass beyond which the surface becomes unimportant and the circulation behaves like that of a giant planet?

Ultimately, unraveling the atmospheric circulation and climate of exoplanets from global-scale observations will be a difficult yet exciting challenge. Degeneracies of interpretation will undoubtedly exist (e.g., multiple circulation patterns explaining a given light curve), and forward progress will require not only high-quality observations but a careful exploration of a hierarchy of models so that the nature of these degeneracies can be understood. Despite the challenge, the potential payoff will be the unleashing of planetary meteorology beyond the confines of our Solar System, leading to not only an improved understanding of basic circulation mechanisms (and how they may vary with planetary rotation rate, gravity, incident stellar flux, and other parameters) but a glimpse of the actual atmospheric circulations, climate, and habitability of planets orbiting other stars in our neighborhood of the Milky Way.

**Acknowledgments.** This paper was supported by NASA Origins grant NNX08AF27G to APS, NASA grants NNG04GN82G and STFC PP/E001858/1 to JYKC, and NASA contract NNG06GF55G to KM.

## REFERENCES

- Atkinson, D. H., A. P. Ingersoll, and A. Seiff, 1997: Deep zonal winds on Jupiter: Update of Doppler tracking the Galileo probe from the orbiter. *Nature*, **388**, 649–650.
- Aurnou, J. M., and M. H. Heimpel, 2004: Zonal jets in rotating convection with mixed mechanical boundary conditions. *Icarus*, **169**, 492–498.
- Aurnou, J. M., and P. L. Olson, 2001: Strong zonal winds from thermal convection in a rotating spherical shell. *Geophys. Res. Lett.*, **28**, 2557–2560.
- Barman, T. S., 2008: On the Presence of Water and Global Circulation in the Transiting Planet HD 189733b. *Astrophys. J. Lett.*, **676**, L61–L64.
- Barry, L., G. C. Craig, and J. Thuburn, 2002: Poleward heat transport by the atmospheric heat engine. *Nature*, **415**, 774–777.
- Batchelor, G. K., 1967: *An Introduction to Fluid Dynamics*. Cambridge University Press.
- Bézard, B., E. Lellouch, D. Strobel, J.-P. Maillard, and P. Drossart, 2002: Carbon Monoxide on Jupiter: Evidence for Both Internal and External Sources. *Icarus*, **159**, 95–111.
- Borucki, W. J., and colleagues, 2009: Kepler's optical phase curve of the exoplanet HAT-P-7b. *Nature*, **325**, 709.
- Burrows, A., T. Guillot, W. B. Hubbard, M. S. Marley, D. Saumon, J. I. Lunine, and D. Sudarsky, 2000: On the Radii of Close-in Giant Planets. *Astrophys. J. Lett.*, **534**, L97–L100.
- Burrows, A., W. B. Hubbard, J. I. Lunine, and J. Liebert, 2001: The theory of brown dwarfs and extrasolar giant planets. *Reviews of Modern Physics*, **73**, 719–765.
- Busse, F. H., 1976: A simple model of convection in the Jovian atmosphere. *Icarus*, **29**, 255–260.
- Busse, F. H., 2002: Convective flows in rapidly rotating spheres and their dynamo action. *Physics of Fluids*, **14**, 1301–1314.
- Caballero, R., R. T. Pierrehumbert, and J. L. Mitchell, 2008: Axisymmetric, nearly inviscid circulations in non-condensing radiative-convective atmospheres. *Quarterly Journal of the Royal Meteorological Society*, **134**, 1269–1285.
- Chabrier, G., and I. Baraffe, 2000: Theory of Low-Mass Stars and Substellar Objects. *Annu. Rev. Astron. Astrophys.*, **38**, 337–377.
- Chabrier, G., and I. Baraffe, 2007: Heat Transport in Giant (Exo)planets: A New Perspective. *Astrophys. J. Lett.*, **661**, L81–L84.
- Chabrier, G., T. Barman, I. Baraffe, F. Allard, and P. H. Hauschildt, 2004: The Evolution of Irradiated Planets: Application to Transits. *Astrophys. J. Lett.*, **603**, L53–L56.
- Charbonneau, D., T. M. Brown, D. W. Latham, and M. Mayor, 2000: Detection of Planetary Transits Across a Sun-like Star. *Astrophys. J. Lett.*, **529**, L45–L48.
- Charbonneau, D., H. A. Knutson, T. Barman, L. E. Allen, M. Mayor, S. T. Megeath, D. Queloz, and S. Udry, 2008: The Broadband Infrared Emission Spectrum of the Exoplanet HD 189733b. *Astrophys. J.*, **686**, 1341–1348.
- Charbonneau, D., et al., 2005: Detection of Thermal Emission from an Extrasolar Planet. *Astrophys. J.*, **626**, 523–529.
- Charney, J. G., 1971: Geostrophic turbulence. *Journal of Atmospheric Sciences*, **28**, 1087–1095.

- Cho, J. Y.-K., 2008: Atmospheric dynamics of tidally synchronized extrasolar planets. *Royal Society of London Philosophical Transactions Series A*, **366**, 4477–4488.
- Cho, J. Y.-K., and L. M. Polvani, 1996a: The morphogenesis of bands and zonal winds in the atmospheres on the giant outer planets. *Science*, **8**(1), 1–12.
- Cho, J. Y.-K., and L. M. Polvani, 1996b: The emergence of jets and vortices in freely evolving, shallow-water turbulence on a sphere. *Physics of Fluids*, **8**, 1531–1552.
- Cho, J. Y.-K., K. Menou, B. M. S. Hansen, and S. Seager, 2003: The Changing Face of the Extrasolar Giant Planet HD 209458b. *Astrophys. J. Lett.*, **587**, L117–L120.
- Cho, J. Y.-K., K. Menou, B. M. S. Hansen, and S. Seager, 2008: Atmospheric Circulation of Close-in Extrasolar Giant Planets. I. Global, Barotropic, Adiabatic Simulations. *Astrophys. J.*, **675**, 817–845.
- Christensen, U. R., 2001: Zonal flow driven by deep convection in the major planets. *Geophys. Res. Lett.*, **28**, 2553–2556.
- Christensen, U. R., 2002: Zonal flow driven by strongly supercritical convection in rotating spherical shells. *Journal of Fluid Mechanics*, **470**, 115–133.
- Cooper, C. S., and A. P. Showman, 2005: Dynamic Meteorology at the Photosphere of HD 209458b. *Astrophys. J. Lett.*, **629**, L45–L48.
- Cooper, C. S., and A. P. Showman, 2006: Dynamics and Disequilibrium Carbon Chemistry in Hot Jupiter Atmospheres, with Application to HD 209458b. *Astrophys. J.*, **649**, 1048–1063.
- Cowan, N. B., E. Agol, and D. Charbonneau, 2007: Hot nights on extrasolar planets: mid-infrared phase variations of hot Jupiters. *Mon. Not. R. Astron. Soc.*, **379**, 641–646.
- Del Genio, A. D., and R. J. Suozzo, 1987: A comparative study of rapidly and slowly rotating dynamical regimes in a terrestrial general circulation model. *Journal of Atmospheric Sciences*, **44**, 973–986.
- Del Genio, A. D., and W. Zhou, 1996: Simulations of Superrotation on Slowly Rotating Planets: Sensitivity to Rotation and Initial Condition. *Icarus*, **120**, 332–343.
- Deming, D., S. Seager, L. J. Richardson, and J. Harrington, 2005: Infrared radiation from an extrasolar planet. *Nature*, **434**, 740–743.
- Deming, D., J. Harrington, S. Seager, and L. J. Richardson, 2006: Strong Infrared Emission from the Extrasolar Planet HD 189733b. *Astrophys. J.*, **644**, 560–564.
- Dima, I. M., and J. M. Wallace, 2003: On the Seasonality of the Hadley Cell. *Journal of Atmospheric Sciences*, **60**, 1522–1527.
- Dobbs-Dixon, I., and D. N. C. Lin, 2008: Atmospheric Dynamics of Short-Period Extrasolar Gas Giant Planets. I. Dependence of Nightside Temperature on Opacity. *Astrophys. J.*, **673**, 513–525.
- Dowling, T. E., 1995: Dynamics of jovian atmospheres. *Annual Review of Fluid Mechanics*, **27**, 293–334.
- Dowling, T. E., and A. P. Ingersoll, 1989: Jupiter's Great Red Spot as a shallow water system. *Journal of Atmospheric Sciences*, **46**, 3256–3278.
- Dritschel, D. G., M. de La Torre Juárez, and M. H. P. Ambaum, 1999: The three-dimensional vortical nature of atmospheric and oceanic turbulent flows. *Physics of Fluids*, **11**, 1512–1520.
- Farrell, B. F., 1990: Equable Climate Dynamics. *Journal of Atmospheric Sciences*, **47**, 2986–2995.
- Fegley, B. J., and K. Lodders, 1994: Chemical models of the deep atmospheres of Jupiter and Saturn. *Icarus*, **110**, 117–154.
- Fels, S. B., and R. S. Lindzen, 1974: The Interaction of Thermally Excited Gravity Waves with Mean Flows. *Geophysical and Astrophysical Fluid Dynamics*, **6**, 149–191.
- Fernando, H. J. S., R.-R. Chen, and D. L. Boyer, 1991: Effects of rotation on convective turbulence. *Journal of Fluid Mechanics*, **228**, 513–547.
- Fortney, J. J., M. S. Marley, and J. W. Barnes, 2007: Planetary Radii across Five Orders of Magnitude in Mass and Stellar Insolation: Application to Transits. *Astrophys. J.*, **659**, 1661–1672.
- Fortney, J. J., K. Lodders, M. S. Marley, and R. S. Freedman, 2008: A Unified Theory for the Atmospheres of the Hot and Very Hot Jupiters: Two Classes of Irradiated Atmospheres. *Astrophys. J.*, **678**, 1419–1435.
- Fortney, J. J., B. Militzer, and I. Baraffe, 2009: Giant planets: theory of interiors and evolution. *Exoplanets*, S. Seager, Ed., Univ. Arizona Press.
- Frierson, D. M. W., J. Lu, and G. Chen, 2007: Width of the Hadley cell in simple and comprehensive general circulation models. *Geophys. Res. Lett.*, **34**, L18,804.
- Gierasch, P. J., and B. J. Conrath, 1985: Energy conversion processes in the outer planets. *Recent Advances in Planetary Meteorology*, G. E. Hunt, Ed., Cambridge Univ. Press, New York, pp. 121–146.
- Gierasch, P. J., et al., 1997: The General Circulation of the Venus Atmosphere: an Assessment. *Venus II: Geology, Geophysics, Atmosphere, and Solar Wind Environment*, S. W. Bougher, D. M. Hunten, and R. J. Phillips, Eds., pp. 459–500.
- Gierasch, P. J., et al., 2000: Observation of moist convection in Jupiter's atmosphere. *Nature*, **403**, 628–630.
- Glatzmaier, G. A., M. Evonuk, and T. M. Rogers, 2009: Differential rotation in giant planets maintained by density-stratified turbulent convection. *Geophys. Astrophys. Fluid Dyn.*, **103**, 31–51.
- Goldman, B., et al., 2008: CLOUDS search for variability in brown dwarf atmospheres. Infrared spectroscopic time series of L/T transition brown dwarfs. *Astron. Astrophys.*, **487**, 277–292.
- Goodman, J., 2009: Thermodynamics of Atmospheric Circulation on Hot Jupiters. *Astrophys. J.*, **693**, 1645–1649.
- Green, J. S. A., 1970: Transfer properties of the large-scale eddies and the general circulation of the atmosphere. *Quarterly Journal of the Royal Meteorological Society*, **96**, 157–185.
- Grillmair, C. J., D. Charbonneau, A. Burrows, L. Armus, J. Stauffer, V. Meadows, J. Van Cleve, and D. Levine, 2007: A Spitzer Spectrum of the Exoplanet HD 189733b. *Astrophys. J. Lett.*, **658**, L115–L118.
- Grillmair, C. J., A. Burrows, D. Charbonneau, L. Armus, J. Stauffer, V. Meadows, J. van Cleve, K. von Braun, and D. Levine, 2008: Strong water absorption in the dayside emission spectrum of the planet HD189733b. *Nature*, **456**, 767–769.

- Grote, E., F. H. Busse, and A. Tilgner, 2000: Regular and chaotic spherical dynamos. *Physics of the Earth and Planetary Interiors*, **117**, 259–272.
- Guillot, T., 2005: The interiors of giant planets: Models and outstanding questions. *Annual Review of Earth and Planetary Sciences*, **33**, 493–530.
- Guillot, T., A. Burrows, W. B. Hubbard, J. I. Lunine, and D. Saumon, 1996: Giant Planets at Small Orbital Distances. *Astrophys. J. Lett.*, **459**, L35–L38.
- Guillot, T., D. J. Stevenson, W. B. Hubbard, and D. Saumon, 2004: The interior of Jupiter. *Jupiter: The Planet, Satellites and Magnetosphere*, F. Bagenal, T. E. Dowling, and W. B. McKinnon, Eds., Cambridge Univ. Press, pp. 35–57.
- Hadley, G., 1735: Concerning the cause of the general trade-winds. *Phil. Trans.*, **39**, 58–62.
- Harrington, J., B. M. Hansen, S. H. Luszcz, S. Seager, D. Deming, K. Menou, J. Y.-K. Cho, and L. J. Richardson, 2006: The Phase-Dependent Infrared Brightness of the Extrasolar Planet *v* Andromedae b. *Science*, **314**, 623–626.
- Hartmann, D. L., and coauthors, 2003: *Understanding Climate Change Feedbacks*. National Research Council of the National Academy of Sciences, The National Academies Press, Washington, D.C.
- Hayashi, Y.-Y., K. Ishioka, M. Yamada, and S. Yoden, 2000: Emergence of circumpolar vortex in two dimensional turbulence on a rotating sphere. *Proceedings of the IUTAM Symposium on Developments in Geophysical Turbulence (Fluid Mechanics and its Applications) V. 58*, R. M. Kerr and Y. Kimura, Eds., Kluwer Academic Pub., pp. 179–192.
- Hayashi, Y.-Y., S. Nishizawa, S.-I. Takehiro, M. Yamada, K. Ishioka, and S. Yoden, 2007: Rossby Waves and Jets in Two-Dimensional Decaying Turbulence on a Rotating Sphere. *Journal of Atmospheric Sciences*, **64**, 4246–4269.
- Haynes, P., 2005: Stratospheric Dynamics. *Annual Review of Fluid Mechanics*, **37**, 263–293.
- Heimpel, M., J. Aurnou, and J. Wicht, 2005: Simulation of equatorial and high-latitude jets on Jupiter in a deep convection model. *Nature*, **438**, 193–196.
- Held, I., 2005: The gap between simulation and understanding in climate modeling. *Bull. Amer. Meteorological Soc.*, **86**, 1609–1614.
- Held, I. M., 1999: The macroturbulence of the troposphere. *Tellus*, **51A-B**, 59–70.
- Held, I. M., 2000: The general circulation of the atmosphere. *Paper presented at 2000 Woods Hole Oceanographic Institute Geophysical Fluid Dynamics Program*, Woods Hole Oceanographic Institute, Woods Hole, MA (available at <http://www.whoi.edu/page.do?pid=13076>).
- Held, I. M., and A. Y. Hou, 1980: Nonlinear Axially Symmetric Circulations in a Nearly Inviscid Atmosphere. *Journal of Atmospheric Sciences*, **37**, 515–533.
- Held, I. M., and V. D. Larichev, 1996: A scaling theory for horizontally homogeneous, baroclinically unstable flow on a beta plane. *Journal of Atmospheric Sciences*, **53**, 946–952.
- Held, I. M., and B. J. Soden, 2000: Water vapor feedback and global warming. *Annu. Rev. Energy Environ.*, **25**, 441–475.
- Henry, G. W., G. W. Marcy, R. P. Butler, and S. S. Vogt, 2000: A Transiting “51 Peg-like” Planet. *Astrophys. J. Lett.*, **529**, L41–L44.
- Herrnstein, A., and T. E. Dowling, 2007: Effects of topography on the spin-up of a Venus atmospheric model. *Journal of Geophysical Research (Planets)*, **112**(E11).
- Hoffert, M. I., A. J. Callegari, C. T. Hsieh, and W. Ziegler, 1981: Liquid water on Mars: an energy balance climate model for CO<sub>2</sub>/H<sub>2</sub>O atmospheres. *Icarus*, **47**, 112–129.
- Hoffman, P. F., and D. Schrag, 2002: Review article: The snowball Earth hypothesis: testing the limits of global change. *Terra Nova*, **14**, 129–155.
- Holton, J. R., 2004: *An Introduction to Dynamic Meteorology*, 4th Ed.. Academic Press, San Diego.
- Huang, H.-P., and W. A. Robinson, 1998: Two-Dimensional Turbulence and Persistent Zonal Jets in a Global Barotropic Model. *Journal of Atmospheric Sciences*, **55**, 611–632.
- Hubbard, W. B., W. J. Nellis, A. C. Mitchell, N. C. Holmes, P. C. McCandless, and S. S. Limaye, 1991: Interior structure of Neptune - Comparison with Uranus. *Science*, **253**, 648–651.
- Hunt, B. G., 1979: The Influence of the Earth’s Rotation Rate on the General Circulation of the Atmosphere. *Journal of Atmospheric Sciences*, **36**, 1392–1408.
- Ingersoll, A. P., 1969: The Runaway Greenhouse: A History of Water on Venus. *Journal of Atmospheric Sciences*, **26**, 1191–1198.
- Ingersoll, A. P., 1990: Atmospheric dynamics of the outer planets. *Science*, **248**, 308–315.
- Ingersoll, A. P., and J. N. Cuzzi, 1969: Dynamics of Jupiter’s cloud bands. *Journal of Atmospheric Sciences*, **26**, 981–985.
- Ingersoll, A. P., and C. C. Porco, 1978: Solar heating and internal heat flow on Jupiter. *Icarus*, **35**, 27–43.
- Ingersoll, A. P., R. F. Beebe, J. L. Mitchell, G. W. Garneau, G. M. Yagi, and J.-P. Muller, 1981: Interaction of eddies and mean zonal flow on Jupiter as inferred from Voyager 1 and 2 images. *J. Geophys. Res.*, **86**, 8733–8743.
- Iro, N., B. Bézard, and T. Guillot, 2005: A time-dependent radiative model of HD 209458b. *Astron. Astrophys.*, **436**, 719–727.
- Irwin, J., D. Charbonneau, P. Nutzman, and E. Falco, 2009: The MEarth project: searching for transiting habitable super-Earths around nearby M dwarfs. *IAU Symposium*, vol. 253 of *IAU Symposium*, pp. 37–43.
- Ishioka, K., M. Yamada, Y.-Y. Hayashi, and S. Yoden, 1999: Pattern formation from two-dimensional decaying turbulence on a rotating sphere. *Nagare Multimedia, The Japan Society of Fluid Mechanics*, [available online at <http://www.nagare.or.jp/mm/99/ishioka/>].
- James, I. N., 1994: *Introduction to Circulating Atmospheres*. Cambridge Atmospheric and Space Science Series, Cambridge University Press, UK.
- Joshi, M., 2003: Climate Model Studies of Synchronously Rotating Planets. *Astrobiology*, **3**, 415–427.
- Joshi, M. M., R. M. Haberle, and R. T. Reynolds, 1997: Simulations of the Atmospheres of Synchronously Rotating Terrestrial Planets Orbiting M Dwarfs: Conditions for Atmospheric Collapse and the Implications for Habitability. *Icarus*, **129**, 450–465.

- Kaspi, Y., G. R. Flierl, and A. P. Showman, 2009: The deep wind structure of the giant planets: results from an anelastic general circulation model. *Icarus*, **202**, 525–542.
- Kasting, J. F., 1988: Runaway and moist greenhouse atmospheres and the evolution of earth and Venus. *Icarus*, **74**, 472–494.
- Kasting, J. F., and D. Catling, 2003: Evolution of a Habitable Planet. *Annu. Rev. Astron. Astrophys.*, **41**, 429–463.
- Kasting, J. F., D. P. Whitmire, and R. T. Reynolds, 1993: Habitable Zones around Main Sequence Stars. *Icarus*, **101**, 108–128.
- Kawamura, K., et al., 2007: Northern hemisphere forcing of climatic cycles in Antarctica over the past 360,000 years. *Nature*, **448**, 912–916.
- Kim, H.-K., and S. Lee, 2001: Hadley Cell Dynamics in a Primitive Equation Model. Part II: Nonaxisymmetric Flow. *Journal of Atmospheric Sciences*, **58**, 2859–2871.
- Kirk, R. L., and D. J. Stevenson, 1987: Hydromagnetic constraints on deep zonal flow in the giant planets. *Astrophys. J.*, **316**, 836–846.
- Knutson, H. A., D. Charbonneau, L. E. Allen, J. J. Fortney, E. Agol, N. B. Cowan, A. P. Showman, C. S. Cooper, and S. T. Megeath, 2007: A map of the day-night contrast of the extrasolar planet HD 189733b. *Nature*, **447**, 183–186.
- Knutson, H. A., D. Charbonneau, L. E. Allen, A. Burrows, and S. T. Megeath, 2008: The 3.6–8.0  $\mu\text{m}$  Broadband Emission Spectrum of HD 209458b: Evidence for an Atmospheric Temperature Inversion. *Astrophys. J.*, **673**, 526–531.
- Knutson, H. A., D. Charbonneau, A. Burrows, F. T. O'Donovan, and G. Mandushev, 2009a: Detection of A Temperature Inversion in the Broadband Infrared Emission Spectrum of TrES-4. *Astrophys. J.*, **691**, 866–874.
- Knutson, H. A., D. Charbonneau, N. B. Cowan, J. J. Fortney, A. P. Showman, E. Agol, G. W. Henry, M. E. Everett, and L. E. Allen, 2009b: Multiwavelength Constraints on the Day-Night Circulation Patterns of HD 189733b. *Astrophys. J.*, **690**, 822–836.
- Korty, R. L., and T. Schneider, 2008: Extent of Hadley circulations in dry atmospheres. *Geophys. Res. Lett.*, **35**, L23,803.
- Langton, J., and G. Laughlin, 2007: Observational Consequences of Hydrodynamic Flows on Hot Jupiters. *Astrophys. J. Lett.*, **657**, L113–L116.
- Langton, J., and G. Laughlin, 2008a: Hydrodynamic Simulations of Unevenly Irradiated Jovian Planets. *Astrophys. J.*, **674**, 1106–1116.
- Langton, J., and G. Laughlin, 2008b: Persistent circumpolar vortices on the extrasolar giant planet HD 37605 b. *Astron. Astrophys.*, **483**, L25–L28.
- Laughlin, G., D. Deming, J. Langton, D. Kasen, S. Vogt, P. Butler, E. Rivera, and S. Meschiari, 2009: Rapid heating of the atmosphere of an extrasolar planet. *Nature*, **457**, 562–564.
- Lee, C., S. R. Lewis, and P. L. Read, 2007: Superrotation in a Venus general circulation model. *Journal of Geophysical Research (Planets)*, **112**(E11).
- Lewis, N., A. P. Showman, J. J. Fortney, and M. S. Marley, 2009: Three-Dimensional Atmospheric Dynamics of Eccentric Extrasolar Planets. *American Astronomical Society Meeting Abstracts*, vol. 213 of *American Astronomical Society Meeting Abstracts*, p. 346.01.
- Lian, Y., and A. P. Showman, 2008: Deep jets on gas-giant planets. *Icarus*, **194**, 597–615.
- Lian, Y., and A. P. Showman, 2009: Generation of equatorial jets by large-scale latent heating on the giant planets. *Icarus*, *in press*.
- Lindzen, R. S., and B. Farrell, 1980a: The role of the polar regions in climate, and a new parameterization of global heat transport. *Monthly Weather Review*, **108**, 2064–2079.
- Lindzen, R. S., and B. Farrell, 1980b: A simple approximate result for the maximum growth rate of baroclinic instabilities. *Journal of the Atmospheric Sciences*, **37**, 1648–1654.
- Lindzen, R. S., and A. V. Hou, 1988: Hadley Circulations for Zonally Averaged Heating Centered off the Equator. *Journal of Atmospheric Sciences*, **45**, 2416–2427.
- Little, B., C. D. Anger, A. P. Ingersoll, A. R. Vasavada, D. A. Senske, H. H. Breneman, W. J. Borucki, and The Galileo SSI Team, 1999: Galileo Images of Lightning on Jupiter. *Icarus*, **142**, 306–323.
- Liu, J., P. M. Goldreich, and D. J. Stevenson, 2008: Constraints on deep-seated zonal winds inside Jupiter and Saturn. *Icarus*, **196**, 653–664.
- Lorenz, E. N., 1967: *The Nature and Theory of the General Circulation of the Atmosphere*. World Meteorological Org., Geneva.
- Lu, J., G. A. Vecchi, and T. Reichler, 2007: Expansion of the Hadley cell under global warming. *Geophys. Res. Lett.*, **34** (L06805).
- Machalek, P., P. R. McCullough, C. J. Burke, J. A. Valenti, A. Burrows, and J. L. Hora, 2008: Thermal Emission of Exoplanet XO-1b. *Astrophys. J.*, **684**, 1427–1432.
- Marcus, P. S., T. Kundu, and C. Lee, 2000: Vortex dynamics and zonal flows. *Physics of Plasmas*, **7**, 1630–1640.
- Marcy, G. W., and R. P. Butler, 1996: A Planetary Companion to 70 Virginis. *Astrophys. J. Lett.*, **464**, L147+.
- Mayor, M., and D. Queloz, 1995: A Jupiter-Mass Companion to a Solar-Type Star. *Nature*, **378**, 355–+.
- Menou, K., and E. Rauscher, 2009: Atmospheric Circulation of Hot Jupiters: A Shallow Three-Dimensional Model. *Astrophys. J.*, **700**, 887–897.
- Menou, K., J. Y.-K. Cho, S. Seager, and B. M. S. Hansen, 2003: “Weather” Variability of Close-in Extrasolar Giant Planets. *Astrophys. J. Lett.*, **587**, L113–L116.
- Morales-Calderón, M., et al., 2006: A Sensitive Search for Variability in Late L Dwarfs: The Quest for Weather. *Astrophys. J.*, **653**, 1454–1463.
- Navarra, A., and G. Boccaletti, 2002: Numerical general circulation experiments of sensitivity to Earth rotation rate. *Climate Dynamics*, **19**, 467–483.
- Noll, K. S., T. R. Geballe, and M. S. Marley, 1997: Detection of Abundant Carbon Monoxide in the Brown Dwarf Gliese 229B. *Astrophys. J. Lett.*, **489**, L87+.
- North, G. R., 1975: Analytical solution to a simple climate model with diffusive heat transport. *Journal of the Atmospheric Sciences*, **32**, 1301–1307.
- North, G. R., R. F. Cahalan, and J. A. J. Coakley, 1981: Energy balance climate models. *Rev. Geophysics Space Physics*, **19**, 91–121.

- Nozawa, T., and S. Yoden, 1997: Formation of zonal band structure in forced two-dimensional turbulence on a rotating sphere. *Physics of Fluids*, **9**, 2081–2093.
- Okuno, A., and A. Masuda, 2003: Effect of horizontal divergence on the geostrophic turbulence on a beta-plane: Suppression of the Rhines effect. *Physics of Fluids*, **15**, 56–65.
- Pedlosky, J., 1987: *Geophysical Fluid Dynamics*, 2nd Ed.. Springer-Verlag, New York.
- Peixoto, J. P., and A. H. Oort, 1992: *Physics of Climate*. American Institute of Physics, New York.
- Podolak, M., W. B. Hubbard, and D. J. Stevenson, 1991: Models of Uranus' interior and magnetic field. *Uranus*, J. T. Bergstrahl, E. D. Miner, and M. S. Matthews, Eds., Univ. Arizona Press, Tucson, AZ, pp. 29–61.
- Prinn, R. G., and S. S. Barshay, 1977: Carbon monoxide on Jupiter and implications for atmospheric convection. *Science*, **198**, 1031–1034.
- Rauscher, E., K. Menou, J. Y.-K. Cho, S. Seager, and B. M. S. Hansen, 2007: Hot Jupiter Variability in Eclipse Depth. *Astrophys. J. Lett.*, **662**, L115–L118.
- Rauscher, E., K. Menou, J. Y.-K. Cho, S. Seager, and B. M. S. Hansen, 2008: On Signatures of Atmospheric Features in Thermal Phase Curves of Hot Jupiters. *Astrophys. J.*, **681**, 1646–1652.
- Reinaud, J. N., D. G. Dritschel, and C. R. Koudella, 2003: The shape of vortices in quasi-geostrophic turbulence. *Journal of Fluid Mechanics*, **474**, 175–192.
- Rhines, P. B., 1975: Waves and turbulence on a beta-plane. *Journal of Fluid Mechanics*, **69**, 417–443.
- Richardson, L. J., D. Deming, K. Horning, S. Seager, and J. Harrington, 2007: A spectrum of an extrasolar planet. *Nature*, **445**, 892–895.
- Salby, M. L., 1996: *Fundamentals of Atmospheric Physics*. San Diego: Academic Press, 1996.
- Sanchez-Lavega, A., J. F. Rojas, and P. V. Sada, 2000: Saturn's Zonal Winds at Cloud Level. *Icarus*, **147**, 405–420.
- Sánchez-Lavega, A., et al., 2008: Depth of a strong jovian jet from a planetary-scale disturbance driven by storms. *Nature*, **451**, 437–440.
- Saravanan, R., 1993: Equatorial Superrotation and Maintenance of the General Circulation in Two-Level Models. *Journal of Atmospheric Sciences*, **50**, 1211–1227.
- Saumon, D., W. B. Hubbard, A. Burrows, T. Guillot, J. I. Lunine, and G. Chabrier, 1996: A Theory of Extrasolar Giant Planets. *Astrophys. J.*, **460**, 993–1018.
- Saumon, D., T. R. Geballe, S. K. Leggett, M. S. Marley, R. S. Freedman, K. Lodders, B. Fegley, Jr., and S. K. Sengupta, 2000: Molecular Abundances in the Atmosphere of the T Dwarf GL 229B. *Astrophys. J.*, **541**, 374–389.
- Saumon, D., M. S. Marley, M. C. Cushing, S. K. Leggett, T. L. Roellig, K. Lodders, and R. S. Freedman, 2006: Ammonia as a Tracer of Chemical Equilibrium in the T7.5 Dwarf Gliese 570D. *Astrophys. J.*, **647**, 552–557.
- Saumon, D., et al., 2007: Physical Parameters of Two Very Cool T Dwarfs. *Astrophys. J.*, **656**, 1136–1149.
- Sayanagi, K. M., A. P. Showman, and T. E. Dowling, 2008: The Emergence of Multiple Robust Zonal Jets from Freely Evolving, Three-Dimensional Stratified Geostrophic Turbulence with Applications to Jupiter. *Journal of Atmospheric Sciences*, **65**, 3947–3962.
- Schneider, T., 2006: The General Circulation of the Atmosphere. *Annual Review of Earth and Planetary Sciences*, **34**, 655–688.
- Schneider, T., and J. Liu, 2009: Formation of Jets and Equatorial Superrotation on Jupiter. *J. Atmos. Sci.*, **66**, 579–601.
- Schneider, T., and C. C. Walker, 2008: Scaling laws and regime transitions of macroturbulence in dry atmospheres. *J. Atmos. Sci.*, **65**, 2153–2173.
- Scott, R. K., and L. Polvani, 2007: Forced-dissipative shallow water turbulence on the sphere and the atmospheric circulation of the giant planets. *J. Atmos. Sci.*, **64**, 3158–3176.
- Scott, R. K., and L. M. Polvani, 2008: Equatorial superrotation in shallow atmospheres. *Geophys. Res. Lett.*, **35**, L24,202.
- Seager, S., D. Deming, and J. A. Valenti, 2008: Transiting Exoplanets with JWST. *ArXiv e-prints*.
- Showman, A. P., 2007: Numerical simulations of forced shallow-water turbulence: effects of moist convection on the large-scale circulation of Jupiter and Saturn. *J. Atmos. Sci.*, **64**, 3132–3157.
- Showman, A. P., and T. Guillot, 2002: Atmospheric circulation and tides of “51 Pegasus b-like” planets. *Astron. Astrophys.*, **385**, 166–180.
- Showman, A. P., P. J. Gierasch, and Y. Lian, 2006: Deep zonal winds can result from shallow driving in a giant-planet atmosphere. *Icarus*, **182**, 513–526.
- Showman, A. P., C. S. Cooper, J. J. Fortney, and M. S. Marley, 2008a: Atmospheric Circulation of Hot Jupiters: Three-dimensional Circulation Models of HD 209458b and HD 189733b with Simplified Forcing. *Astrophys. J.*, **682**, 559–576.
- Showman, A. P., K. Menou, and J. Y.-K. Cho, 2008b: Atmospheric Circulation of Hot Jupiters: A Review of Current Understanding. *Extreme Solar Systems*, D. Fischer, F. A. Rasio, S. E. Thorsett, and A. Wolszczan, Eds., vol. 398 of *Astronomical Society of the Pacific Conference Series*, pp. 419–441.
- Showman, A. P., J. J. Fortney, Y. Lian, M. S. Marley, R. S. Freedman, H. A. Knutson, and D. Charbonneau, 2009: Atmospheric Circulation of Hot Jupiters: Coupled Radiative-Dynamical General Circulation Model Simulations of HD 189733b and HD 209458b. *Astrophys. J.*, **699**, 564–584.
- Smith, K. S., 2004: A local model for planetary atmospheres forced by small-scale convection. *J. Atmos. Sciences*, **61**, 1420–1433.
- Spiegel, D. S., K. Menou, and C. A. Scharf, 2008: Habitable Climates. *Astrophys. J.*, **681**, 1609–1623.
- Spiegel, D. S., K. Menou, and C. A. Scharf, 2009: Habitable Climates: The Influence of Obliquity. *Astrophys. J.*, **691**, 596–610.
- Stevens, B., 2005: Atmospheric Moist Convection. *Annual Review of Earth and Planetary Sciences*, **33**, 605–643.
- Stevenson, D. J., 1979: Turbulent thermal convection in the presence of rotation and a magnetic field - A heuristic theory. *Geophysical and Astrophysical Fluid Dynamics*, **12**, 139–169.

- Stevenson, D. J., 1991: The search for brown dwarfs. *Annu. Rev. Astron. Astrophys.*, **29**, 163–193.
- Stone, P. H., 1972: A simplified radiative-dynamical model for the static stability of rotating atmospheres. *Journal of the Atmospheric Sciences*, **29**, 406–418.
- Stone, P. H., 1978: Baroclinic Adjustment. *Journal of Atmospheric Sciences*, **35**, 561–571.
- Suarez, M. J., and D. G. Duffy, 1992: Terrestrial Superrotation: A Bifurcation of the General Circulation. *Journal of Atmospheric Sciences*, **49**, 1541–1556.
- Sukoriansky, S., N. Dikovskaya, and B. Galperin, 2007: On the “arrest” of inverse energy cascade and the Rhines scale. *J. Atmos. Sci.*, **64**, 3312–3327.
- Swain, M. R., G. Vasht, and G. Tinetti, 2008: The presence of methane in the atmosphere of an extrasolar planet. *Nature*, **452**, 329–331.
- Swain, M. R., G. Vasht, G. Tinetti, J. Bouwman, P. Chen, Y. Yung, D. Deming, and P. Deroo, 2009: Molecular Signatures in the Near-Infrared Dayside Spectrum of HD 189733b. *Astrophys. J. Lett.*, **690**, L114–L117.
- Tabeling, P., 2002: Two-dimensional turbulence: a physicist approach. *Phys. Rep.*, **362**, 1–62.
- Thompson, A. F., and W. R. Young, 2007: Two-layer baroclinic eddy heat fluxes: zonal flows and energy balance. *J. Atmos. Sci.*, **64**, 3214–3231.
- Tinetti, G., et al., 2007: Water vapour in the atmosphere of a transiting extrasolar planet. *Nature*, **448**, 169–171.
- Vallis, G. K., 2006: *Atmospheric and Oceanic Fluid Dynamics: Fundamentals and Large-Scale Circulation*. Cambridge Univ. Press, Cambridge, UK.
- Vasavada, A. R., and A. P. Showman, 2005: Jovian atmospheric dynamics: an update after Galileo and Cassini. *Reports of Progress in Physics*, **68**, 1935–1996.
- Walker, C. C., and T. Schneider, 2005: Response of idealized Hadley circulations to seasonally varying heating. *Geophys. Res. Lett.*, **32**, L06,813.
- Walker, C. C., and T. Schneider, 2006: Eddy Influences on Hadley Circulations: Simulations with an Idealized GCM. *Journal of Atmospheric Sciences*, **63**, 3333–3350.
- Ward, W. R., 1974: Climatic variations on Mars. I. Astronomical theory of insolation. *J. Geophys. Res.*, **79**, 3375–3386.
- Williams, D. M., and J. F. Kasting, 1997: Habitable Planets with High Obliquities. *Icarus*, **129**, 254–267.
- Williams, D. M., and D. Pollard, 2002: Earth-like worlds on eccentric orbits: excursions beyond the habitable zone. *International Journal of Astrobiology*, **1**, 61–69.
- Williams, D. M., and D. Pollard, 2003: Extraordinary climates of Earth-like planets: three-dimensional climate simulations at extreme obliquity. *International Journal of Astrobiology*, **2**, 1–19.
- Williams, G. P., 1978: Planetary circulations. I - Barotropic representation of Jovian and terrestrial turbulence. *Journal of Atmospheric Sciences*, **35**, 1399–1426.
- Williams, G. P., 1979: Planetary circulations. II - The Jovian quasi-geostrophic regime. *Journal of Atmospheric Sciences*, **36**, 932–968.
- Williams, G. P., 1988a: The dynamical range of global circulations – I. *Climate Dynamics*, **2**, 205–260.
- Williams, G. P., 1988b: The dynamical range of global circulations – II. *Climate Dynamics*, **3**, 45–84.
- Williams, G. P., 2003: Jovian Dynamics. Part III: Multiple, Migrating, and Equatorial Jets. *Journal of Atmospheric Sciences*, **60**, 1270–1296.
- Williams, G. P., and J. L. Holloway, 1982: The range and unity of planetary circulations. *Nature*, **297**, 295–299.
- Yamamoto, M., and M. Takahashi, 2006: Superrotation Maintained by Meridional Circulation and Waves in a Venus-Like AGCM. *Journal of Atmospheric Sciences*, **63**, 3296–3314.
- Yoden, S., K. Ishioka, Y.-Y. Hayashi, and M. Yamada, 1999: A further experiment on two-dimensional decaying turbulence on a rotating sphere. *Nuovo Cimento C Geophysics Space Physics C*, **22**, 803–812.
- Zurita-Gotor, P., and R. S. Lindzen, 2006: Theories of baroclinic adjustment and eddy equilibration. *The Global Circulation of the Atmosphere*, T. Schneider and A. H. Sobel, Eds., Princeton University Press, pp. 22–46.
- Zurita-Gotor, P., and G. K. Vallis, 2009: Equilibration of baroclinic turbulence in primitive equations and quasigeostrophic models. *J. Atmos. Sci.*, **66**, 837–863.